Structures and Materials Research
Department of Civil Engineering
Division of Structural Engineering
and Structural Mechanics

Report No. UCSESM 74-4

STATIC AND DYNAMIC GEOMETRIC AND MATERIAL NONLINEAR ANALYSIS

by

Klaus-Jürgen Bathe

Haluk Ozdemir

Edward L. Wilson

Structural Engineering Laboratory
University of California
Berkeley, California

February 1974

ABSTRACT

The purpose of this report is to present the theory and implementation of the analysis procedures that have been tested and are currently used in the general linear and nonlinear, static and dynamic finite element analysis program NONSAP. First, the continuum mechanics formulations employed are briefly summarized. For finite element discretization, one-, two- and three-dimensional isoparametric elements have been implemented. The two- and three-dimensional elements can have variable number of nodes. Next, the various linear and nonlinear material models available in the program to represent elastic, hyperelastic (rubber) and hypoelastic (elastic-plastic) material behavior are presented. Finally, a selected number of sample analyses are described to show some of the current solution capabilities of the program.

TABLE OF CONTENTS

TABLE OF CONTENTS (cont'd.)

TABLE OF CONTENTS (cont'd.)

NOTATION

All notation is defined in the text when used first. The following is only a list of some frequently used symbols.

With regard to tensor and vector subscripts and superscripts, the following convention is employed:

A left superscript denotes the time of the configuration in which the quantity occurs.

A left subscript can have two different meanings. If the quantity considered is a derivative, the left subscript denotes the time of the configuration, in which is measured the coordinate with respect to which is differentiated. Otherwise the left subscript denotes the time of the configuration in which the quantity is measured.

Right lower case subscripts denote the components of a tensor or vector. Components are referred to a fixed Cartesian coordinate system; $i,j,\ldots = 1,2,3$. Differentiation is denoted by a right lower case subscript following a comma, with the subscript indicating the coordinate with respect to which is differentiated.

${}^{0}_{A}$	=	Area of body in the configuration at time 0
C_{ijrs}	=	Component of constant constitutive tensor
${}^{t}_{0}C_{ijrs}$, ${}^{t}_{t}C_{ijrs}$	=	Component of constitutive tensor at time t referred to the configuration at time 0, t
${}_{0}C_{ijrs}$, ${}_{t}C_{ijrs}$	=	Component of tangent constitutive tensor at time t referred to the configuration at time 0, t
${}^{t+\Delta t}_{0}f_{i}$	=	Component of body force vector per unit mass, at time $t+\Delta t$, referred to the configuration at time 0

h_k = Finite element interpolation function associated with nodal point k

$^{t+\Delta t}R$ = External virtual work expression corresponding to the configuration at time $t+\Delta t$ defined in Eq. (2.2)

r,s,t = Natural element coordinates

$^{t}_{0}S_{ij}$, $^{t+\Delta t}_{0}S_{ij}$ = Component of 2nd Piola - Kirchhoff stress tensor in the configuration at time t, $t+\Delta t$ referred to the configuration at time 0

$^{t+\Delta t}_{t}S_{ij}$ = Component of 2nd Piola - Kirchhoff stress tensor in the configuration at time $t+\Delta t$ referred to the configuration at time t

$^{0}S_{ij}$, $^{t}S_{ij}$ = Component of 2nd Piola - Kirchhoff stress increment at time t

t , $t+\Delta t$ = time t and $t+\Delta t$, before and after time increment Δt

$^{t+\Delta t}_{0}t_i$ = Component of surface traction vector per unit area, at time $t+\Delta t$, referred to the configuration at time 0

$^{t}u_i$, $^{t+\Delta t}u_i$ = Component of displacement vector from the initial configuration at time 0 to the configuration at time t, $t+\Delta t$

u_i = Increment in displacement component, $u_i = {}^{t+\Delta t}u_i - {}^{t}u_i$

$^{t}u^{k}_{i}$ = Displacement component of nodal point k in the configuration at time t

u_i^k	=	Increment in ${}^t u_i^k$
${}^t_0 u_{i,j}$, ${}^{t+\Delta t}_0 u_{i,j}$	=	Derivative of displacement component to the configuration at time t, t+Δt with respect to coordinate ${}^0 x_j$
${}^0 u_{i,j}$, ${}^t u_{i,j}$, ${}^{t+\Delta t} u_{i,j}$	=	Derivative of displacement increment with respect to coordinate ${}^0 x_j$, ${}^t x_j$, ${}^{t+\Delta t} x_j$
${}^0 V$, ${}^t V$, ${}^{t+\Delta t} V$	=	Volume of body in the configuration at time 0, t, t+Δt
${}^0 x_i$, ${}^t x_i$, ${}^{t+\Delta t} x_i$	=	Cartesian coordinate in the configuration at time 0, t, t+Δt
${}^0 x_i^k$, ${}^t x_i^k$, ${}^{t+\Delta t} x_i^k$	=	Cartesian coordinate of nodal point k in the configuration at time 0, t, t+Δt
${}^0_t x_{i,j}$, ${}^t_0 x_{i,j}$	=	Derivative of coordinate in the configuration at time 0, t with respect to coordinate ${}^t x_j$, ${}^0 x_j$
δ	=	Denoting "variation in"
${}^{t+\Delta t}_0 \epsilon_{ij}$, ${}^t_0 \epsilon_{ij}$	=	Component of Almansi strain tensor in the configuration at time t+Δt, t, referred to the configuration at time 0
${}^{t+\Delta t}_0 \epsilon_{ij}$, ${}^t_0 \epsilon_{ij}$	=	Component of Green - Lagrange strain tensor in the configuration at time t+Δt, t, referred to the configuration at time 0
${}^{t+\Delta t}_t \epsilon_{ij}$	=	Component of Green - Lagrange strain tensor in the configuration at time t+Δt, referred to the configuration at time t (i.e. using displacements from the configuration at time t to the configuration at time t+Δt)

$_0\varepsilon_{ij}$, $_t\varepsilon_{ij}$ = Component of strain increment tensor (Green - Lagrange), referred to the configuration at time 0, t

$_{t+\Delta t}e_{ij}$, $_te_{ij}$ = Component of total infinitesimal strain tensor at time t+Δt, t

e_{ij} = Increment in $_te_{ij}$

$_0e_{ij}$, $_te_{ij}$ = Linear part of strain increment $_0\varepsilon_{ij}$, $_t\varepsilon_{ij}$

$_0\eta_{ij}$, $_t\eta_{ij}$ = Nonlinear part of strain increment $_0\varepsilon_{ij}$, $_t\varepsilon_{ij}$

$_0\rho$, $_t\rho$ = Specific mass of body in the configuration at time 0, t

$_t\sigma_{ij}$ = Component of stress tensor at time t calculated assuming infinitesimal displacements

σ_{ij} = Increment in σ_{ij}

$_t\tau_{ij}$, $_{t+\Delta t}\tau_{ij}$ = Component of Cauchy stress tensor in the configuration at time t, t+Δt

$_t\tau^{\nabla}_{ij}$ = Component of Jaumann stress rate tensor in the configuration at time t

$_t\Omega_{pi}$ = Components of spin tensor in the configuration at time t

Matrices:

$_0^tB_L$, $_t^tB_L$ = Linear strain-displacement matrix in the configuration at time t referred to the configuration at time 0, t

B_L	=	Linear strain-displacement matrix assuming small displacements
${}_0^tB_{NL}$, ${}_t^tB_{NL}$	=	Nonlinear strain-displacement matrix in the configuration at time t referred to the configuration at time 0, t
C	=	Stress-strain material property matrix
${}_0^tC$, ${}_t^tC$	=	Tangent material property matrix at time t and referred to the configuration at time 0, t
${}^tF$, ${}_0^tF$, ${}_t^tF$	=	Vector of nodal point forces at time t
K	=	Time independent linear elastic, small displacement stiffness matrix
${}_0^tK_L$, ${}_t^tK_L$	=	Linear strain stiffness matrix in the configuration at time t referred to the configuration at time 0, t
${}_0^tK_{NL}$, ${}_t^tK_{NL}$	=	Nonlinear strain stiffness matrix in the configuration at time t referred to the configuration at time 0, t
${}^tK$	=	Tangent stiffness matrix at time t
M	=	Mass matrix
${}^{t+\Delta t}R$	=	Vector of external loads at time $t+\Delta t$
${}_0^tS$, ${}_0^t\hat{S}$	=	2nd Piola - Kirchhoff stress matrix and vector in the configuration at time t and referred to the configuration at time 0
${}^tu$, ${}^{t+\Delta t}u$	=	Vector of displacements at time t, $t+\Delta t$
u	=	Vector of incremental displacements at time t

$\overset{t}{\underset{\sim}{\hat{\Sigma}}}$ = Vector of stresses at time t in materially nonlinear only analysis

$\overset{t}{\tau}$, $\overset{t}{\hat{\tau}}$ = Cauchy stress matrix and vector in the configuration at time t

1. INTRODUCTION

The importance of investigating the nonlinear behavior of various types of structures for adequate design is currently recognized to an increasing extent. In some cases the behavior of the materials is significantly nonlinear at even relatively small loading [24] [38], and for other structures the influence of the geometry changes on the response of the structure cannot be neglected [11] [16] [27] [31] [52].

A most important aspect is in many cases the ultimate load behavior of the structure, which is largely governed by nonlinear effects [12] [21] [42] [44] [45] [47]. If the ultimate load can be obtained accurately, the safety of the structure is increased and in many instances the cost can be reduced. In certain designs, for example, as found in the automotive and nuclear industries, extensive testing is carried out in order to assess accurately the response of the structure considered. However, the realization that reliable test data are very expensive and the need for parametric studies has increased emphasis on theoretical analysis. If appropriate analysis techniques are available, testing can be reduced significantly and a better understanding of the structural behavior can be obtained.

The finite element analysis of structures has proven to be very effective in linear analysis [1] [53]. With regard to nonlinear analysis, practical solutions to many different problems have also been obtained (see references).

The earliest nonlinear finite element analyses were essentially based on extensions of linear analyses and have been developed for specific applications (for a comprehensive list of references, see the books

by Oden [40], Zienkiewicz [53], Martin and Carey [32] and Desai and Abel [10]). The procedures were primarily developed on an intuitive basis in order to obtain solutions to the specific problems considered. However, to provide general analysis capabilities, much research is still required to improve the stability, accuracy and effectiveness of nonlinear solutions. Also, for the analysis of some problems the required techniques are not yet available.

In nonlinear analysis, stability and accuracy are a great deal more difficult to obtain than in linear analysis and depend on various factors. An important aspect is the use of a consistent continuum mechanics formulation and an effective finite element discretization. During recent years the isoparametric finite element procedure has proven to be very effective in linear analysis [53], and lately it has been shown that general nonlinear continuum mechanics formulations can also efficiently be implemented.

A second important aspect is the use of material models which accurately represent the actual materials under field conditions. Specific attention need be given that the implementation of the material models does not introduce instabilities in the solution [42].

In dynamic analysis it is further necessary to use numerical time integration, which introduces additional errors [2] [6] [25] [39]. Extensive research is currently being devoted to the development of stable and accurate integration schemes. However, it need be realized that a proper evaluation and use of an integration method is only possible if a consistent nonlinear finite element formulation is used.

Currently, the general purpose nonlinear finite element program NONSAP is being developed at the University of California, Berkeley [5].

The purpose of this report is to present the continuum mechanics formulations used, the resulting finite element matrices, the material models so far implemented and sample solutions. For a description of the computer program the reader is referred to [7].

The program has been developed to solve static and dynamic, linear and nonlinear problems. The nonlinearities may be due to material nonlinearity, in which case elastic, hyperelastic and hypoelastic material behavior may be considered, or the nonlinear effects may arise from large displacements and large strains. The continuum mechanics formulations include all nonlinear effects, and the isoparametric finite element discretization used is shown to be very effective for general application. The finite elements implemented have a variable number of nodes, which allows efficient mesh selection.

To demonstrate the applicability of the program to the solution of practical problems, a variety of sample analyses are presented. Solutions are obtained of linear and nonlinear static and dynamic response of beams, arches, plates and shells. The nonlinear behavior is due to large displacements, large strains and various nonlinear material characteristics.

2. FORMULATION OF THE CONTINUUM MECHANICS INCREMENTAL EQUATIONS OF MOTION

In nonlinear dynamic finite element analysis involving large deformations and material nonlinearities, it is necessary to use an incremental formulation of the equations of motion. In the development to follow we assume that the continuum can experience large displacements, large strains and the media are described by general constitutive laws, several of which are presented in Chapter 4 of this report. The formulations given herein include all nonlinear effects. However, as will be discussed, for the solution of certain problems some simplifying approximations can be made.

Consider the motion of a body in a Cartesian coordinate system as shown in Fig. 1.1. The aim is to evaluate the equilibrium positions of the body at the discrete time points 0, Δt, $2\Delta t$, $3\Delta t$, ..., where Δt is an increment in time. Assume that the solution for the kinematic and static variables for all time steps from time 0 to time t, inclusive, have been solved for, and that the solution for time $t+\Delta t$ is required next. It is noted that the solution process for the next required equilibrium position is typical and would be applied repetitively until the complete solution path has been solved for.

Nomenclature

It is useful at this point to lay out the notation which will be employed.

The motion of the body is considered in a fixed Cartesian coordinate system, Fig. 1.1, in which all kinematic and static variables are defined.

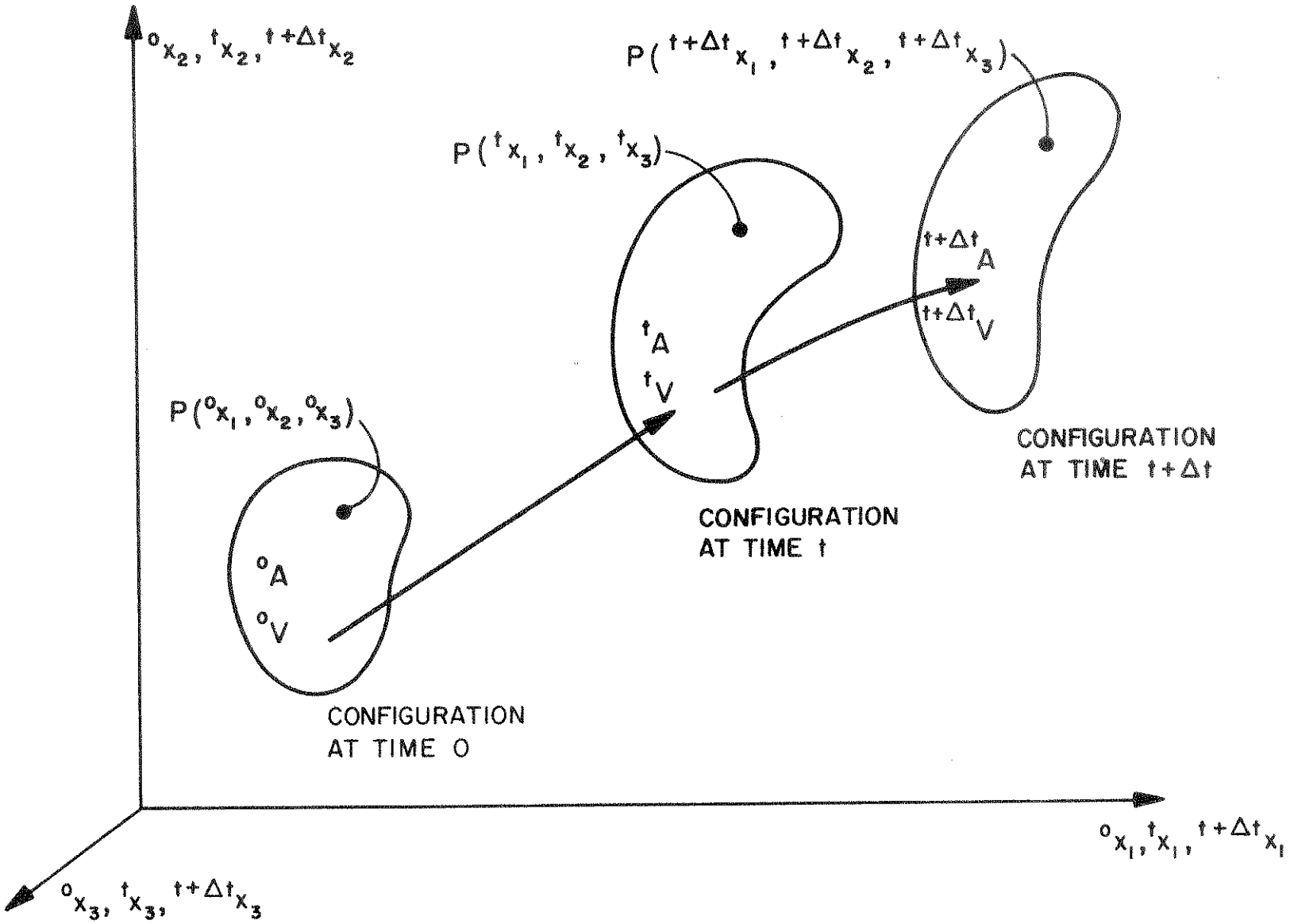

FIGURE I.I MOTION OF BODY IN CARTESIAN COORDINATE SYSTEM

The coordinates describing the configuration of the body at time 0 are ${}^0x_1$, ${}^0x_2$, ${}^0x_3$; at time t are ${}^tx_1$, ${}^tx_2$, ${}^tx_3$; and at time $t+\Delta t$ are ${}^{t+\Delta t}x_1$, ${}^{t+\Delta t}x_2$, ${}^{t+\Delta t}x_3$, where the left superscripts refer to the configuration of the body and the subscripts to the coordinate axes.

The notation for the displacements of the body is similar to the notation for the coordinates; at time t the displacements are ${}^tu_i$, i = 1,2,3 and at time $t+\Delta t$ the displacements are ${}^{t+\Delta t}u_i$, i = 1,2,3; therefore we have

$$\left.\begin{aligned} {}^tx_i &= {}^0x_i + {}^tu_i \\ {}^{t+\Delta t}x_i &= {}^0x_i + {}^{t+\Delta t}u_i \end{aligned}\right\} \quad i = 1,2,3$$

The increments in the displacements from time t to $t+\Delta t$ are denoted as

$$u_i = {}^{t+\Delta t}u_i - {}^tu_i \quad ; \quad i = 1,2,3$$

During motion of the body, its volume, surface area, mass density, stresses and strains are changing continuously. We denote the specific mass, area and volume of the body at times 0, t and $t+\Delta t$ as ${}^0\rho$, ${}^t\rho$, ${}^{t+\Delta t}\rho$; ${}^0A$, ${}^tA$, ${}^{t+\Delta t}A$; and ${}^0V$, ${}^tV$, ${}^{t+\Delta t}V$; respectively.

Since the configuration of the body at time $t+\Delta t$ is not known, we will refer applied forces, stresses and strains to a known equilibrium configuration. In analogy to the notation used for coordinates and displacements a left superscript indicates in which configuration the quantity (body force, surface traction, stress, ...) occurs; in addition, a left subscript indicates the configuration with respect to which the quantity is measured.

The surface and body force components per unit mass at time $t+\Delta t$, but measured in configuration t, are ${}^{t+\Delta t}_t f_k$, ${}^{t+\Delta t}_t f_k$, k = 1,2,3.

Considering stresses, we denote the Cartesian components of the Cauchy stress tensor at time $t+\Delta t$ as ${}^{t+\Delta t}\tau_{ij}$ (since Cauchy stresses are always referred to the configuration in which they do occur ${}^{t+\Delta t}\tau_{ij} \equiv {}^{t+\Delta t}_{t+\Delta t}\tau_{ij}$), and the Cartesian components of the 2nd Piola - Kirchhoff stress tensor corresponding to the configuration at time $t+\Delta t$ but measured in configuration at time t by ${}^{t+\Delta t}_{t}S_{ij}$.

Considering strains, the Cartesian components of Cauchy's infintesimal strain tensor referred to the configuration at time $t+\Delta t$ are denoted by ${}_{t+\Delta t}e_{ij}$; and the Cartesian components of the Green - Lagrange strain tensor using the displacements from the configuration at time t to the configuration at time $t+\Delta t$ referred to the configuration at time t are denoted by ${}^{t+\Delta t}_{t}\epsilon_{ij}$.

The reference configurations, which will be used for applied forces, Kirchhoff - Piola stresses and Green - Lagrange strains are those at time 0 and at time t.

In the formulation of the governing equilibrium equations we need to consider derivatives of displacements and coordinates. In the notation adopted, a comma denotes differentiation with respect to the coordinate following, and the left time subscripts indicate the configuration in which this coordinate is measured; thus we have, for example,

$$ {}^{t+\Delta t}_{0}u_{i,j} = \frac{\partial^{t+\Delta t}u_i}{\partial^{0}x_j} $$

and

$$ {}^{0}_{t+\Delta t}x_{m,n} = \frac{\partial^{0}x_m}{\partial^{t+\Delta t}x_n} $$

Principle of Virtual Displacements

With the notation having been explained briefly, we now consider again the body in Fig. 1.1. Since the solution is known at all discrete time points 0, Δt, $2\Delta t$, ..., t, the basic aim of the formulation is to establish an equation of virtual work from which the unknown static and kinematic variables in the configuration at time $t+\Delta t$ can be solved. Since the isoparametric displacement based finite element procedure shall be employed for numerical solution, we use the principle of virtual displacements to express the equilibrium of the body in the configuration at time $t+\Delta t$. Assuming that the direction and magnitude of the body and surface loading is independent of the configuration, i.e., conservative loading only is considered, the principle of virtual displacements requires that

$$\int_{t+\Delta t_V} {}^{t+\Delta t}\tau_{ij}\ \delta\,{}_{t+\Delta t}e_{ij}\ {}^{t+\Delta t}dv = {}^{t+\Delta t}\mathcal{R} \tag{2.1}$$

where ${}^{t+\Delta t}\mathcal{R}$ is the external virtual work expression,

$${}^{t+\Delta t}\mathcal{R} = \int_{{}^0A} {}_0^{t+\Delta t}t_k\ \delta u_k\ {}^0da + \int_{{}^0V} {}^0\rho\ {}_0^{t+\Delta t}f_k\ \delta u_k\ {}^0dv \tag{2.2}$$

In Eqs. (2.1) and (2.2) δu_k is a (virtual) variation in the current displacement components ${}^{t+\Delta t}u_k$, and $\delta\,{}_{t+\Delta t}e_{ij}$ are the corresponding (virtual) variations in strains, i.e.,

$$\delta\,{}_{t+\Delta t}e_{ij} = \delta\,\tfrac{1}{2}\left({}_{t+\Delta t}u_{i,j} + {}_{t+\Delta t}u_{j,i}\right) \tag{2.3}$$

We should note that in Eq. (2.1) and the equations to follow the summation convention of tensor notation is implied.

Equation (2.1) cannot be solved directly since the configuration at time $t+\Delta t$ is unknown. An approximate solution can be obtained by

referring all variables to a known previously calculated equilibrium configuration. This solution can, in general, be improved by iteration (see Chapter 5).

For the purpose of obtaining a first approximate solution, in principle, any one of the already calculated equilibrium configurations could be used. In practice, however, the choice lies essentially between two formulations which have been termed total Lagrangian (T.L.) formulation and updated Lagrangian (U.L.) formulation during the course of this work [4] [5]. The T.L. formulation has generally been referred to as Lagrangian formulation [4] [13] [18] [27] [40] [48]. In this solution scheme all static and kinematic variables are referred to the initial configuration at time 0. The U.L. formulation is based on the same procedures that are used in the T.L. formulation, but in the solution all static and kinematic variables are referred to the configuration at time t [4] [5] [50]. The application of both formulations in the analysis of linear and nonlinear elastic materials was presented in [4], where it was shown, in particular, that both the T.L. and U.L. formulations include all nonlinear effects due to large displacements, large strains and material nonlinearities. The only advantage of using one formulation rather than the other is its better numerical efficiency, which largely depends on the definition of the material law.

The first step in both formulations is to obtain an approximate solution to Eq. (2.1) by linearizing the equation about the last calculated equilibrium configuration at time t. This approximate solution can then be improved by equilibrium iteration until Eq. (2.1) is satisfied to a required tolerance. In Chapter 6 specific emphasis is directed to the importance of equilibrium iteration in some dynamic analyses.

Using the notation outlined above, in the T.L. formulation, Eq. (2.1) is transformed to [30]

$$\int_{{}^0V} {}_0^{t+\Delta t}S_{ij} \; \delta\, {}_0^{t+\Delta t}\varepsilon_{ij} \; {}^0dv = {}^{t+\Delta t}\mathcal{R} \tag{2.4}$$

Similarly, in the U.L. formulation Eq. (2.1) becomes

$$\int_{{}^tV} {}_t^{t+\Delta t}S_{ij} \; \delta\, {}_t^{t+\Delta t}\varepsilon_{ij} \; {}^tdv = {}^{t+\Delta t}\mathcal{R} \tag{2.5}$$

As pointed out above, an approximate solution to Eqs. (2.4) or (2.5) is obtained by linearizing the equation. Tables 1 and 2 summarize the relations used to arrive at the linearized equations of motion in the T.L. and the U.L. formulations. As shown in the tables, the linearized equilibrium equations are in the T.L. formulation

$$\int_{{}^0V} {}_0C_{ijrs} \; {}_0e_{rs} \; \delta\, {}_0e_{ij} \; {}^0dv + \int_{{}^0V} {}_0^tS_{ij} \; \delta\, {}_0\eta_{ij} \; {}^0dv$$

$$= {}^{t+\Delta t}\mathcal{R} - \int_{{}^0V} {}_0^tS_{ij} \; \delta\, {}_0e_{ij} \; {}^0dv \tag{2.6}$$

and in the U.L. formulation

$$\int_{{}^tV} {}_tC_{ijrs} \; {}_te_{rs} \; \delta\, {}_te_{ij} \; {}^tdv + \int_{{}^tV} {}_t\tau_{ij} \; \delta\, {}_t\eta_{ij} \; {}^tdv$$

$$= {}^{t+\Delta t}\mathcal{R} - \int_{{}^tV} {}_t\tau_{ij} \; \delta\, {}_te_{ij} \; {}^tdv \tag{2.7}$$

where ${}_0C_{ijrs}$ and ${}_tC_{ijrs}$ are the incremental material property tensors in

TABLE 1 TOTAL LAGRANGIAN FORMULATION

1. Equations of Motion

$$\int_{{}^0V} {}^{t+\Delta t}_{\ 0}S_{ij}\ \delta\,{}^{t+\Delta t}_{\ 0}\epsilon_{ij}\ {}^0dv = {}^{t+\Delta t}R$$

where

$${}^{t+\Delta t}_{\ 0}S_{ij} = \frac{{}^0\rho}{{}^{t+\Delta t}\rho}\ {}^0x_{i,s}\ {}^{t+\Delta t}\tau_{sr}\ {}^0x_{j,r} \quad ; \quad \delta\,{}^{t+\Delta t}_{\ 0}\epsilon_{ij} = \delta\,\tfrac{1}{2}\left({}^{t+\Delta t}_{\ 0}u_{i,j} + {}^{t+\Delta t}_{\ 0}u_{j,i} + {}^{t+\Delta t}_{\ 0}u_{k,i}\ {}^{t+\Delta t}_{\ 0}u_{k,j}\right)$$

2. Incremental Decompositions

a. stresses

$${}^{t+\Delta t}_{\ 0}S_{ij} = {}^t_0S_{ij} + {}^0S_{ij}$$

b. strains

$${}^{t+\Delta t}_{\ 0}\epsilon_{ij} = {}^t_0\epsilon_{ij} + {}^0\epsilon_{ij} \quad ; \quad {}^0\epsilon_{ij} = {}^0e_{ij} + {}^0\eta_{ij}$$

$${}^0e_{ij} = \tfrac{1}{2}\left({}^0u_{i,j} + {}^0u_{j,i} + {}^t_0u_{k,i}\ {}^0u_{k,j} + {}^0u_{k,i}\ {}^t_0u_{k,j}\right) \quad ; \quad {}^0\eta_{ij} = \tfrac{1}{2}{}^0u_{k,i}\ {}^0u_{k,j}$$

TABLE 1 (cont'd.)

3. Equations of Motion with Incremental Decompositions

Noting that $\delta\,{}^{t+\Delta t}_{0}\epsilon_{ij} = \delta_0\epsilon_{ij}$ and ${}_0S_{ij} = {}_0C_{ijrs}\,{}_0\epsilon_{rs}$

the equations of motion are

$$\int_{{}^0V} {}_0C_{ijrs}\;{}_0\epsilon_{rs}\;\delta_0\epsilon_{ij}\;{}^0dv + \int_{{}^0V} {}^t_0S_{ij}\;\delta_0\eta_{ij}\;{}^0dv = {}^{t+\Delta t}\mathcal{R} - \int_{{}^0V} {}^t_0S_{ij}\;\delta_0e_{ij}\;{}^0dv$$

4. Linearization of Equations of Motion

Using the approximations ${}_0S_{ij} = {}_0C_{ijrs}\;{}_0e_{ij}$, $\delta\,{}_0\epsilon_{ij} = \delta_0e_{ij}$

we obtain as approximate equations of motion

$$\int_{{}^0V} {}_0C_{ijrs}\;{}_0e_{rs}\;\delta_0e_{ij}\;{}^0dv + \int_{{}^0V} {}^t_0S_{ij}\;\delta_0\eta_{ij}\;{}^0dv = {}^{t+\Delta t}\mathcal{R} - \int_{{}^0V} {}^t_0S_{ij}\;\delta_0e_{ij}\;{}^0dv$$

TABLE 2 UPDATED LAGRANGIAN FORMULATION

1. Equations of Motion

$$\int_{{}^{t}V} {}^{t+\Delta t}_{t}S_{ij}\, \delta\, {}^{t+\Delta t}_{t}\epsilon_{ij}\, {}^{t}dv = {}^{t+\Delta t}R$$

where

$${}^{t+\Delta t}_{t}S_{ij} = \frac{{}^{t}\rho}{{}^{t+\Delta t}\rho}\, {}^{t}_{t+\Delta t}x_{i,s}\, {}^{t+\Delta t}\tau_{sr}\, {}^{t}_{t+\Delta t}x_{j,r} \quad ; \quad \delta\, {}^{t+\Delta t}_{t}\epsilon_{ij} = \delta\, \tfrac{1}{2}\left({}^{t}u_{i,j} + {}^{t}u_{j,i} + {}^{t}u_{k,i}\, {}^{t}u_{k,j} \right)$$

2. Incremental Decompositions

a. stresses

$${}^{t+\Delta t}_{t}S_{ij} = {}^{t}\tau_{ij} + {}^{t}S_{ij}$$

b. strains

$${}^{t+\Delta t}_{t}\epsilon_{ij} = {}^{t}\epsilon_{ij} \quad ; \quad {}^{t}\epsilon_{ij} = {}^{t}e_{ij} + {}^{t}\eta_{ij}$$

$${}^{t}e_{ij} = \tfrac{1}{2}\left({}^{t}u_{i,j} + {}^{t}u_{j,i} \right) \quad ; \quad {}^{t}\eta_{ij} = \tfrac{1}{2}\, {}^{t}u_{k,i}\, {}^{t}u_{k,j}$$

TABLE 2 (cont'd.)

3. Equations of Motion with Incremental Decompositions

Noting that ${}_t^tS_{ij} = {}_t^tC_{ijrs}\ {}_t^t\epsilon_{rs}$ the equations of motion are

$$\int_{{}^tV} {}_t^tC_{ijrs}\ {}_t^t\epsilon_{rs}\ \delta\,{}_t\epsilon_{ij}\ {}^tdv + \int_{{}^tV} {}^t\tau_{ij}\ \delta\,{}_t\eta_{ij}\ {}^tdv = {}^{t+\Delta t}\mathcal{R} - \int_{{}^tV} {}^t\tau_{ij}\ \delta\,{}_te_{ij}\ {}^tdv$$

4. Linearization of Equations of Motion

Using the approximations ${}_t^tS_{ij} = {}_t^tC_{ijrs}\ {}_t^te_{ij}$, $\delta\,{}_t\epsilon_{ij} = \delta\ {}_t^te_{ij}$

we obtain as approximate equations of motion

$$\int_{{}^tV} {}_t^tC_{ijrs}\ {}_t^te_{rs}\ \delta\,{}_te_{ij}\ {}^tdv + \int_{{}^tV} {}^t\tau_{ij}\ \delta\,{}_t\eta_{ij}\ {}^tdv = {}^{t+\Delta t}\mathcal{R} - \int_{{}^tV} {}^t\tau_{ij}\ \delta\,{}_te_{ij}\ {}^tdv$$

the configuration at time t, and referred to the configuration at times 0 and t, respectively. The derivation of ${}_0C_{ijrs}$ and ${}_tC_{ijrs}$ for the material models in NONSAP is presented in Chapter 4. We should note that in Eqs. (2.6) and (2.7) ${}^t_0S_{ij}$ and ${}^t\tau_{ij}$ are given 2nd Piola - Kirchhoff and Cauchy stresses acting in the configuration at time t; and ${}_0e_{ij}$, ${}_0\eta_{ij}$ and ${}_te_{ij}$, ${}_t\eta_{ij}$ are the linear and nonlinear incremental strains referred to the configurations at times 0 and t, respectively.

Comparing the U.L. and T.L. formulations in Tables 1 and 2, we observe that they are quite analogous and that, in fact, the only theoretical difference between the two formulations lies in the choice of different reference configurations for kinematic and static variables. Indeed, if in the numerical solution the appropriate constitutive tensors are used, identical results are obtained (see Chapter 4). Although not indicated in Table 2, we should also note that in the T.L. formulation, Cauchy stresses need be calculated from 2nd Piola - Kirchhoff stresses whenever program output is required.

The choice between the U.L. and T.L. formulations depends, in practice, on their relative numerical effectiveness, which can be evaluated once the finite element solutions of Eqs. (2.6) and (2.7) have been presented.

The T.L. and U.L. formulations in Tables 1 and 2 include all nonlinear effects due to large displacements, large strains and material nonlinearities; however, in practice, it is often sufficient to account for nonlinear material effects only. In this case, the nonlinear strain components and the displacements at time t are neglected in the formulations. Therefore, Eqs. (2.6) and (2.7) reduce to the same equations of

motion, namely

$$\int_{{}^0V} C_{ijrs}\ e_{rs}\ \delta e_{ij}\ {}^0dv = {}^{t+\Delta t}\mathcal{R} - \int_{{}^0V} {}^t\sigma_{ij}\ \delta e_{ij}\ {}^0dv \qquad (2.8)$$

where ${}^t\sigma_{ij}$ is the actual physical stress at time t referred to unit area in the original configuration, which is also the configuration at time t (hence ${}^t\sigma_{ij} \equiv {}^t\tau_{ij} \equiv {}^t_0S_{ij}$). The increment in stress σ_{ij} is obtained from the increment in infinitesimal strains e_{ij}, i.e.,

$$\sigma_{ij} = C_{ijrs}\ e_{rs} \quad ; \quad e_{ij} = \tfrac{1}{2}\left({}^0u_{i,j} + {}^0u_{j,i}\right) \qquad (2.9)$$

It should be noted that in order to distinguish the strain increments in Eqs. (2.8) and (2.9) from the linear strain increments in the T.L. and U.L. formulations, we do not use a left subscript, since the configuration at time 0 corresponds also to the configurations at times Δt, $2\Delta t$, ..., t, ... For the same reason, a left subscript is also not used on the stresses ${}^t\sigma_{ij}$, σ_{ij} and on the material tensor C_{ijrs}.

From the incremental equilibrium equations, Eq. (2.8), we may derive the conventional equations of motion used in linear elastic, infinitesimal displacement analysis. In this case we have

$${}^t\sigma_{ij} = C_{ijrs}\ {}^te_{rs} \qquad (2.10)$$

where C_{ijrs} is now a constant material tensor relating total (or incremental) stresses to total (or incremental) strains, and ${}^te_{rs}$ is the total infinitesimal strain at time t,

$${}^te_{rs} = \tfrac{1}{2}\left({}^t_0u_{r,s} + {}^t_0u_{s,r}\right) \qquad (2.11)$$

Substituting for ${}^{t}\sigma_{ij}$ from Eq. (2.10) into Eq. (2.8) we obtain the equations of motion used in linear elastic infinitesimal strain analysis

$$\int_{{}^{0}V} C_{ijrs}\, {}^{t+\Delta t}e_{rs}\, \delta e_{ij} = {}^{t+\Delta t}R \tag{2.12}$$

where ${}^{t+\Delta t}e_{rs}$ is the total infinitesimal strain at time $t+\Delta t$,

$${}^{t+\Delta t}e_{rs} = \tfrac{1}{2}\left({}^{t+\Delta t}_{0}u_{r,s} + {}^{t+\Delta t}_{0}u_{s,r}\right) \tag{2.13}$$

In program NONSAP, options exist to use for a finite element the U.L. or T.L. formulations, to allow for material nonlinearity only by using Eq. (2.8), or to perform a conventional linear elastic small displacement analysis. The advantage of being able to use these four types of descriptions for a finite element allows effective nonlinear analysis. Namely, it is thus possible to study first the linear response of the element assemblage, after which varying degrees of nonlinearities may be assigned to specific parts of the structure. This enables the analyst to assess the influence of material nonlinearities only, geometric nonlinearities only, and both types of nonlinearities together. The separate influence of material and geometric nonlinearities on the response of some systems is studied in Chapter 6.

3. FINITE ELEMENT DISCRETIZATION

The objective is to perform static and dynamic analysis, where in dynamic analysis the applied body forces include inertia forces. Assuming that the mass of the body is preserved, the inertia forces are conservative and can in both the T.L. and U.L. formulations be evaluated using $\int_{{}^0V} {}^0\rho \; {}^{t+\Delta t}\ddot{u}_k \; \delta u_k \; {}^0dv$. Corresponding to Eqs. (2.12), (2.8), (2.6) and (2.7), respectively, we now have the following equations of motion to be solved by finite element discretization;

in linear analysis

$$\int_{{}^0V} {}^0\rho \; {}^{t+\Delta t}\ddot{u}_k \; \delta u_k \; {}^0dv + \int_{{}^0V} C_{ijrs} \; {}^{t+\Delta t}e_{rs} \; \delta e_{ij} \; {}^0dv = {}^{t+\Delta t}\mathcal{R} \tag{3.1}$$

in nonlinear analysis, including nonlinear material effects only

$$\int_{{}^0V} {}^0\rho \; {}^{t+\Delta t}\ddot{u}_k \; \delta u_k \; {}^0dv + \int_{{}^0V} C_{ijrs} \; e_{rs} \; \delta e_{ij} \; {}^0dv = {}^{t+\Delta t}\mathcal{R} - \int_{{}^0V} {}^t\sigma_{ij} \; \delta e_{ij} \; {}^0dv \tag{3.2}$$

using the T.L. formulation

$$\int_{{}^0V} {}^0\rho \; {}^{t+\Delta t}\ddot{u}_k \; \delta u_k \; {}^0dv + \int_{{}^0V} {}^0C_{ijrs} \; {}^0e_{rs} \; \delta {}^0e_{ij} \; {}^0dv$$

$$+ \int_{{}^0V} {}^t_0S_{ij} \; \delta {}^0\eta_{ij} \; {}^0dv = {}^{t+\Delta t}R - \int_{{}^0V} {}^t_0S_{ij} \; \delta {}^0e_{ij} \; {}^0dv \qquad (3.3)$$

using the U.L. formulation

$$\int_{{}^0V} {}^0\rho \; {}^{t+\Delta t}\ddot{u}_k \; \delta u_k \; {}^0dv + \int_{{}^tV} {}^tC_{ijrs} \; {}^te_{rs} \; \delta {}^te_{ij} \; {}^tdv$$

$$+ \int_{{}^tV} {}^t\tau_{ij} \; \delta {}^t\eta_{ij} \; {}^tdv = {}^{t+\Delta t}R - \int_{{}^tV} {}^t\tau_{ij} \; \delta {}^te_{ij} \; {}^tdv \qquad (3.4)$$

where the definition for ${}^{t+\Delta t}R$ is still given in Eq. (2.2), but it need be noted that the body forces no longer include inertia forces.

In program NONSAP, isoparametric finite element discretization is used. The element library includes a one-dimensional truss element, 3 to 8 variable-number-nodes two-dimensional plane stress, plane strain and axisymmetric elements and 8 to 21 variable-number-nodes three-dimensional elements. Referring to the standard procedures for assembling the structure matrices, in the derivation of the required finite element matrices, attention need only be given to the calculation of the matrices corresponding to a single element [40] [53].

In the isoparametric finite element solution the coordinates and displacements of an element are interpolated using

$$ {}^{0}x_j = \sum_{k=1}^{N} h_k \, {}^{0}x_j^k \quad ; \quad {}^{t}x_j = \sum_{k=1}^{N} h_k \, {}^{t}x_j^k \qquad j = 1,2,3 $$

$$ {}^{t+\Delta t}x_j = \sum_{k=1}^{N} h_k \, {}^{t+\Delta t}x_j^k \qquad (3.5) $$

$$ {}^{t}u_j = \sum_{k=1}^{N} h_k \, {}^{t}u_j^k \quad ; \quad u_j = \sum_{k=1}^{N} h_k \, u_j^k \qquad j = 1,2,3 \qquad (3.6) $$

where ${}^{t}x_j^k$ is the coordinate of nodal point k corresponding to direction j at time t, ${}^{t}u_j^k$ is defined similarly to ${}^{t}x_j^k$, h_k is the interpolation function corresponding to nodal point k, and N is the number of nodal points of the elements [53]. We should note that the coordinates, displacements and displacement increments of an element are interpolated by the same functions h_k at any time of the solution.

Using the relations in Eqs. (3.5) and (3.6) for the evaluation of the integrals in Eqs. (3.1) to (3.4), the following matrix equations are obtained,

in linear analysis

$$ M \, {}^{t+\Delta t}\ddot{u} + K \, {}^{t+\Delta t}u = {}^{t+\Delta t}R \qquad (3.7) $$

in nonlinear analysis, including nonlinear material effects only

$$ M \, {}^{t+\Delta t}\ddot{u} + {}^{t}K \, u = {}^{t+\Delta t}R - {}^{t}F \qquad (3.8) $$

using the T.L. formulation

$$ M \, {}^{t+\Delta t}\ddot{u} + \left({}^{t}_{0}K_L + {}^{t}_{0}K_{NL} \right) u = {}^{t+\Delta t}R - {}^{t}_{0}F \qquad (3.9) $$

using the U.L. formulation

$$ M \, {}^{t+\Delta t}\ddot{u} + \left({}^{t}_{t}K_L + {}^{t}_{t}K_{NL} \right) u = {}^{t+\Delta t}R - {}^{t}_{t}F \qquad (3.10) $$

where

M = time independent mass matrix; in NONSAP a lumped mass matrix M_ℓ and a consistent mass matrix M_c can be used.

K = time independent linear elastic, small displacement stiffness matrix

${}_0^tK_L$, ${}_t^tK_L$ = linear strain incremental stiffness matrices

${}_0^tK_{NL}$, ${}_t^tK_{NL}$ = nonlinear strain (geometric or initial stress) incremental stiffness matrices

${}^tK$ = linear strain incremental stiffness matrix, not including the initial displacement effect

${}^{t+\Delta t}R$ = vectors of externally applied element nodal loads

${}_0^tF$, ${}_t^tF$ = vectors of nodal point forces equivalent to the element stresses at time t

${}^tF$ = vector of nodal point forces equivalent to the element stresses at time t, not including the initial displacement effect

u = vector of incremental nodal displacements, assembled from u_j^k

${}^{t+\Delta t}u$ = vector of total nodal displacements at time $t+\Delta t$, assembled from ${}^{t+\Delta t}u_j^k$

${}^{t+\Delta t}\ddot{u}$ = vector of nodal point accelerations

Table 3 summarizes the various integrals considered and the corresponding matrix evaluations. The following notation is used for the calculation of the element matrices.

H_S , H = surface- and volume-displacement transformation matrices

${}^{t+\Delta t}_{0}t$, ${}^{t+\Delta t}_{0}f$ = vectors of surface and body forces defined per unit area and per unit mass of the body at time 0

B_L , ${}^{t}_{0}B_L$, ${}^{t}_{t}B_L$ = linear strain-displacement transformation matrices

${}^{t}_{0}B_{NL}$, ${}^{t}_{t}B_{NL}$ = nonlinear strain-displacement transformation matrices

C = stress-strain material property matrix (incremental or total)

${}_{0}C$, ${}_{t}C$ = incremental stress-strain material property matrices

${}^{t}_{\tau}$, ${}^{t}\hat{}_{\tau}$ = matrix and vector of Cauchy stresses

${}^{t}_{0}S$, ${}^{t}_{0}\hat{S}$ = matrix and vector of 2nd Piola - Kirchhoff stresses

${}^{t}\hat{}_{\Sigma}$ = vector of stresses in materially nonlinear only analysis

The above matrices used in Table 3 depend on the specific element considered. In the following sections, we establish the displacement and strain-displacement transformation matrices, the element stress matrices and vectors. The evaluation of the material property matrices depends on the material model used and is considered in Chapter 4.

TABLE 3 FINITE ELEMENT MATRICES

ANALYSIS TYPE	INTEGRAL	MATRIX EVALUATION
IN ALL ANALYSES	$\int_{{}^0V} {}^0\rho \; {}^{t+\Delta t}\ddot{u}_k \; \delta u_k \; {}^0dv$	$M \; {}^{t+\Delta t}\ddot{u} = {}^0\rho \left(\int_{{}^0V} H^T \; H \; {}^0dv \right) \; {}^{t+\Delta t}\ddot{u}$
	${}^{t+\Delta t}R = \int_{{}^0A} {}^{t+\Delta t}_{\;\;0}t_k \; \delta u_k \; {}^0da$	${}^{t+\Delta t}R = \int_{{}^0A} H_S^T \; {}^{t+\Delta t}_{\;\;0}t \; {}^0da$
	$+ \int_{{}^0V} {}^0\rho \; {}^{t+\Delta t}_{\;\;0}f_k \; \delta u_k \; {}^0dv$	$+ {}^0\rho \int_{{}^0V} H^T \; {}^{t+\Delta t}_{\;\;0}f \; {}^0dv$
A. LINEAR ANALYSIS	$\int_{{}^0V} C_{ijrs} \; {}^{t+\Delta t}e_{rs} \; \delta e_{ij} \; {}^0dv$	$K \; {}^{t+\Delta t}u = \left(\int_{{}^0V} B_L^T \; C \; B_L \; {}^0dv \right) \; {}^{t+\Delta t}u$

TABLE 3 (cont'd.)

ANALYSIS TYPE	INTEGRAL	MATRIX EVALUATION
B. MATERIAL NONLINEARITY ONLY	$\int_{0_V} C_{ijrs}\ e_{rs}\ \delta e_{ij}\ {}^0dv$	${}^tK\ u = \left(\int_{0_V} B_L^T\ C\ B_L\ {}^0dv\right) u$
	$\int_{0_V} {}^t\sigma_{ij}\ \delta e_{ij}\ {}^0dv$	${}^tF = \int_{0_V} B_L^T\ {}^t\hat{\Sigma}\ {}^0dv$
C. TOTAL LAGRANGIAN FORMULATION	$\int_{0_V} {}^0C_{ijrs}\ {}^0e_{rs}\ \delta\,{}^0e_{ij}\ {}^0dv$	${}^t_0K_L\ u = \left(\int_{0_V} {}^t_0B_L^T\ {}^0C\ {}^t_0B_L\ {}^0dv\right) u$
	$\int_{0_V} {}^t_0S_{ij}\ \delta\,{}_0\eta_{ij}\ {}^0dv$	${}^t_0K_{NL}\ u = \left(\int_{0_V} {}^t_0B_{NL}^T\ {}^tS\ {}^t_0B_{NL}\ {}^0dv\right) u$
	$\int_{0_V} {}^t_0S_{ij}\ \delta\,{}^0e_{ij}\ {}^0dv$	${}^t_0F = \int_{0_V} {}^t_0B_L^T\ {}^t\hat{S}\ {}^0dv$

TABLE 3 (cont'd.)

ANALYSIS TYPE	INTEGRAL	MATRIX EVALUATION
D. UPDATED LAGRANGIAN FORMULATION	$\int_{t_V} {}_t C_{ijrs} \; {}^t e_{rs} \; \delta {}^t e_{ij} \; {}^t dv$	${}^t_t K_L \; u = \left(\int_{t_V} {}^t_t B_L^T \; {}^t C \; {}^t_t B_L \; {}^t dv \right) u$
	$\int_{t_V} {}^t \tau_{ij} \; \delta {}_t \eta_{ij} \; {}^t dv$	${}^t_t K_{NL} \; u = \left(\int_{t_V} {}^t_t B_{NL}^T \; {}^t \tau \; {}^t_t B_{NL} \; {}^t dv \right) u$
	$\int_{t_V} {}^t \tau_{ij} \; \delta {}^t e_{ij} \; {}^t dv$	${}^t_t F = \int_{t_V} {}^t_t B_L^T \; {}^t \hat{\tau} \; {}^t dv$

3.1 Truss Element

A truss element is a two node member capable of transmitting axial force only. The member may have an arbitrary orientation in the global Cartesian coordinate system as shown in Fig. 3.1

For the truss element the following formulations have been incorporated into NONSAP:

1. Linear elastic, small displacement analysis, i.e. (A) in Table 3.
2. Small displacement analysis with material nonlinearities only, i.e., (B) in Table 3.
3. Updated Lagrangian formulation, i.e. (D) in Table 3, but assuming small strains (with large displacements).

The reason for incorporating only the U.L. formulation and not the T.L. formulation lies in the better numerical efficiency of the U.L. solution. The U.L. formulation is practically always more effective, since no initial displacement transformation matrix need be included (see Section 3.2).

The small strain assumption is believed to be appropriate for truss elements, since the material models considered are only defined for small strains. Therefore, small strains are assumed in the calculation of stresses and in neglecting changes in the cross sectional areas of the truss elements during deformation.

In the following section we derive the mass matrices and the stiffness and stress matrices corresponding to the U.L. formulation. Considering geometrically linear analyses, the nonlinear strain incremental stiffness matrix ${}^{t}_{t}K_{NL}$ is not included and all matrices are evaluated using the initial geometry of the element (see Table 3).

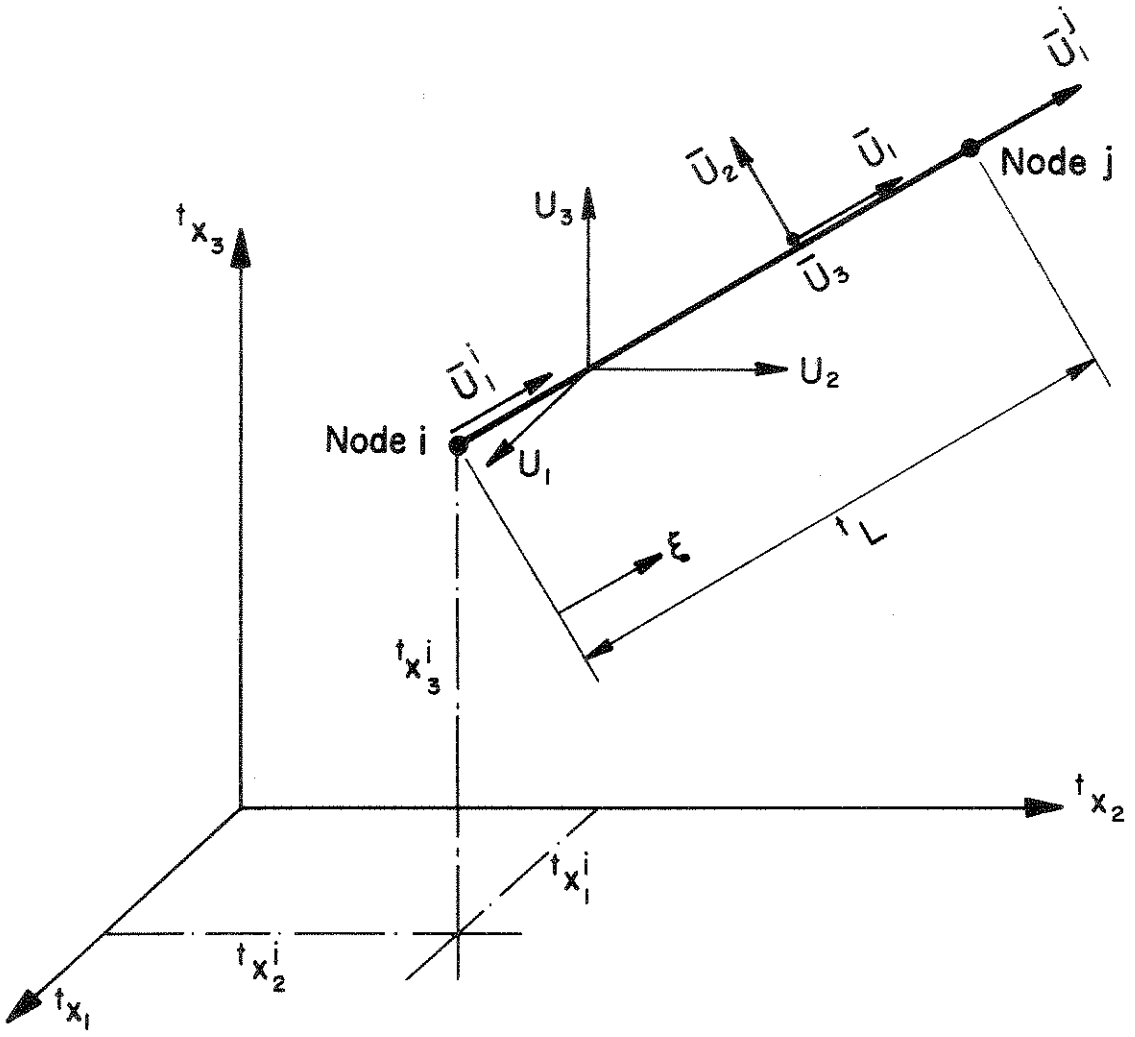

FIGURE 3.1 THREE-DIMENSIONAL TRUSS IN CONFIGURATION AT TIME t

Stiffness Matrix

Referring to Eq. (3.10) the complete incremental element stiffness matrix is the sum of the linear strain stiffness matrix ${}^{t}_{t}K_{L}$ and nonlinear strain stiffness matrix ${}^{t}_{t}K_{NL}$.

In global coordinates the element linear strain stiffness matrix is

$$ {}^{t}_{t}K_{L} = \int_{{}^{t}V} {}^{t}_{t}B_{L}^{T} \; {}^{t}C \; {}^{t}_{t}B_{L} \; {}^{t}dv \qquad (3.11) $$

and, as shown in Table 3, is the result of evaluating the term $\int_{{}^{t}V} {}^{t}C_{ijrs} \; {}^{t}e_{rs} \; \delta {}^{t}e_{ij} \; {}^{t}dv$. However, since the truss transmits axial force only along the direction from node i to node j of the element, it is expedient to calculate first a linear strain stiffness matrix ${}^{t}_{t}k_{L}$ corresponding to the local displacement increments $\bar{u}_{1}^{i}$ and $\bar{u}_{1}^{j}$, Fig. 3.1, where

$$ {}^{t}_{t}k_{L} = \int_{{}^{t}V} {}^{t}_{t}b_{L}^{T} \; E \; {}^{t}_{t}b_{L} \; {}^{t}dv \qquad (3.12) $$

In Eq. (3.12) E is Young's modulus of the material in the configuration at time t, and ${}^{t}_{t}b_{L}$ is the linear strain-displacement matrix in local coordinates. Referring to Fig. 3.1 we have

$$ {}^{t}\bar{e}_{11} = {}^{t}_{t}b_{L} \; \bar{u} \qquad (3.13) $$

in which $\bar{u}$ is a vector containing the two axial node displacement increments measured relative to the configuration at time t, i.e.

$$\bar{u}^T = \begin{bmatrix} \bar{u}_1^i & \bar{u}_1^j \end{bmatrix} \tag{3.14}$$

Let ξ measure the distance along the truss element, positive from node i to node j, then the finite element displacement assumption for the axial displacement $\bar{u}_1(\xi)$ along the element is

$$\bar{u}_1(\xi) = \begin{bmatrix} (1-\xi/{}^tL) & (\xi/{}^tL) \end{bmatrix} \bar{u} \tag{3.15}$$

Since ${}_t\bar{e}_{11}(\xi) = d\left(\bar{u}_1(\xi)\right)/d\xi$ we have

$${}_t\bar{e}_{11}(\xi) = \begin{bmatrix} (-1/{}^tL) & (1/{}^tL) \end{bmatrix} \bar{u} \tag{3.16}$$

and we obtain

$${}^t_t b_L = \begin{bmatrix} (-1/{}^tL) & (1/{}^tL) \end{bmatrix} \tag{3.17}$$

where ${}^tL$ is the length of the element in the configuration at time t.

Substituting Eq. (3.17) into Eq. (3.12) we have

$${}^t_t k_L = \frac{AE}{{}^tL} \begin{bmatrix} 1 & -1 \\ -1 & 1 \end{bmatrix} \tag{3.18}$$

where A is the cross sectional area of the member assumed constant with length. Since we consider small strain conditions, A is the cross section of the element in the configuration at time 0. To calculate ${}^t_t K_L$ we relate the axial node displacement increments $\bar{u}_1^i$, $\bar{u}_1^j$ to the global Cartesian node displacement increments, u_k^i , u_k^j , k = 1,2,3, using

$$\bar{u} = N \; u \tag{3.19}$$

where

$$u^T = \begin{bmatrix} u_1^i & u_2^i & u_3^i & u_1^j & u_2^j & u_3^j \end{bmatrix} \tag{3.20}$$

$$N = \begin{bmatrix} \ell_1 & \ell_2 & \ell_3 & 0 & 0 & 0 \\ 0 & 0 & 0 & \ell_1 & \ell_2 & \ell_3 \end{bmatrix} \tag{3.21}$$

and the ℓ_n are the direction cosines of the element axis in the configuration at time t, i.e.,

$$\ell_n = \frac{{}^t x_n^j - {}^t x_n^i}{{}^t L} \tag{3.22}$$

As in Eq. (3.5), ${}^t x_n^j$ is the coordinate of nodal point j corresponding to direction n and at time t. Using Eq. (3.21) the local element stiffness ${}^t_t k_L$ is transformed to obtain

$${}^t_t K_L = N^T \; {}^t_t k_L \; N \tag{3.23}$$

Considering now the nonlinear strain stiffness matrix, it is given by

$${}^t_t K_{NL} = \int_{{}^t V} {}^t_t B_{NL}^T \; {}^t\tau \; {}^t_t B_{NL} \; {}^t dv \tag{3.24}$$

and, as shown in Table 3, results from the evaluation of $\int_{{}^t V} {}^t\tau_{ij} \; \delta \, {}^t\eta_{ij} \; {}^t dv$. For the truss element in local coordinates the only non-zero component of the Cauchy stress tensor is ${}^t\bar{\tau}_{11}$, i.e., the axial stress in the member at time t. Also, the corresponding quadratic portion of the total strain increment ${}^t\bar{\eta}_{ij}$ is for the element

$${}^t\bar{\eta}_{11} = \tfrac{1}{2} \; {}^t\bar{u}_{k,1} \; {}^t\bar{u}_{k,1} \tag{3.25}$$

which can be written using the global Cartesian components of displacements

$${}^t\bar{\eta}_{11} = \tfrac{1}{2} \left(\left(\frac{\partial u_1}{\partial \xi} \right)^2 + \left(\frac{\partial u_2}{\partial \xi} \right)^2 + \left(\frac{\partial u_3}{\partial \xi} \right)^2 \right) \tag{3.26}$$

Hence ${}^t\bar{\tau}_{11} \; \delta \, {}^t\bar{\eta}_{11}$ can be written in matrix form as

$$ {}^{t}\bar{\tau}_{11} \quad \delta\, {}_{t}\bar{\eta}_{11} = \delta \left\{ \frac{1}{2} \begin{bmatrix} u_{1,\xi} & u_{2,\xi} & u_{3,\xi} \end{bmatrix} \begin{bmatrix} {}^{t}\bar{\tau}_{11} & & \\ & {}^{t}\bar{\tau}_{11} & \\ & & {}^{t}\bar{\tau}_{11} \end{bmatrix} \begin{bmatrix} u_{1,\xi} \\ u_{2,\xi} \\ u_{3,\xi} \end{bmatrix} \right\} \tag{3.27} $$

where no variation is taken on ${}^{t}\bar{\tau}_{11}$. Since the displacement components of the truss are assumed to vary linearly with ξ we have

$$ \begin{bmatrix} u_{1,\xi} \\ u_{2,\xi} \\ u_{3,\xi} \end{bmatrix} = {}^{t}_{t}B_{NL} \; u \tag{3.28} $$

where

$$ {}^{t}_{t}B_{NL} = \frac{1}{{}^{t}L} \begin{bmatrix} -1 & 0 & 0 & 1 & 0 & 0 \\ 0 & -1 & 0 & 0 & 1 & 0 \\ 0 & 0 & -1 & 0 & 0 & 1 \end{bmatrix} \quad ; \quad u = \begin{bmatrix} u_1^{\,i} \\ u_2^{\,i} \\ u_3^{\,i} \\ u_1^{\,j} \\ u_2^{\,j} \\ u_3^{\,j} \end{bmatrix} \tag{3.29} $$

Substituting from Eq. (3.29) for ${}^{t}_{t}B_{NL}$ into Eq. (3.24) and using

$$ {}^{t}\tau = {}^{t}\bar{\tau}_{11} \; I_3 \tag{3.30} $$

where I_3 is the 3 x 3 identity matrix, we have

$$ {}^{t}_{t}K_{NL} = \frac{{}^{t}P}{{}^{t}L} \begin{bmatrix} I_3 & -I_3 \\ -I_3 & I_3 \end{bmatrix} \tag{3.31} $$

where ${}^{t}P$ is the axial force in the truss element at time t.

Mass Matrices

In NONSAP the lumped mass matrix M_ℓ or consistent mass matrix M_c can be used. Both matrices are evaluated in the configuration at time 0.

The lumped mass matrix is obtained by simply lumping half of the mass of the truss element at each of the element's two nodes,

$$ M_\ell = A \frac{{}^{0}\rho \, {}^{0}L}{2} I_6 \tag{3.32} $$

where ${}^{0}\rho$ are the material density and ${}^{0}L$ are the length of the truss at time 0; I_6 is the identity matrix of order 6.

The consistent mass matrix is calculated as shown in Table 3,

$$ M_c = {}^{0}\rho \int_{{}^{0}V} H^T H \, {}^{0}dv \tag{3.33} $$

where H is the matrix of displacement interpolation functions, i.e.

$$ H = \left[(1 - \xi/{}^{0}L) I_3 \quad (\xi/{}^{0}L) I_3 \right] \tag{3.34} $$

Substituting for H into Eq. (3.33) and using ${}^{0}dv = A \, d\xi$, we obtain

$$ M_c = A \frac{{}^{0}\rho \, {}^{0}L}{6} \begin{bmatrix} 2I_3 & I_3 \\ I_3 & 2I_3 \end{bmatrix} \tag{3.35} $$

Internal Resisting Force Vector

Referring to Table 3, the nodal force vector equivalent to the Cauchy stresses ${}^{t}\tau_{ij}$ is

$$ {}^{t}_{t}F_{e} = \int_{{}^{t}V} {}^{t}_{t}B_{L}^{T} \; {}^{t}\hat{\tau} \; {}^{t}dv \tag{3.36} $$

where ${}^{t}_{t}F_{e}$ is referred to the Cartesian coordinate system. For the truss element Eq. (3.36) can be written in local coordinates

$$ {}^{t}_{t}f_{e} = \int_{0}^{{}^{t}L} {}^{t}_{t}b_{L}^{T} \; {}^{t}\bar{\tau}_{11} \; A \; d\xi \tag{3.37} $$

Substituting from Eq. (3.17) for ${}^{t}_{t}b_{L}$ gives

$$ {}^{t}_{t}f_{e}^{T} = [\; -{}^{t}P \quad {}^{t}P \;] \tag{3.38} $$

To calculate ${}^{t}_{t}F_{e}$ we use the transformation in Eq. (3.19) from local to Cartesian displacement components, and obtain

$$ {}^{t}_{t}F_{e} = N^{T} \; {}^{t}_{t}f_{e} \tag{3.39} $$

3.2 Two-Dimensional Elements

The two-dimensional elements available in NONSAP are the axisymmetric, the plane stress and plane strain elements. Figure 3.2 shows typical structures that these elements would model.

For the two-dimensional elements the following formulations have been incorporated into NONSAP:

1. Linear elastic, small displacement analysis, i.e., (A) in Table 3.
2. Small displacement analysis with material nonlinearities only, i.e., (B) in Table 3.
3. Total Lagrangian formulation, i.e., (C) in Table 3.
4. Updated Lagrangian formulations, i.e., (D) in Table 3. For the analysis of elastic-plastic problems various constitutive assumptions have been implemented (see Section 4.4.4).

All formulations given in Table 3 have been incorporated into NONSAP for the two-dimensional elements, in order to be able to investigate the differences that arise from the various assumptions on the magnitude of the displacements and on the material behavior.

For the derivation of the required element matrices consider a typical two-dimensional element in its configuration at time 0 and at time t, as shown in Fig. 3.3. An isoparametric formulation of the element matrices is used, in which the element can have any number of nodes between 3 to 8. Figure 3.4 shows some typical element node configurations.

The global coordinates of the nodal points of the element in Fig. 3.3 are at time 0, ${}^0x_1^i$, ${}^0x_2^i$ and at time t, ${}^tx_1^i$, ${}^tx_2^i$, where i = 1, ...N, and N is the number of element nodes. A system of natural

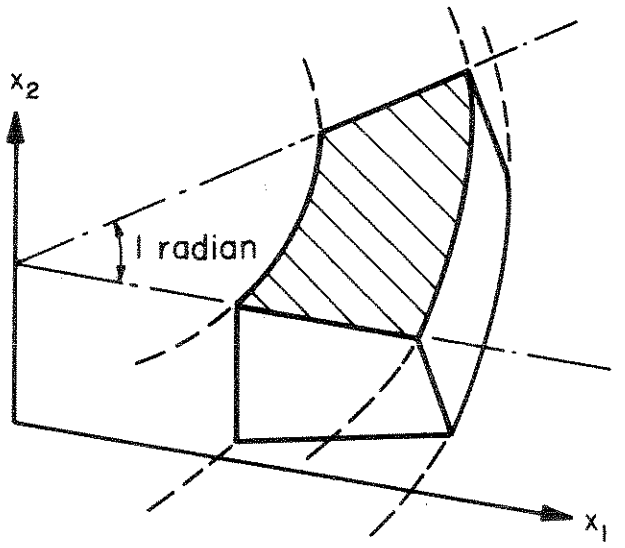

AXISYMMETRIC FINITE ELEMENT MODEL OF A RING

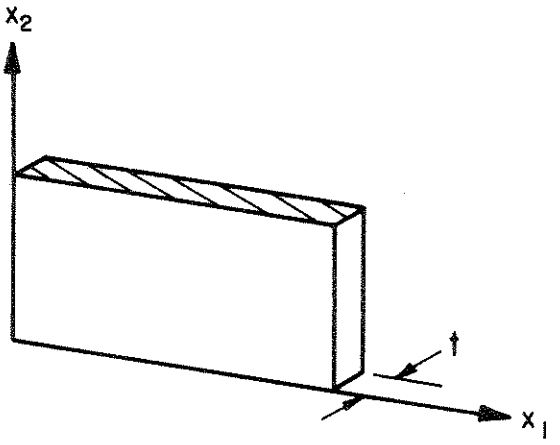

PLANE STRESS FINITE ELEMENT MODEL OF A CANTILEVER

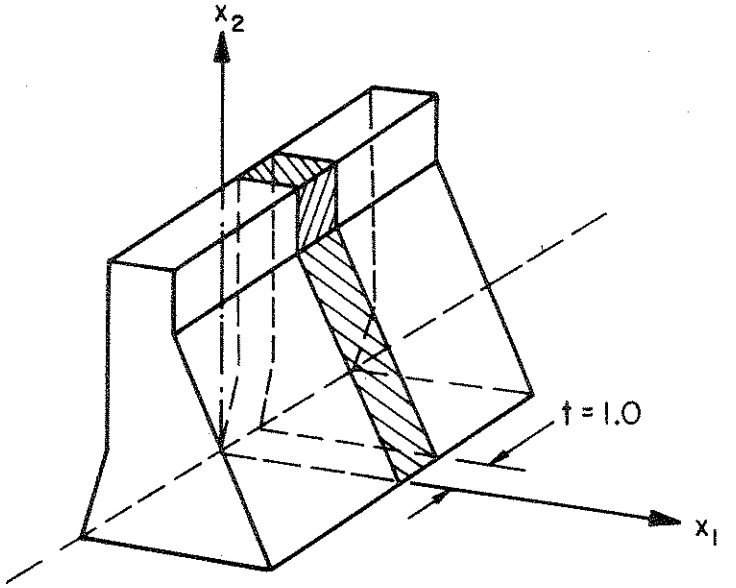

PLANE STRAIN FINITE ELEMENT MODEL OF A DAM

FIGURE 3.2 POSSIBLE TWO-DIMENSIONAL FINITE ELEMENT ANALYSES

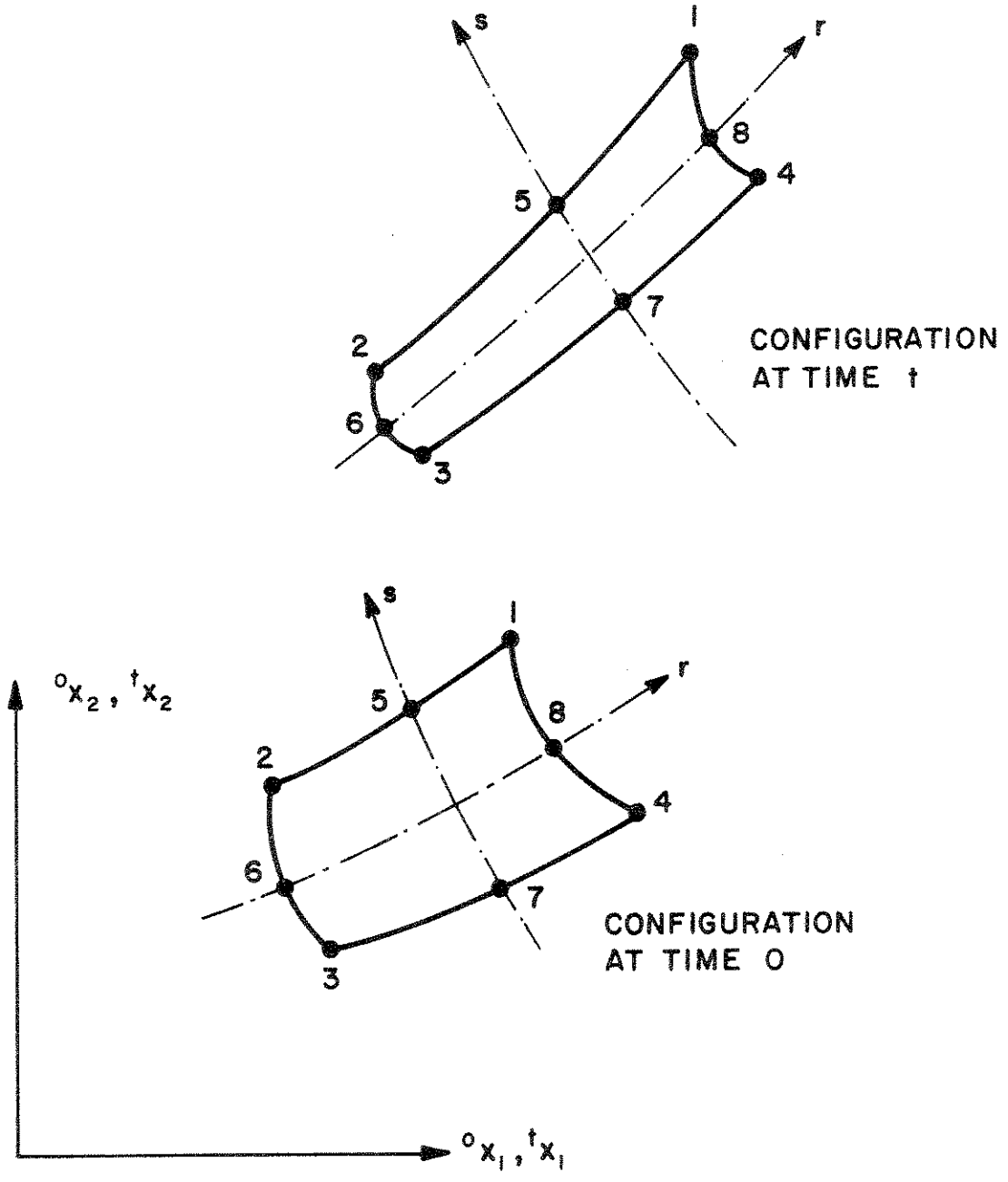

FIGURE 3.3 TWO-DIMENSIONAL ELEMENT SHOWN IN THE GLOBAL $^{t}x_1$-$^{t}x_2$ PLANE

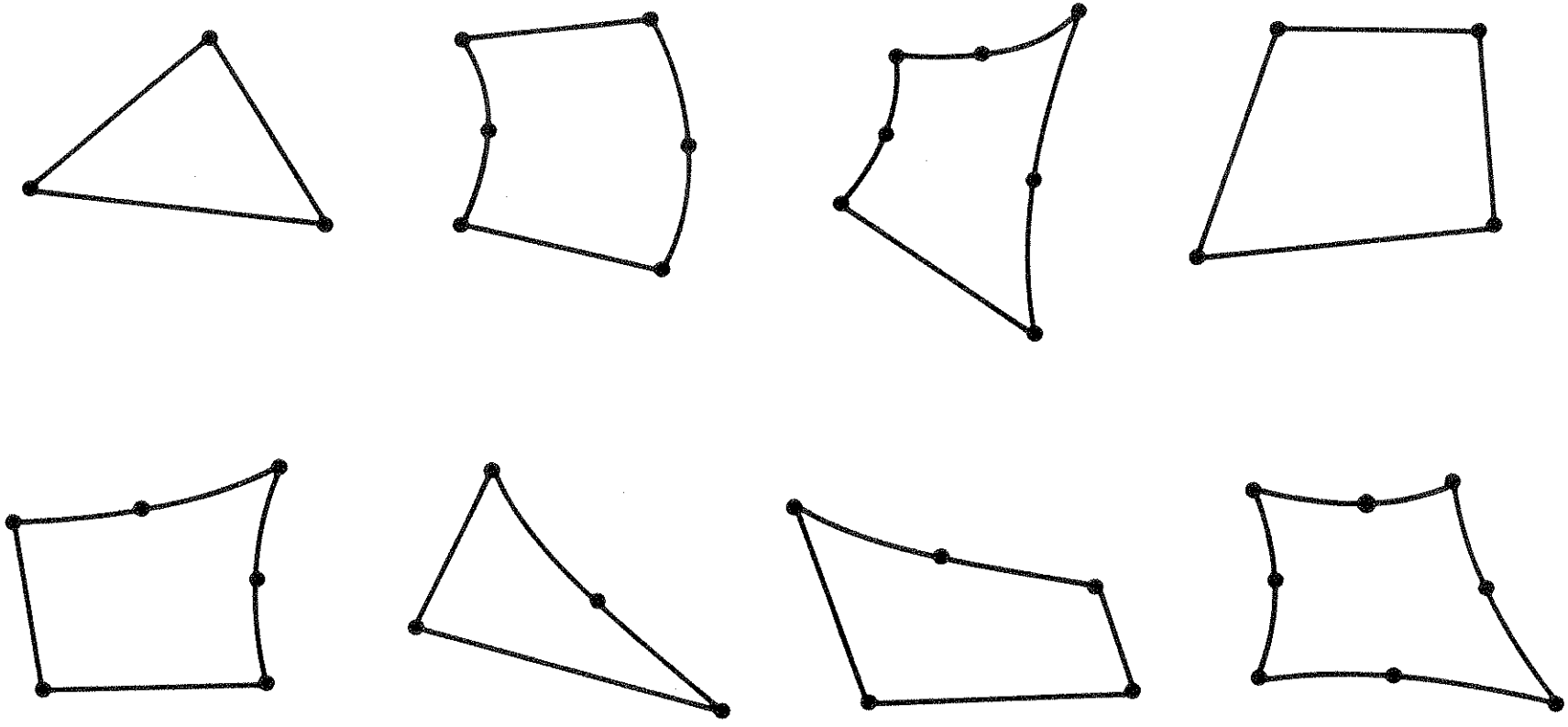

FIGURE 3.4 TYPICAL NODAL POINT CONFIGURATIONS FOR 2/D CONTINUUM ELEMENTS DERIVED FROM THE GENERAL 8-NODE ELEMENT IN FIGURE 3.5

coordinates r, s is chosen for the element such that r = -1 along element edge 2-6-3 and r = +1 on 4-8-1; similarly s = -1 along edge 3-7-4 and s = +1 on 1-5-2. Figure 3.5 illustrates the mapping of a general element into its r-s plane.

The element stiffness matrices, mass matrices, and force vectors are evaluated using Gauss numerical integration [40] [53]. Therefore, we require the displacement and strain-displacement transformation matrices for the different formulations at the integration points.

Interpolation Functions

For the two-dimensional elements natural r,s and global coordinates are related by, at time 0

$$ {}^0x_1 = \sum_{k=1}^{N} h_k \, {}^0x_1^k \quad ; \quad {}^0x_2 = \sum_{k=1}^{N} h_k \, {}^0x_2^k \tag{3.40} $$

and at time t

$$ {}^tx_1 = \sum_{k=1}^{N} h_k \, {}^tx_1^k \quad ; \quad {}^tx_2 = \sum_{k=1}^{N} h_k \, {}^tx_2^k \tag{3.41} $$

where the h_k are the interpolation functions.

Since we use isoparametric finite element discretization, the element displacements are interpolated in the same way as the geometry (see Eqs. (3.5) and (3.6)), i.e.,

$$ {}^tu_1 = \sum_{k=1}^{N} h_k \, {}^tu_1^k \quad ; \quad {}^tu_2 = \sum_{k=1}^{N} h_k \, {}^tu_2^k \tag{3.42} $$

$$ u_1 = \sum_{k=1}^{N} h_k \, u_1^k \quad ; \quad u_2 = \sum_{k=1}^{N} h_k \, u_2^k \tag{3.43} $$

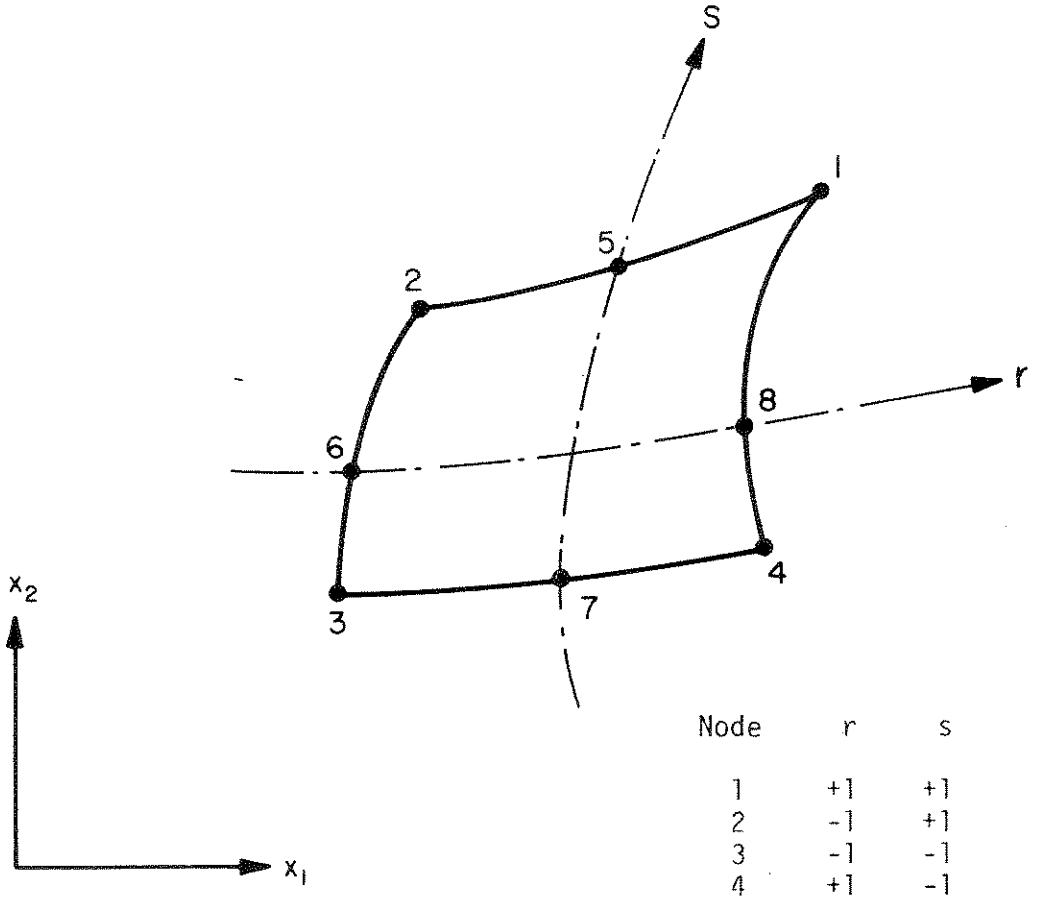

Node	r	s
1	+1	+1
2	-1	+1
3	-1	-1
4	+1	-1
5	0	+1
6	-1	0
7	0	-1
8	+1	0

FIGURE 3.5 ELEMENT NODE NUMBER INPUT SEQUENCE FOR 2/D CONTINUUM ELEMENTS

Defining

$$
\begin{aligned}
R &= 1 + r \\
S &= 1 + s \\
\bar{R} &= 1 - r \\
\bar{S} &= 1 - s \\
R^* &= 1 - r^2 \\
S^* &= 1 - s^2
\end{aligned}
\tag{3.44}
$$

we use

		delete if node I is not included			
		I = 5	I = 6	I = 7	I = 8
h_1	$= (1/4)\ R\ S$	$-(1/2)h_5$			$-(1/2)h_8$
h_2	$= (1/4)\ \bar{R}\ S$	$-(1/2)h_5$	$-(1/2)h_6$		
h_3	$= (1/4)\ \bar{R}\ \bar{S}$		$-(1/2)h_6$	$-(1/2)h_7$	
h_4	$= (1/4)\ R\ \bar{S}$			$-(1/2)h_7$	$-(1/2)h_8$
h_5	$= (1/2)\ R^*\ S$				
h_6	$= (1/2)\ \bar{R}\ S^*$				
h_7	$= (1/2)\ R^*\ \bar{S}$				
h_8	$= (1/2)\ R\ S^*$				

(3.45)

The above interpolation functions are written for all 8 nodes. If any one node from 5 to 8 is omitted, the corresponding interpolation function is deleted and the interpolation functions $h_1, \ldots, h_4$ are modified accordingly.

The evaluation of strains requires the following derivatives:

$$
\frac{\partial u_i}{\partial {}^0x_j} = \sum_{k=1}^{N} \left(\frac{\partial h_k}{\partial {}^0x_j} \right) u_i{}^k \qquad \begin{matrix} i = 1,2 \\ j = 1,2 \end{matrix} \tag{3.46}
$$

$$\frac{\partial u_i}{\partial {}^t x_j} = \sum_{k=1}^{N} \left(\frac{\partial h_k}{\partial {}^t x_j} \right) u_i^k \qquad \begin{matrix} i = 1,2 \\ j = 1,2 \end{matrix} \tag{3.47}$$

The derivatives are calculated using a Jacobian transformation. Consider the evaluation in the configuration at time t, since the evaluation at time 0 is obtained simply by replacing ${}^t x_j$ with ${}^0 x_j$.

The chain rule relating ${}^t x_1$, ${}^t x_2$ to r,s derivatives is written as

$$\begin{bmatrix} \frac{\partial}{\partial r} \\ \\ \frac{\partial}{\partial s} \end{bmatrix} = J \begin{bmatrix} \frac{\partial}{\partial {}^t x_1} \\ \\ \frac{\partial}{\partial {}^t x_2} \end{bmatrix} \tag{3.48}$$

in which

$$J = \begin{bmatrix} \frac{\partial {}^t x_1}{\partial r} & \frac{\partial {}^t x_2}{\partial r} \\ \\ \frac{\partial {}^t x_1}{\partial s} & \frac{\partial {}^t x_2}{\partial s} \end{bmatrix} \tag{3.49}$$

Inverting the Jacobian operator J, we obtain

$$\begin{bmatrix} \frac{\partial}{\partial {}^t x_1} \\ \\ \frac{\partial}{\partial {}^t x_2} \end{bmatrix} = \frac{1}{\det J} \begin{bmatrix} \frac{\partial {}^t x_2}{\partial s} & -\frac{\partial {}^t x_2}{\partial r} \\ \\ -\frac{\partial {}^t x_1}{\partial s} & \frac{\partial {}^t x_1}{\partial r} \end{bmatrix} \begin{bmatrix} \frac{\partial}{\partial r} \\ \\ \frac{\partial}{\partial s} \end{bmatrix} \tag{3.50}$$

where the Jacobian determinant is

$$\det J = \frac{\partial {}^t x_1}{\partial r} \frac{\partial {}^t x_2}{\partial s} - \frac{\partial {}^t x_1}{\partial s} \frac{\partial {}^t x_2}{\partial r} \tag{3.51}$$

Hence, for the evaluation of the Jacobian operator and of Eq. (3.47) we need the derivatives of the interpolation functions with respect to r and s, tabulated as follows:

$$
\begin{aligned}
h_{1,r} &= (1/4)\, S - (1/2)h_{5,r} - (1/2)h_{8,r} \\
h_{2,r} &= -(1/4)\, S - (1/2)h_{5,r} - (1/2)h_{6,r} \\
h_{3,r} &= -(1/4)\, \bar{S} - (1/2)h_{6,r} - (1/2)h_{7,r} \\
h_{4,r} &= (1/4)\, \bar{S} - (1/2)h_{7,r} - (1/2)h_{8,r} \\
h_{5,r} &= - r\, S \\
h_{6,r} &= -(1/2)\, S^{*} \\
h_{7,r} &= - r\, \bar{S} \\
h_{8,r} &= (1/2)\, S^{*}
\end{aligned}
\tag{3.52}
$$

and

$$
\begin{aligned}
h_{1,s} &= (1/4)\, R - (1/2)h_{5,s} - (1/2)h_{8,s} \\
h_{2,s} &= (1/4)\, \bar{R} - (1/2)h_{5,s} - (1/2)h_{6,s} \\
h_{3,s} &= -(1/4)\, \bar{R} - (1/2)h_{6,s} - (1/2)h_{7,s} \\
h_{4,s} &= -(1/4)\, R - (1/2)h_{7,s} - (1/2)h_{8,s} \\
h_{5,s} &= (1/2)\, R^{*} \\
h_{6,s} &= - s\, \bar{R} \\
h_{7,s} &= -(1/2)\, R^{*} \\
h_{8,s} &= - s\, R
\end{aligned}
\tag{3.53}
$$

As in the case of the interpolation functions in Eq. (3.45), only those functions whose nodal points are defined for the element considered should be included in Eqs. (3.52) and (3.53).

With all required derivatives being defined it is now possible to establish the strain-displacement transformation matrices for the

elements. Table 4 gives the required matrices for the U.L. and T.L. formulations. In the numerical integration these matrices are evaluated at the Gauss integration points.

It should be noted that in linear elastic analysis, and nonlinear analysis with material nonlinearities only, i.e. (A) and (B)in Table 3, we have $B_L = {}^{t}_{0}B_{LO}$, where B_L is defined in Table 3 and ${}^{t}_{0}B_{LO}$ in Table 4.

As was pointed out earlier, the choice between the T.L. and U.L. formulations essentially depends on their relative numerical effectiveness. Table 4 shows that all matrices of the two formulations have corresponding patterns of zero elements, except that ${}^{t}_{0}B_{L}$ is a full matrix whereas ${}^{t}_{t}B_{L}$ is sparse. The strain-displacement transformation matrix ${}^{t}_{0}B_{L}$ is full because of the initial displacement effect in the linear strain terms (see Tables 1 and 4). Therefore, the calculation of the matrix product ${}^{t}_{t}B_{L}^{T}\ {}_{t}C\ {}^{t}_{t}B_{L}$ in the U.L. formulation requires less time than the matrix product ${}^{t}_{0}B_{L}^{T}\ {}_{0}C\ {}^{t}_{0}B_{L}$ in the T.L. formulation.

The second numerical difference between the two formulations is that in the T.L. formulation all derivatives of interpolation functions are with respect to the initial coordinates, whereas in the U.L. formulation all derivatives are with respect to the coordinates at time t. Therefore, in the T.L. formulation they could be calculated only once in the first load step, and stored on back-up storage for use in all subsequent load steps. However, in practice, the use of tape or disc to store and retrieve the required derivatives may be more costly than simply to recalculate them in each time step. Also, the required back-up storage is a problem size governing factor, since saturation of back-up storage may be reached; and it is primarily for this reason that in

TABLE 4 MATRICES USED IN TWO-DIMENSIONAL ANALYSIS

A. TOTAL LAGRANGIAN FORMULATION

1. Incremental Strains

$$ {}_0\epsilon_{11} = {}_0u_{1,1} + {}^t_0u_{1,1}\,{}_0u_{1,1} + {}^t_0u_{2,1}\,{}_0u_{2,1} + \tfrac{1}{2}\left[({}_0u_{1,1})^2 + ({}_0u_{2,1})^2 \right] $$

$$ {}_0\epsilon_{22} = {}_0u_{2,2} + {}^t_0u_{1,2}\,{}_0u_{1,2} + {}^t_0u_{2,2}\,{}_0u_{2,2} + \tfrac{1}{2}\left[({}_0u_{1,2})^2 + ({}_0u_{2,2})^2 \right] $$

$$ {}_0\epsilon_{12} = \tfrac{1}{2}\left[{}_0u_{1,2} + {}_0u_{2,1}\right] + \tfrac{1}{2}\left[{}^t_0u_{1,1}\,{}_0u_{1,2} + {}^t_0u_{2,1}\,{}_0u_{2,2} + {}^t_0u_{1,2}\,{}_0u_{1,1} + {}^t_0u_{2,2}\,{}_0u_{2,1} \right] + \tfrac{1}{2}\left[{}_0u_{1,1}\,{}_0u_{1,2} + {}_0u_{2,1}\,{}_0u_{2,2}\right] $$

$$ {}_0\epsilon_{33} = \frac{u_1}{{}_0x_1} + \frac{{}^t_0u_1 u_1}{({}_0x_1)^2} + \tfrac{1}{2}\left(\frac{u_1}{{}_0x_1}\right)^2 \qquad \text{(for axisymmetric analysis)} $$

where $ {}_0u_{i,j} = \dfrac{\partial u_i}{\partial {}_0x_j} $; $ {}^t_0u_{i,j} = \dfrac{\partial {}^tu_i}{\partial {}_0x_j} $

2. Linear Strain-Displacement Transformation Matrix

Using $ {}_0e = {}^t_0B_L\, u $

where $ {}_0e^T = [{}_0\epsilon_{11}\ {}_0\epsilon_{22}\ 2{}_0\epsilon_{12}\ {}_0\epsilon_{33}] $; $ u^T = [u_1^1\ u_2^1\ u_1^2\ u_2^2\ \ldots\ u_1^N\ u_2^N] $

TABLE 4 (cont'd.)

and $$ {}^{t}_{0}B_{L} = {}^{t}_{0}B_{L0} + {}^{t}_{0}B_{L1} $$

$$ {}^{t}_{0}B_{L0} = \begin{bmatrix} {}^{0}h_{1,1} & 0 & {}^{0}h_{2,1} & 0 & {}^{0}h_{3,1} & 0 & \cdots & {}^{0}h_{N,1} & 0 \\ 0 & {}^{0}h_{1,2} & 0 & {}^{0}h_{2,2} & 0 & {}^{0}h_{3,2} & \cdots & 0 & {}^{0}h_{N,2} \\ {}^{0}h_{1,2} & {}^{o}h_{1,1} & {}^{0}h_{2,2} & {}^{0}h_{2,1} & {}^{0}h_{3,2} & {}^{0}h_{3,1} & \cdots & {}^{0}h_{N,2} & {}^{0}h_{N,1} \\ \dfrac{h_1}{{}^{0}\bar{x}_1} & 0 & \dfrac{h_2}{{}^{0}\bar{x}_1} & 0 & \dfrac{h_3}{{}^{0}\bar{x}_1} & 0 & \cdots & \dfrac{h_N}{{}^{0}\bar{x}_1} & 0 \end{bmatrix} $$

where $$ {}^{0}h_{k,j} = \frac{\partial h_k}{\partial {}^{0}x_j} \quad ; \quad u^{k}_{j} = {}^{t+\Delta t}u^{k}_{j} - {}^{t}u^{k}_{j} \quad ; \quad {}^{0}\bar{x}_1 = \sum_{k=1}^{N} h_k \, {}^{0}x^{k}_{1} \quad ; $$

N = number of nodes

and

TABLE 4 (cont'd.)

$$
{}^{t}_{0}B_{L1} = \begin{bmatrix}
\ell_{11}\,{}^{0}h_{1,1} & \ell_{21}\,{}^{0}h_{1,1} & \ell_{11}\,{}^{0}h_{2,1} & \ell_{21}\,{}^{0}h_{2,1} & \cdots & \ell_{11}\,{}^{0}h_{N,1} & \ell_{21}\,{}^{0}h_{N,1} \\
\ell_{12}\,{}^{0}h_{1,2} & \ell_{22}\,{}^{0}h_{1,2} & \ell_{12}\,{}^{0}h_{2,2} & \ell_{22}\,{}^{0}h_{2,2} & \cdots & \ell_{12}\,{}^{0}h_{N,2} & \ell_{22}\,{}^{0}h_{N,2} \\
(\ell_{11}\,{}^{0}h_{1,2} + \ell_{12}\,{}^{0}h_{1,1}) & (\ell_{21}\,{}^{0}h_{1,2} + \ell_{22}\,{}^{0}h_{1,1}) & (\ell_{11}\,{}^{0}h_{2,2} + \ell_{12}\,{}^{0}h_{2,1}) & (\ell_{21}\,{}^{0}h_{2,2} + \ell_{22}\,{}^{0}h_{2,1}) & \cdots & (\ell_{11}\,{}^{0}h_{N,2} + \ell_{12}\,{}^{0}h_{N,1}) & (\ell_{21}\,{}^{0}h_{N,2} + \ell_{22}\,{}^{0}h_{N,1}) \\
\ell_{33}\,\dfrac{h_1}{0\bar{x}_1} & 0 & \ell_{33}\,\dfrac{h_2}{0\bar{x}_1} & 0 & & \ell_{33}\,\dfrac{h_N}{0\bar{x}_1} & 0
\end{bmatrix}
$$

where

$$
\ell_{11} = \sum_{k=1}^{N} {}^{0}h_{k,1}\,{}^{t}u_1^k \;;\; \ell_{22} = \sum_{k=1}^{N} {}^{0}h_{k,2}\,{}^{t}u_2^k \;;\; \ell_{21} = \sum_{k=1}^{N} {}^{0}h_{k,1}\,{}^{t}u_2^k \;;\; \ell_{12} = \sum_{k=1}^{N} {}^{0}h_{k,2}\,{}^{t}u_1^k \;;\; \ell_{33} = \left(\sum_{k=1}^{N} h_k\,{}^{t}u_1^k\right) \Big/ 0\bar{x}_1
$$

TABLE 4 (cont'd.)

3. Nonlinear Strain Displacement Transformation Matrix

$$
{}^{t}_{0}B_{NL} = \begin{bmatrix}
{}^{0}h_{1,1} & 0 & {}^{0}h_{2,1} & 0 & {}^{0}h_{3,1} & 0 & \cdots & {}^{0}h_{N,1} & 0 \\
{}^{0}h_{1,2} & 0 & {}^{0}h_{2,2} & 0 & {}^{0}h_{3,2} & 0 & \cdots & {}^{0}h_{N,2} & 0 \\
0 & {}^{0}h_{1,1} & 0 & {}^{0}h_{2,1} & 0 & {}^{0}h_{3,1} & \cdots & 0 & {}^{0}h_{N,1} \\
0 & {}^{0}h_{1,2} & 0 & {}^{0}h_{2,2} & 0 & {}^{0}h_{3,2} & \cdots & 0 & {}^{0}h_{N,2} \\
\dfrac{h_1}{{}^{0}\bar{x}_1} & 0 & \dfrac{h_2}{{}^{0}\bar{x}_1} & 0 & \dfrac{h_3}{{}^{0}\bar{x}_1} & 0 & \cdots & \dfrac{h_N}{{}^{0}\bar{x}_1} & 0
\end{bmatrix}
$$

4. 2nd Piola-Kirchhoff Stress Matrix and Vector

$$
{}^{t}_{0}S = \begin{bmatrix}
{}^{t}_{0}S_{11} & {}^{t}_{0}S_{12} & 0 & 0 & 0 \\
{}^{t}_{0}S_{21} & {}^{t}_{0}S_{22} & 0 & 0 & 0 \\
0 & 0 & {}^{t}_{0}S_{11} & {}^{t}_{0}S_{12} & 0 \\
0 & 0 & {}^{t}_{0}S_{21} & {}^{t}_{0}S_{22} & 0 \\
0 & 0 & 0 & 0 & {}^{t}_{0}S_{33}
\end{bmatrix}
\quad ; \quad
{}^{t}_{0}\hat{S} = \begin{bmatrix}
{}^{t}_{0}S_{11} \\
{}^{t}_{0}S_{22} \\
{}^{t}_{0}S_{12} \\
{}^{t}_{0}S_{33}
\end{bmatrix}
$$

TABLE 4 (cont'd.)

B. UPDATED LAGRANGIAN FORMULATION

1. Incremental Strains

$$ {}^{t}\epsilon_{11} = {}^{t}u_{1,1} + \tfrac{1}{2}\left[({}^{t}u_{1,1})^2 + ({}^{t}u_{2,1})^2 \right] $$

$$ {}^{t}\epsilon_{22} = {}^{t}u_{2,2} + \tfrac{1}{2}\left[({}^{t}u_{1,2})^2 + ({}^{t}u_{2,2})^2 \right] $$

$$ {}^{t}\epsilon_{12} = \tfrac{1}{2}\left[{}^{t}u_{1,2} + {}^{t}u_{2,1} \right] + \tfrac{1}{2}\left[{}^{t}u_{1,1}\, {}^{t}u_{1,2} + {}^{t}u_{2,1}\, {}^{t}u_{2,2} \right] $$

$$ {}^{t}\epsilon_{33} = \frac{u_1}{{}^{t}x_1} + \tfrac{1}{2}\left(\frac{u_1}{{}^{t}x_1}\right)^2 \qquad \text{(for axisymmetric analysis)} $$

where $$ {}^{t}u_{i,j} = \frac{\partial u_i}{\partial {}^{t}x_j} $$

2. Linear Strain-Displacement Transformation Matrix

Using $$ {}^{t}e = {}^{t}_{t}B_L \, u $$

where $$ {}^{t}e^{T} = \left[{}^{t}e_{11} \;\; {}^{t}e_{22} \;\; {}^{2}{}^{t}e_{12} \;\; {}^{t}e_{33} \right] \quad ; \quad u^{T} = \left[u_1^1 \;\; u_2^1 \;\; u_1^2 \;\; u_2^2 \;\; \ldots \;\; u_1^N \;\; u_2^N \right] $$

TABLE 4 (cont'd.)

$$
{}^{t}_{t}B_{L} = \begin{bmatrix}
{}^{t}h_{1,1} & 0 & {}^{t}h_{2,1} & 0 & {}^{t}h_{3,1} & 0 & \cdots & {}^{t}h_{N,1} & 0 \\
0 & {}^{t}h_{1,2} & 0 & {}^{t}h_{2,2} & 0 & {}^{t}h_{3,2} & \cdots & 0 & {}^{t}h_{N,2} \\
{}^{t}h_{1,2} & {}^{t}h_{1,1} & {}^{t}h_{2,2} & {}^{t}h_{2,1} & {}^{t}h_{3,2} & {}^{t}h_{3,1} & \cdots & {}^{t}h_{N,2} & {}^{t}h_{N,1} \\
\dfrac{h_1}{t_{\bar{x}_1}} & 0 & \dfrac{h_2}{t_{\bar{x}_1}} & 0 & \dfrac{h_3}{t_{\bar{x}_1}} & 0 & \cdots & \dfrac{h_N}{t_{\bar{x}_1}} & 0
\end{bmatrix}
$$

where ${}^{t}h_{k,j} = \dfrac{\partial h_k}{\partial {}^{t}x_j}$; $u^k_j = {}^{t+\Delta t}u^k_j - {}^{t}u^k_j$; $t_{\bar{x}_1} = \sum_{k=1}^{N} h_k \, {}^{t}x^k_1$; N = number of nodes

3. Nonlinear Strain Displacement Transformation Matrix

$$
{}^{t}_{t}B_{NL} = \begin{bmatrix}
{}^{t}h_{1,1} & 0 & {}^{t}h_{2,1} & 0 & {}^{t}h_{3,1} & 0 & \cdots & {}^{t}h_{N,1} & 0 \\
{}^{t}h_{1,2} & 0 & {}^{t}h_{2,2} & 0 & {}^{t}h_{3,2} & 0 & \cdots & {}^{t}h_{N,2} & 0 \\
0 & {}^{t}h_{1,1} & 0 & {}^{t}h_{2,1} & 0 & {}^{t}h_{3,1} & \cdots & 0 & {}^{t}h_{N,1} \\
0 & {}^{t}h_{1,2} & 0 & {}^{t}h_{2,2} & 0 & {}^{t}h_{3,2} & \cdots & 0 & {}^{t}h_{N,2} \\
\dfrac{h_1}{t_{\bar{x}_1}} & 0 & \dfrac{h_2}{t_{\bar{x}_1}} & 0 & \dfrac{h_3}{t_{\bar{x}_1}} & 0 & \cdots & \dfrac{h_N}{t_{\bar{x}_1}} & 0
\end{bmatrix}
$$

TABLE 4 (cont'd)

4. Cauchy Stress Matrix and Stress Vector

$$
{}^{t}_{\tau} = \begin{bmatrix}
{}^{t}\tau_{11} & {}^{t}\tau_{12} & 0 & 0 & 0 \\
{}^{t}\tau_{21} & {}^{t}\tau_{22} & 0 & 0 & 0 \\
0 & 0 & {}^{t}\tau_{11} & {}^{t}\tau_{12} & 0 \\
0 & 0 & {}^{t}\tau_{21} & {}^{t}\tau_{22} & 0 \\
0 & 0 & 0 & 0 & {}^{t}\tau_{33}
\end{bmatrix} \quad ; \quad
{}^{t}\tilde{\tau} = \begin{bmatrix}
{}^{t}\tau_{11} \\
{}^{t}\tau_{22} \\
{}^{t}\tau_{12} \\
{}^{t}\tau_{33}
\end{bmatrix}
$$

NONSAP the derivatives of the interpolation functions are recalculated in each time step.

In two-dimensional analysis the differences in numerical operations using the T.L. or U.L. formulations when measured on the total efforts of solution are generally small and, in NONSAP, the choice is in most cases decided by the definition of the material law used. This is further discussed in Chapter 4, in which the different material models are presented.

Mass Matrices

The lumped mass matrix is evaluated by simply lumping 1/N th of the total element mass at each node. The consistent mass matrix is given in Table 3, i.e. $M = \rho \int_{{}^0V} H^T H \, {}^0dv$, in which H is a matrix of the interpolation functions tabulated in Eq. (3.45).

Internal Resisting Force Vectors

The internal resisting force vectors calculated in the different formulations are given in Table 3. The matrices used in the evaluation by Gauss numerical integration are presented in Table 4. We should note that in nonlinear analysis with material nonlinearities only $B_L = {}^t_0B_{LO}$, where B_L is used in Table 3 and ${}^t_0B_{LO}$ is defined in Table 4.

3.3 Three-Dimensional Elements

A general three-dimensional isoparametric element is available in NONSAP. Figure 3.6 shows some typical structures which could be analyzed using the element.

For the three-dimensional element the following formulations have been incorporated into NONSAP:

1. Linear elastic small displacement analysis, i.e. (A) in Table 3.
2. Small displacement analysis with material nonlinearities only, i.e. (B) in Table 3.

Therefore, only material nonlinearities can so far be considered in three-dimensional nonlinear analysis using NONSAP. However, the matrices to be used in geometrically nonlinear analysis would be very similar to those employed in two-dimensional analysis, and could be derived using Table 4. Since the formulation of the three-dimensional elements is quite analogous to the formulation of the two-dimensional elements, only the interpolation functions used will be given.

Interpolation Functions

The general three-dimensional element in NONSAP is an 8 to 21 variable-number-nodes element. This means that the element may have any number of nodes from 8 to 21, in which the first 8 nodes are the corner nodes of the element. Figure 3.7 shows some typical element configurations. The coordinates and displacements are interpolated using

$$ {}^{0}x_i = \sum_{k=1}^{N_x} h_k \, {}^{0}x_i^k \qquad i = 1,2,3 \qquad (3.53) $$

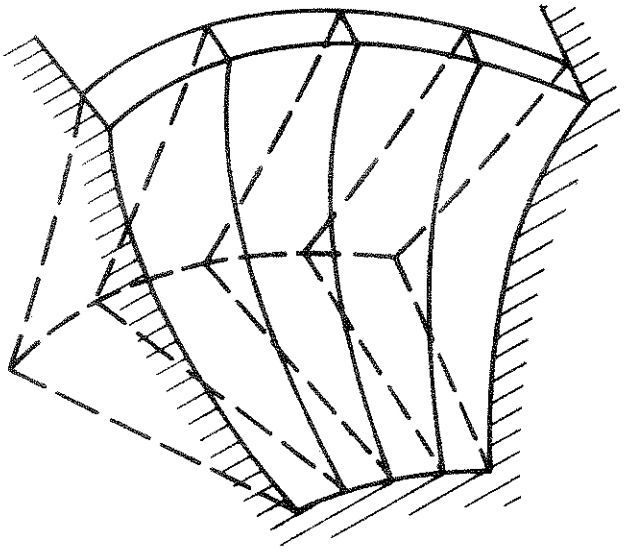

3/D CONTINUUM ELEMENT MODEL OF ARCH DAM

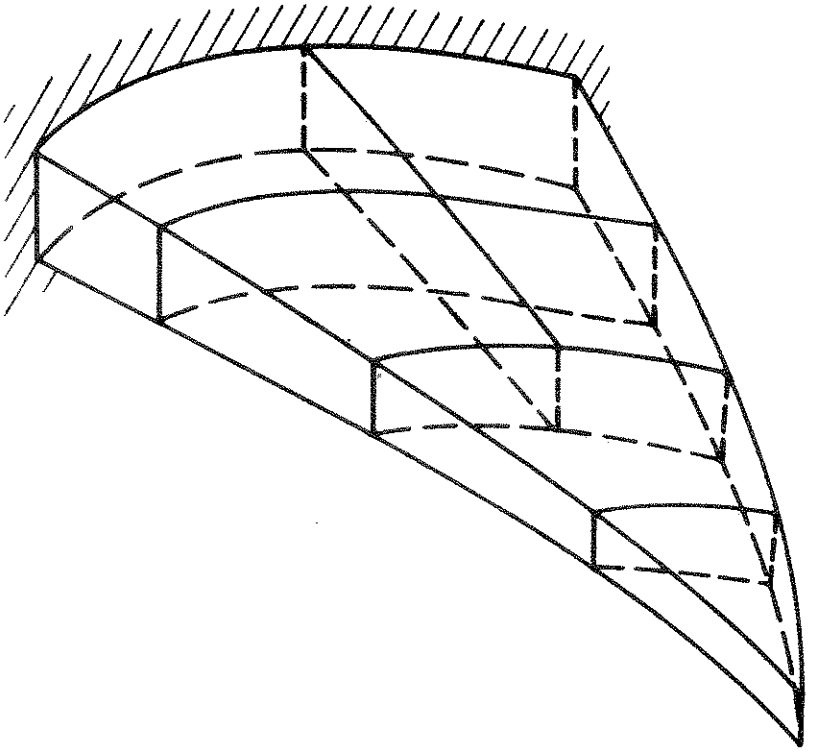

3/D CONTINUUM ELEMENT MODEL OF THICK SHELL

FIGURE 3.6 POSSIBLE THREE-DIMENSIONAL FINITE ELEMENT ANALYSES

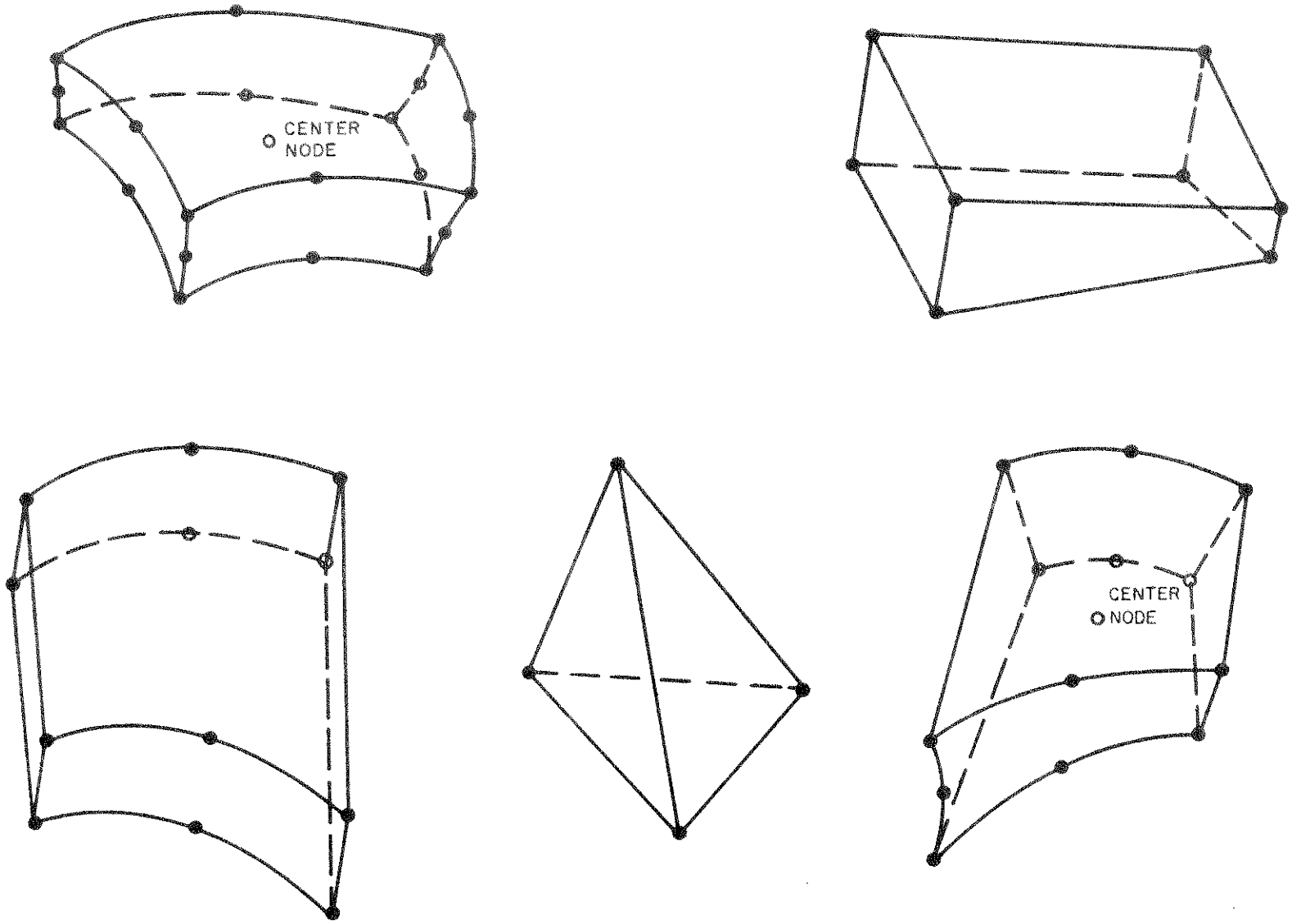

FIGURE 3.7 TYPICAL 3/D CONTINUUM ELEMENTS DERIVED FROM THE GENERAL 21-NODE ELEMENT

$$u_i = \sum_{k=1}^{N_u} h_k \, u_i^k \qquad i = 1,2,3 \qquad (3.54)$$

where the h_k are the interpolation functions listed in Table 5, and N_x and N_u are the number of nodes used for coordinate and displacement interpolation, respectively. The element is isoparametric if $N_x = N_u$, and subparametric if $N_x < N_u$ [53]. In three-dimensional finite element analysis the element formation time is, in general, significant and the option of using subparametric elements has been included to increase the efficiency of the analysis. As in the case of the two-dimensional elements, in Table 5 the interpolation functions have been written for all 21 possible nodes, and for any one node which is not included the corresponding interpolation functions should be deleted.

TABLE 5 INTERPOLATION FUNCTIONS OF THREE-DIMENSIONAL ELEMENT

	9	10	11	12	13	14	15	16	17	18	19	20	21
$h_1=(1/8)R\ S\ T$	$-(1/2)h_9$			$-(1/2)h_{12}$					$-(1/2)h_{17}$				$-(1/8)h_{21}$
$h_2=(1/8)\bar{R}\ S\ T$	$-(1/2)h_9$	$-(1/2)h_{10}$								$-(1/2)h_{18}$			$-(1/8)h_{21}$
$h_3=(1/8)\bar{R}\ \bar{S}\ T$		$-(1/2)h_{10}$	$-(1/2)h_{11}$								$-(1/2)h_{19}$		$-(1/8)h_{21}$
$h_4=(1/8)R\ \bar{S}\ T$			$-(1/2)h_{11}$	$-(1/2)h_{12}$								$-(1/2)h_{20}$	$-(1/8)h_{21}$
$h_5=(1/8)R\ S\ \bar{T}$					$-(1/2)h_{13}$			$-(1/2)h_{16}$	$-(1/2)h_{17}$				$-(1/8)h_{21}$
$h_6=(1/8)\bar{R}\ S\ \bar{T}$					$-(1/2)h_{13}$	$-(1/2)h_{14}$				$-(1/2)h_{18}$			$-(1/8)h_{21}$
$h_7=(1/8)\bar{R}\ \bar{S}\ \bar{T}$						$-(1/2)h_{14}$	$-(1/2)h_{15}$				$-(1/2)h_{19}$		$-(1/8)h_{21}$
$h_8=(1/8)R\ \bar{S}\ \bar{T}$							$-(1/2)h_{15}$	$-(1/2)h_{16}$				$-(1/2)h_{20}$	$-(1/8)h_{21}$
$h_9=(1/4)R^*\ S\ T$													$-(1/4)h_{21}$
$h_{10}=(1/4)\bar{R}\ S^*\ T$													$-(1/4)h_{21}$
$h_{11}=(1/4)R^*\ \bar{S}\ T$													$-(1/4)h_{21}$
$h_{12}=(1/4)R\ S^*\ T$													$-(1/4)h_{21}$
$h_{13}=(1/4)R^*\ S\ \bar{T}$													$-(1/4)h_{21}$
$h_{14}=(1/4)\bar{R}\ S^*\ \bar{T}$													$-(1/4)h_{21}$
$h_{15}=(1/4)R^*\ \bar{S}\ \bar{T}$													$-(1/4)h_{21}$
$h_{16}=(1/4)R\ S^*\ \bar{T}$													$-(1/4)h_{21}$
$h_{17}=(1/4)R\ S\ T^*$													$-(1/4)h_{21}$
$h_{18}=(1/4)\bar{R}\ S\ T^*$													$-(1/4)h_{21}$
$h_{19}=(1/4)\bar{R}\ \bar{S}\ T^*$													$-(1/4)h_{21}$
$h_{20}=(1/4)R\ \bar{S}\ T^*$													$-(1/4)h_{21}$
$h_{21}=R^*\ S^*\ T^*$													$-(1/4)h_{21}$

where

$R = 1 + r$
$S = 1 + s$
$T = 1 + t$
$\bar{R} = 1 - r$
$\bar{S} = 1 - s$
$\bar{T} = 1 - t$
$R^* = 1 - r^2$
$S^* = 1 - s^2$
$T^* = 1 - t^2$

4. MATERIAL MODELS

An important aspect in the solution of materially nonlinear problems is the calculation of the constitutive tensors, which define the stress-strain matrices in the finite element evaluations. In the isoparametric finite element discretization used in NONSAP, it is necessary to evaluate the stress-strain matrices at the element integration points, and they are required for the calculation of the element stiffness matrices and stress vectors (see Tables 3 and 4). The purpose in this chapter is to present the constitutive relations used in NONSAP and to demonstrate the specific computer implementation.

We recall that materials may be classed as elastic, hyperelastic or hypoelastic, as summarized by Fung [14].

4.1 Linear Elasticity and Hyperelasticity

Elastic and hyperelastic materials are relatively easy to deal with in practical analyses. Since both the T.L. and U.L. formulations reduce to the linear elastic infinitesimal displacement analysis procedure, we consider directly large displacement and large strain analysis. In the T.L. formulation we have

$$ {}^{t}_{0}S_{ij} = {}^{t}_{0}C_{ijrs} \, {}^{t}_{0}\varepsilon_{rs} \tag{4.1} $$

where ${}^{t}_{0}S_{ij}$ is the 2nd Piola - Kirchhoff stress tensor, ${}^{t}_{0}\varepsilon_{rs}$ is the Green - Lagrange strain tensor and ${}^{t}_{0}C_{ijrs}$ is the material property tensor in the configuration at time t. The relation in Eq. (4.1) can be written for all configurations at time 0, Δt, $2\Delta t$, ... In the U.L. formulation the constitutive relation equivalent to Eq. (4.1) is

$$ {}^{t}\tau_{ij} = {}^{t}_{t}C_{ijrs} \, {}^{t}\varepsilon_{rs} \tag{4.2} $$

in which ${}^{t}\tau_{ij}$ is the Cauchy stress tensor, ${}^{t}\varepsilon_{rs}$ is the Almansi strain tensor and ${}^{t}_{t}C_{ijrs}$ is the material property tensor at time t.

Considering linear elasticity ${}^{t}_{0}C_{ijrs}$ and ${}^{t}_{t}C_{ijrs}$ are both constant and defined in terms of the Young's moduli and Poisson's ratios of the material. However, it should be noted that specifying constant ${}^{t}_{t}C_{ijrs}$ is equivalent to using a material tensor ${}^{t}_{0}C_{ijrs}$, which is deformation dependent, and vice versa; namely

$$ {}^{t}_{0}C_{mnpq} = \frac{{}^{0}\rho}{{}^{t}\rho} \, {}^{0}_{t}x_{m,i} \, {}^{0}_{t}x_{n,j} \, {}^{t}_{t}C_{ijrs} \, {}^{0}_{t}x_{p,r} \, {}^{0}_{t}x_{q,s} \tag{4.3} $$

$$ {}^{t}_{t}C_{mnpq} = \frac{{}^{t}\rho}{{}^{0}\rho} \, {}^{t}_{0}x_{m,i} \, {}^{t}_{0}x_{n,j} \, {}^{t}_{0}C_{ijrs} \, {}^{t}_{0}x_{p,r} \, {}^{t}_{0}x_{q,s} \tag{4.4} $$

Considering hyperelasticity the stress-strain relations are derived from the strain energy function, usually defined per unit mass of the material and corresponding to the T.L. formulation [14] [22].

However, if ${}^{t}_{0}C_{ijrs}$ is defined, say, for example, by an experiment on a rubber-like material, we may calculate at any given time ${}^{t}_{t}C_{ijrs}$ for the U.L. formulation using Eq. (4.4), and vice versa.

The constitutive relations in Eqs. (4.1) and (4.2) are used in the evaluation of the element stress matrices and stress vectors (see Tables 3 and 4), i.e., we calculate from total Green - Lagrange or Almansi strains directly the total 2nd Piola - Kirchhoff or Cauchy stresses, respectively. However, in the calculation of the linear strain stiffness matrices at time t, we need tangent material property tensors (see Tables 1, 2 and 3). In linear elasticity we simply have

$$ {}_{0}C_{ijrs} = {}^{t}_{0}C_{ijrs} \quad ; \quad {}_{t}C_{ijrs} = {}^{t}_{t}C_{ijrs} \tag{4.5} $$

and for the hyperelastic material considered in Section 4.4.3 we have

$$ {}_{0}C_{ijrs} = \frac{\partial\, {}^{t}_{0}S_{ij}}{\partial\, {}^{t}_{0}\epsilon_{rs}} \tag{4.6} $$

We should note that in the analysis of elastic and hyperelastic materials identical numerical results are obtained using the T.L. and the U.L. formulations provided the material tensors are related as given in Eqs. (4.3) and (4.4). Also, since the material constants are independent of the history of solution, analysis errors result only from the iso-parametric finite element formulation and the time integration scheme, provided equilibrium iterations are performed (see Chapter 5). Therefore, in the analysis of elastic and hyperelastic materials the analysis errors are quite similar to those in small displacement linear elastic analysis.

4.2 Hypoelasticity

For a hypoelastic material the constitutive tensor relates increments in stresses to increments in deformations. Therefore, total stresses cannot be related directly to total strains but depend on the path of deformation [12] [38] [46].

Consider first the analysis of a small displacement problem, i.e., a problem with material nonlinearities only. In this case we have

$$\sigma_{ij} = C_{ijrs} \, e_{rs} \tag{4.7}$$

in which σ_{ij} and e_{rs} are increments in engineering stresses and infinitesimal strains at time t, respectively (see Eqs. 2.9 to 2.11). In this analysis the configuration of the body is assumed to remain unchanged. Therefore, increments in stresses and increments in infinitesimal strains can simply be added to obtain total strains and stresses. In general, the material tensor C_{ijrs} depends on the stress and strain history. The plasticity models, the variable tangent moduli model and the general curve description model described in the next sections define hypoelastic materials.

In large deformation analysis it is necessary to make an assumption on which strain increments are related to which stress increments. In this context it should be noted that a great deal of additional research is still required to formulate and evaluate appropriate material constants for hypoelastic materials, in particular, for the identification of large strain behavior [22] [27] [28]. Although the formulations presented below are applicable to large strain conditions, in actual practical analysis the material law is likely to be defined only for small strains. An important such case is elastic-plastic material behavior characterized using the flow

theory, which can be used in the analysis of large displacement but small strain problems.

Using the T.L. formulation, hypoelastic material behavior can be described by

$$ {}_0S_{ij} = {}_0C_{ijrs} \; {}_0\epsilon_{rs} \tag{4.8} $$

in which ${}_0S_{ij}$ and ${}_0\epsilon_{rs}$ are increments in 2nd Piola - Kirchhoff stresses and Green - Lagrange strains, respectively. In the solution we approximate ${}_0\epsilon_{rs}$ by ${}_0e_{rs}$ and calculate the 2nd Piola - Kirchhoff stresses at time $t+\Delta t$ using

$$ {}^{t+\Delta t}_{0}S_{ij} = {}^{t}_{0}S_{ij} + {}_0S_{ij} \tag{4.9} $$

as shown in Table 1.

In the analysis using Eq. (4.8) it is assumed that the material tensor ${}_0C_{ijrs}$ is evaluated in the same way as in small displacement analysis, but the stress and strain variables of the T.L. formulation are used to define the history of the material. A main advantage of adopting this material description is that it is relatively simple to use. Namely, assume that a subroutine to calculate C_{ijrs} in Eq. (4.7) has been written, then the same subroutine would also define ${}_0C_{ijrs}$ in large displacement analysis by simply using Green - Lagrange strains and 2nd Piola - Kirchhoff stresses to define the stress and strain history.

Similarly to Eq. (4.8), in the U.L. formulation we may use

$$ {}^tS_{ij} = {}^tC_{ijrs} \; {}^t\epsilon_{rs} \tag{4.10} $$

and assume that ${}^tC_{ijrs}$ is defined by the history of Cauchy stresses. In the solution we approximate ${}^t\epsilon_{rs}$ by ${}^te_{rs}$. The constitutive relation in Eq. (4.10) may be more appealing than the T.L. material law in Eq. (4.8),

since we work with physical stress components to define the material constants and ${}_t e_{rs}$ can kinematically be understood to be the addition of elastic and plastic strain increments, just as in small displacement analysis. Having calculated ${}_t S_{ij}$ from the relation ${}_t S_{ij} = C_{ijrs}\ {}_t e_{rs}$, the Cauchy stresses at time $t+\Delta t$ are obtained, using the relations given in Table 2,

$$ {}^{t+\Delta t}_{t}S_{ij} = {}^{t}\tau_{ij} + {}_t S_{ij} \tag{4.11} $$

and

$$ {}^{t+\Delta t}\tau_{sr} = \frac{{}^{t+\Delta t}\rho}{{}^{t}\rho}\ {}^{t+\Delta t}_{t}x_{s,i}\ {}^{t+\Delta t}_{t}S_{ij}\ {}^{t+\Delta t}_{t}x_{r,j} \tag{4.12} $$

A third possibility suggested by Hibbitt, et al. [18], Heifitz and Constantino [17] and Lee [28], is to characterize the material behavior using a stress rate which is defined with respect to the current moving coordinates within the time interval t to $t+\Delta t$. The stress rate used must be invariant with respect to rigid body rotation, and one possibility is to use the Jaumann stress rate, which, at time t, is defined as

$$ {}^{t}\tau^{\nabla}_{ij} = \frac{D}{Dt}\ {}^{t}\tau_{ij} - {}^{t}\tau_{ip}\ {}^{t}\Omega_{pj} - {}^{t}\tau_{jp}\ {}^{t}\Omega_{pi} \tag{4.13} $$

where $\frac{D}{Dt}$ denotes time derivative with ${}^{t}x_i$, $i = 1,2,3$, kept constant,

$$ {}^{t}\tau^{\nabla}_{ij} = {}_t C_{ijrs}\ \frac{D}{Dt}\ {}_t e_{rs} \tag{4.14} $$

and ${}^{t}\Omega_{pj}$ are Cartesian components of the spin tensor,

$$ {}^{t}\Omega_{pj} = \tfrac{1}{2}\frac{D}{Dt}\ \left({}_t u_{j,p} - {}_t u_{p,j}\right) \tag{4.15} $$

In small displacement analysis the spin tensor is not considered and Eqs. (4.13) to (4.15) reduce to Eq. (4.7).

We should note that the Jaumann stress rate definition considers instantaneous conditions. In the numerical solution, however, we need to

consider finite time steps. Therefore, the solution will only be accurate if small enough time steps are taken.

Equations (4.13) to (4.15) need be considered in the evaluation of the tangent stiffness matrix and in the calculation of the current stress conditions. The constitutive tensor relating the Jaumann stress rate tensor ${}^{t}_{\nabla}\tau_{ij}$ to the incremental strain rate tensor $\frac{D}{Dt}\ {}^{t}e_{rs}$ is calculated in the same way as in small displacement analysis, but using Cauchy stresses to define the history of the material. In the evaluation of the tangent stiffness matrix it appears that the contribution from the stresses to the material constants is negligible, i.e., ${}^{t}C_{ijrs}\ \frac{D}{Dt}\ {}^{t}e_{rs} \gg {}^{t}\tau_{ip}\ {}^{t}\Omega_{pj}$. Therefore, neglecting the stress contribution, we have

$$D^{t}\tau_{ij} = {}^{t}C_{ijrs}\ {}^{t}e_{rs} \tag{4.16}$$

since $D_{t}e_{rs} \equiv {}^{t}e_{rs}$. Alternatively, the stress rotation contribution may be taken account of in the calculation of the force vector ${}^{t}_{t}F_{e}$. Considering the calculation of Cauchy stresses at time $t+\Delta t$, ${}^{t+\Delta t}\tau_{ij}$, it is important to use Eqs. (4.13) to (4.15) in small enough increments of time. In elastic-plastic analysis it is in any case necessary to evaluate the stress increment by numerical integration of the elastic-plastic material law times the strain increment, and it is efficient to include Eq. (4.13) in this integration (see Section 4.4.4).

Since the material descriptions given in Eqs. (4.10) to (4.12) and in Eqs. (4.13) to (4.16) have both been implemented with the U.L. formulation in NONSAP, they will be referred to as U.L. with transformation, U.L.(T), and U.L. with Jaumann stress rate, U.L.(J), respectively.

With the different descriptions available for the material behavior, the question must be which one should be used in actual practical analysis. This depends naturally on the specific material considered and the definition chosen for the material parameters. For example, in elastic-plastic analysis if Eq. (4.8) is used, yielding is defined as a function of the 2nd Piola - Kirchhoff stresses, whereas if Eq. (4.10) is used, the Cauchy stress conditions define yielding. We consider in Chapter 6 some results obtained using the different descriptions.

In the above enumeration it was assumed that the solution procedure, namely the T.L. or U.L. formulation, is chosen according to the definition of the constitutive tensor. This was merely done to avoid the necessary transformations given in Eqs. (4.3) and (4.4). It is of interest to note that Hibbitt, et al. define the material tensor first in the current configuration at time t and then transform it for use in the T.L. formulation [18].

4.3 Truss Element Models

The truss element in NONSAP is assumed to have constant area, and either a constant Young's modulus or the stress defined as a function of the current total strain. Therefore, linear and nonlinear elastic truss elements can currently be considered. Figure 4.1 illustrates a typical nonlinear stress-strain definition. We recall that in the material property definition small strains are assumed (see Section 3.1).

4.4 Two-Dimensional Element Models

It is probable that in most analyses with NONSAP two-dimensional elements will be used. For this reason the main library of material models has been incorporated for the two-dimensional elements. The use of a constitutive model in two-dimensional analysis may also indicate how useful the model would be in a more expensive three-dimensional analysis.

In the preceding sections we discussed the formulation of constitutive relations using tensor quantities. We now consider the material laws in matrix forms as they are implemented in NONSAP.

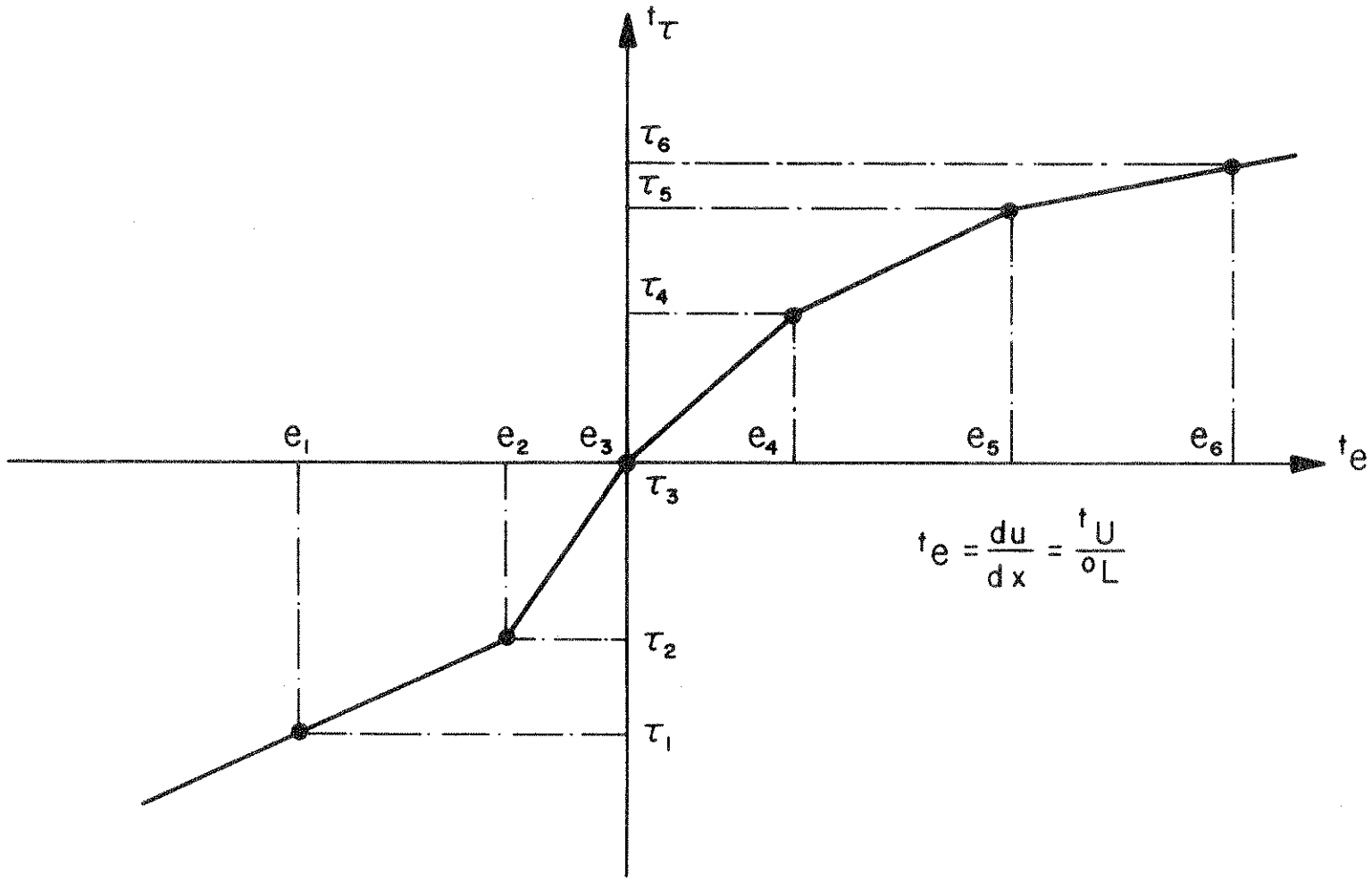

FIGURE 4.1 NONLINEAR STRESS-STRAIN DEFINITION FOR A TRUSS ELEMENT

4.4.1 Linear Elastic Isotropic Model

This model assumes that the elements of the constitutive matrix are constant, i.e., independent of magnitude or history of stresses and strains. The material matrix is formed from the two elastic constants E and ν, which are Young's modulus and Poisson's ratio, respectively. For axisymmetric analysis the material matrix is

$$C = \begin{bmatrix} c_1 & c_2 & 0 & c_2 \\ c_2 & c_1 & 0 & c_2 \\ 0 & 0 & c_3 & 0 \\ c_2 & c_2 & 0 & c_1 \end{bmatrix} \tag{4.17}$$

where $c_3 = E/2(1+\nu)$, $c_2 = 2\nu c_3/(1-2\nu)$, $c_1 = c_2 + c_3$, and the corresponding stress and strain vectors are, for example, in small displacement analysis (see Eq. (2.11)),

$$\begin{bmatrix} {}^t\sigma_{11} \\ {}^t\sigma_{22} \\ {}^t\sigma_{12} \\ {}^t\sigma_{33} \end{bmatrix} \quad ; \quad \begin{bmatrix} {}^te_{11} \\ {}^te_{22} \\ 2\,{}^te_{12} \\ {}^te_{33} \end{bmatrix}$$

respectively.

It should be noted that the material matrix in Eq. (4.17) is also used in the T.L. formulation to relate 2nd Piola - Kirchhoff stresses to Green - Lagrange strains, and in the U.L. formulation to relate Cauchy stresses to Almansi - strains, i.e., C in Eq. (4.17) also corresponds to the constitutive tensors ${}^t_tC_{ijrs}$ in Table 2 and ${}^t_0C_{ijrs}$ in Table 1.

Using Eqs. (4.5) and (4.6), it then follows that C also corresponds to the incremental constitutive tensors ${}_t^{}C_{ijrs}$ and ${}_0^{}C_{ijrs}$ in the tables. Since the same Young's modulus and Poisson's ratio are used to relate different stress and strain quantities in the T.L. and U.L. formulations, depending on the magnitude of the deformation gradients, different numerical results need be expected. To obtain identical numerical results for any level of displacements, the same definition of material constants need be used, i.e., the appropriate transformation in Eq. (4.3) or Eq. (4.4) must be performed.

To obtain from the material law in Eq. (4.17) the constitutive matrix for plane strain analysis, we use the condition that the strain in direction 3 is zero, and operate only with the 3 x 3 upper left matrix in C. In plane stress analysis we use the condition that the stress in direction 3 is zero, and condense the matrix C in Eq. (4.17) to the required 3 x 3 matrix [53].

Before presenting the next material models, it should be pointed out that the same ordering of stresses and strains in the stress and strain vectors is used throughout, and that the plane stress and plane strain constitutive relations are always derived from the general matrix C in Eq. (4.17) as described above.

4.4.2 Linear Elastic Orthotropic Model

This material model is used in the same way as the linear elastic isotropic model, but the elements of the matrix C are defined to represent orthotropic media.

Consider the finite element in Fig. 4.2, for which the in-plane orthogonal material axes are "a" and "b". The third orthogonal material direction is "c" and is perpendicular to the plane defined by "a" and "b". The material constants are defined in the principal material directions (a, b, c), for which we have

$$C_{\ell}^{-1} = \begin{bmatrix} 1/E_a & -\nu_{ab}/E_b & 0 & -\nu_{ac}/E_c \\ -\nu_{ba}/E_a & 1/E_b & 0 & -\nu_{bc}/E_c \\ 0 & 0 & 1/G_{ab} & 0 \\ -\nu_{ca}/E_a & -\nu_{cb}/E_b & 0 & 1/E_c \end{bmatrix} \tag{4.18}$$

where the subscript "ℓ" in C_{ℓ}^{-1} indicates that the material law is given in the local system of material axes. The seven independent constants (E_a, E_b, E_c, ν_{ab}, ν_{ac}, ν_{bc}, G_{ab}) define the symmetric matrix C_{ℓ}^{-1}.

In order to evaluate the stiffness matrix or element stresses, the stress-strain law in global coordinates ${}^{0}x_i$, ${}^{t}x_i$, ${}^{t+\Delta t}x_i$, $i = 1, 2, 3$ must be computed. First we calculate C_{ℓ} using Eq. (4.18); then we evaluate the transformation matrix Q which calculates strains in the global system from strains in the (a, b, c) local system [53],

$$Q = \begin{bmatrix} \cos^2\gamma & \sin^2\gamma & \cos\gamma\,\sin\gamma & 0 \\ \sin^2\gamma & \cos^2\gamma & -\cos\gamma\,\sin\gamma & 0 \\ -2\cos\gamma\,\sin\gamma & 2\cos\gamma\,\sin\gamma & \cos^2\gamma - \sin^2\gamma & 0 \\ 0 & 0 & 0 & 1 \end{bmatrix} \tag{4.19}$$

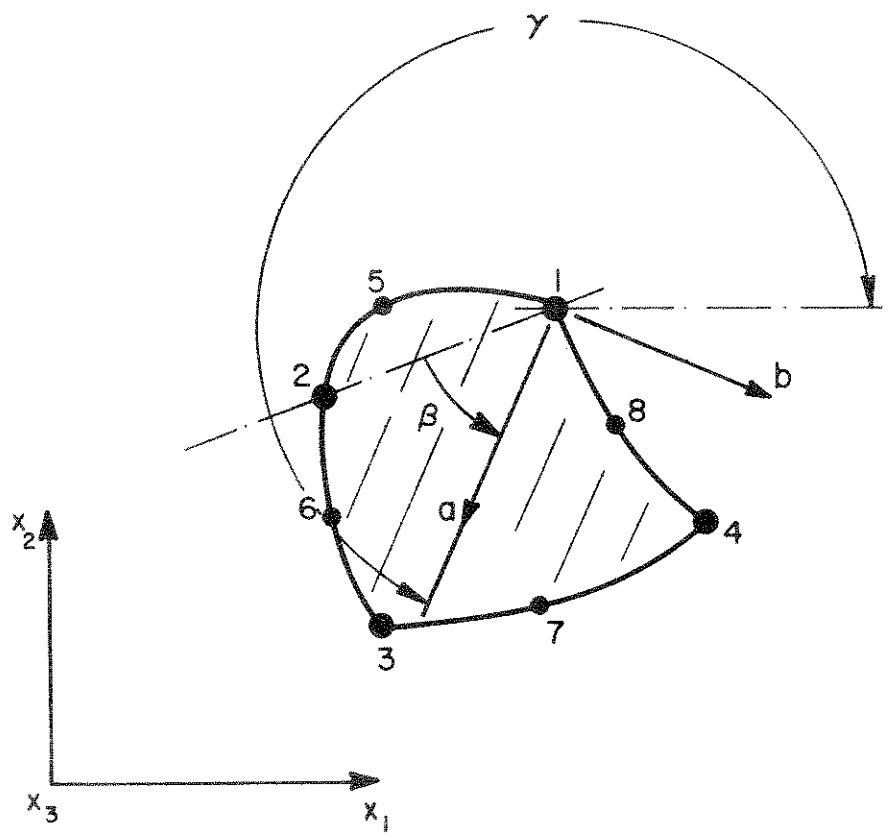

FIGURE 4.2 PRINCIPAL IN-PLANE MATERIAL AXES ORIENTATION FOR THE LINEAR ORTHOTROPIC MATERIAL MODEL

in which the angle γ is measured from the global ${}^{0}x_1$, ${}^{t}x_1$ or ${}^{t+\Delta t}x_1$ axes to the material axis "a", positive being clockwise. The required stress-strain relation in global coordinates is thus

$$C = Q^T C_\ell Q \tag{4.20}$$

As in the definition of the isotropic material law, Eq. (4.17), the material law in Eq. (4.20) is used in small displacement analysis, and in the T.L. formulation. If the material law is used directly in the U.L. formulation, it is assumed that the directions of orthotropy are at all times defined as given in Fig. 4.2.

4.4.3 Hyperelastic Incompressible Material Model

The material model presented in this section can only be used in plane stress analysis. Namely, in other than plane stress analysis, it is necessary to include the unknown hydrostatic pressure as an additional variable.

The constitutive relation is given corresponding to the T.L. formulation, and can be written as [4] [22]

$$\begin{bmatrix} {}^{t}_{0}S_{11} \\ {}^{t}_{0}S_{22} \\ {}^{t}_{0}S_{12} \end{bmatrix} = 2C_1 \left\{ \begin{bmatrix} 1 \\ 1 \\ 0 \end{bmatrix} - \left({}^{t}C_{33}\right)^2 \begin{bmatrix} {}^{t}C_{22} \\ {}^{t}C_{11} \\ -{}^{t}C_{12} \end{bmatrix} \right\} + 2C_2 \left\{ {}^{t}C_{33} \begin{bmatrix} 1 \\ 1 \\ 0 \end{bmatrix} + \left[1 - \left({}^{t}C_{33}\right)^2 \left({}^{t}C_{11} + {}^{t}C_{22}\right)\right] \begin{bmatrix} {}^{t}C_{22} \\ {}^{t}C_{11} \\ -{}^{t}C_{12} \end{bmatrix} \right\} \tag{4.21}$$

in which

$${}^{t}C_{ij} = 2\,{}^{t}_{0}\epsilon_{ij} + \delta_{ij} \tag{4.22}$$

where δ_{ij} is the Kronecker delta. Since the material is incompressible,

$${}^{t}C_{33} = \left[{}^{t}C_{11}\ {}^{t}C_{22} - \left({}^{t}C_{12}\right)^2\right]^{-1} \tag{4.23}$$

The variables C_1 , C_2 are the material constants of a Mooney - Rivlin type material [22] [40].

Equation (4.21) relates total 2nd Piola - Kirchhoff stresses to total Green - Lagrange strains. Using Eq. (4.5) to calculate the incremental material law we obtain

$$
{}_0C = 4C_1 \left({}^tC_{33}\right)^2 \left\{ 2\,{}^tC_{33}\ {}^t\hat{C} + \begin{bmatrix} 0 & -1 & 0 \\ -1 & 0 & 0 \\ 0 & 0 & 1 \end{bmatrix} \right\}
$$

$$
+ 4C_2 \left({}^tC_{33}\right)^2 \left\{ 2\,{}^tC_{33} \left({}^tC_{11} + {}^tC_{22}\right) {}^t\hat{C} \right.
$$

$$
+ \left({}^tC_{11} + {}^tC_{22}\right) \begin{bmatrix} 0 & -2 & 0 \\ -2 & 0 & 0 \\ 0 & 0 & 0.5 \end{bmatrix}
$$

$$
\left. + \begin{bmatrix} -2\,{}^tC_{22} & \dfrac{1}{\left({}^tC_{33}\right)^2} & {}^tC_{12} \\ \dfrac{1}{\left({}^tC_{33}\right)^2} & -2\,{}^tC_{11} & {}^tC_{12} \\ {}^tC_{12} & {}^tC_{12} & -\dfrac{1}{2\left({}^tC_{33}\right)^2} \end{bmatrix} \right\} \tag{4.24}
$$

where

$$
{}^t\hat{C} = \begin{bmatrix} \left({}^tC_{22}\right)^2 & {}^tC_{11}\ {}^tC_{22} & -{}^tC_{12}\ {}^tC_{22} \\ & \left({}^tC_{11}\right)^2 & -{}^tC_{12}\ {}^tC_{11} \\ \text{symmetric} & & \left({}^tC_{12}\right)^2 \end{bmatrix} \tag{4.25}
$$

4.4.4 Elastic-Plastic Models

It was discussed in Section 4.2 that, depending on the description used, i.e. the material nonlinearity only analysis, the T.L. formulation, or the U.L. formulation, an elastic-plastic constitutive law relates different stress and strain quantities. The constitutive matrix is found in the same way in either analysis; however, the appropriate stress and strain measures need be used. In the following we derive first the elastic-plastic constitutive relations used in small displacement analysis, and enumerate afterwards the specific changes that need be made using the T.L. or U.L. formulation.

Before presenting the elastic-plastic model it is useful to define the notation adopted in this section.

Notation used

$^{t}e_{ij}$ = total strains (the left superscript always refers to time "t")

$^{t}e^{E}_{ij}$ = total elastic strains

$^{t}e^{P}_{ij} = {}^{t}e_{ij} - {}^{t}e^{E}_{ij}$ = total plastic strains

e_{ij}, e^{E}_{ij}, e^{P}_{ij} = incremental strain quantities (at time t is implied)

$^{t}\sigma_{ij}$ = total stresses

σ_{ij} = incremental stresses

$^{t}\sigma_{m} = {}^{t}\sigma_{ii}/3$ = mean stress

$^{t}s_{ij} = {}^{t}\sigma_{ij} - {}^{t}\sigma_{m}\delta_{ij}$ = deviatoric stresses

Tensor components are also written in vector form, e.g.

$$ {}^{t}\sigma^{T} = [\ {}^{t}\sigma_{11}\ \ {}^{t}\sigma_{22}\ \ {}^{t}\sigma_{12}\ \ {}^{t}\sigma_{33}\ ]\ ;\ {}^{t}e = [\ e_{11}\ \ e_{22}\ \ 2e_{12}\ \ e_{33}\ ] $$

$$ F\ (\ {}^{t}\sigma\ ,\ {}^{t}e^{P}\ ,\ {}^{t}\varkappa\ ) = \text{yield function} $$

$$ {}^{t}\varkappa = \text{strain hardening parameter} $$

$$ {}^{t}q_{ij} = \frac{\partial F}{\partial\ {}^{t}\sigma_{ij}} $$

$$ {}^{t}q^{T} = [\ {}^{t}q_{11}\ ,\ {}^{t}q_{22}\ ,\ 2\,{}^{t}q_{12}\ ,\ {}^{t}q_{33}\ ] $$

$$ p_{ij} = -\frac{\partial F}{\partial\ {}^{t}e^{P}_{ij}} $$

$$ {}^{t}p^{T} = [\ {}^{t}p_{11}\ ,\ {}^{t}p_{22}\ ,\ {}^{t}p_{12}\ ,\ {}^{t}p_{33}\ ] $$

C^{E} = elastic stress-strain relation, i.e. $C^{E} \equiv C$ in Eq. (4.17).

In elastic-plastic analysis the material behavior is described using three properties in addition to the elastic stress-strain relations, C^{E}, namely (1) a yield condition, which specifies the state of multi-axial stress corresponding to start of plastic flow; (2) a flow rule relating plastic strain increments to the current stresses and the stress increments subsequent to yielding; and (3) a hardening rule, which specifies how the yield condition is modified during plastic flow.

The initial and subsequent yield condition for isothermal kinematic or isotropic hardening can be written as [14] [27] [42]

$$ F\ (\ {}^{t}e^{P},\ {}^{t}\sigma,\ {}^{t}\varkappa\ ) = 0 \qquad (4.21) $$

in which, for isotropic hardening, ${}^{t}\varkappa$ is a function of ${}^{t}e^{P}$, and for kinematic hardening, ${}^{t}\varkappa$ is a constant. As indicated, the effects of temperature and creep are neglected. Restricting the analysis to asso-

ciated flow rules, the function F in Eq. (4.21) is the plastic potential function to which the normality rule is applicable, i.e.,

$$e^{P}_{ij} = \lambda \frac{\partial F}{\partial {}^{t}\sigma_{ij}} \tag{4.22}$$

or in matrix form

$$e^{P} = \lambda \, {}^{t}q \tag{4.23}$$

where λ is a scalar to be determined. Since during plastic deformation $F = 0$, we also have

$$\frac{\partial F}{\partial {}^{t}\sigma_{ij}} \sigma_{ij} + \frac{\partial F}{\partial {}^{t}e^{P}_{ij}} e^{P}_{ij} = 0 \tag{4.24}$$

or in matrix form

$${}^{t}q^{T} \sigma = {}^{t}p^{T} e^{P} \tag{4.25}$$

The stress increments are calculated from

$$\sigma = C^{E} (e - e^{P}) \tag{4.26}$$

Using Eqs. (4.23) to (4.26) to eliminate e^{P} and σ, we obtain

$$\lambda = \frac{{}^{t}q^{T} C^{E} e}{{}^{t}p^{T} {}^{t}q + {}^{t}q^{T} C^{E} {}^{t}q} \tag{4.27}$$

Substituting in Eq. (4.26) from Eqs. (4.23) and (4.27) for e^{P} and λ, the elastic-plastic material law at time t becomes

$$\sigma = {}^{t}C^{EP} e \tag{4.28}$$

where

$${}^{t}C^{EP} = C^{E} - \frac{C^{E} {}^{t}q (C^{E} {}^{t}q)^{T}}{{}^{t}p^{T} {}^{t}q + {}^{t}q^{T} C^{E} {}^{t}q} \tag{4.29}$$

In NONSAP the von Mises and the Drucker-Prager yield conditions have been implemented. Currently the von Mises condition can be used assuming either perfectly plastic conditions or isotropic hardening; whereas the Drucker-Prager yield condition is limited to elastic perfectly plastic analysis. In both cases an initially isotropic elastic material is assumed, i.e. the material matrix C^E in Eq. (4.29) is equal to the matrix C in Eq. (4.17).

Von Mises Yield Condition

When the von Mises yield condition is used the loading surface for isothermal classical isotropic (or kinematic) hardening is given by

$$F\left({}^t\sigma, {}^t e^P\right) = \tfrac{1}{2}\left({}^t s_{ij} - {}^t\alpha_{ij}\right)\left({}^t s_{ij} - {}^t\alpha_{ij}\right) - {}^t\kappa \qquad (4.30)$$

where ${}^t\alpha_{ij}$ is a tensor denoting the translation of the yield surface. In the case of isotropic hardening (which includes perfectly plastic conditions), we have

$${}^t\alpha_{ij} = 0 \quad ; \quad {}^t\kappa = \frac{{}^t\sigma_y^{\,2}}{3} \qquad (4.31)$$

where ${}^t\sigma_y$ is the yield stress in simple tension at time t and is a function of the plastic work per unit volume ${}^tW^P$,

$${}^tW^P = \int_0^{{}^t e^P_{ij}} {}^t\sigma_{ij}\; de^P_{ij} \qquad (4.32)$$

Evaluating ${}^tq$ and ${}^tp$ we obtain

$${}^tq^T = \left[\, {}^t s_{11} \quad {}^t s_{22} \quad 2\,{}^t s_{12} \quad {}^t s_{33} \,\right] \qquad (4.33)$$

and

$$ {}^{t}_{p}T = {}^{t}_{H} \left[{}^{t}\sigma_{11} \quad {}^{t}\sigma_{22} \quad {}^{t}\sigma_{12} \quad {}^{t}\sigma_{33} \right] \tag{4.34} $$

where

$$ {}^{t}_{H} = \frac{2}{3} \, {}^{t}\sigma_{y} \, \frac{d\,{}^{t}\sigma_{y}}{d\,{}^{t}_{W}P} \tag{4.35} $$

We can now calculate the material property matrix in Eq. (4.29) and obtain

$$C^{EP} = \frac{E}{1+\nu}\begin{pmatrix} \frac{1-\nu}{1-2\nu} - \beta^t s_{11}{}^t s_{11} & & & \text{Symmetric} \\ \frac{\nu}{1-2\nu} - \beta^t s_{22}{}^t s_{11} & ; & \frac{1-\nu}{1-2\nu} - \beta^t s_{22}{}^t s_{22} & \\ -\beta^t s_{12}{}^t s_{11} & ; & -\beta^t s_{12}{}^t s_{22} & ; \quad \frac{1}{2} - \beta^t s_{12}{}^t s_{12} \\ \frac{\nu}{1-2\nu} - \beta^t s_{33}{}^t s_{11} & ; & \frac{\nu}{1-2\nu} - \beta^t s_{33}{}^t s_{22} & ; \quad -\beta^t s_{33}{}^t s_{12} \quad ; \quad \frac{1-\nu}{1-2\nu} - \beta^t s_{33}{}^t s_{33} \end{pmatrix} \tag{4.36}$$

where

$$\beta = \frac{3}{2}\frac{1}{{}^t\sigma_y^2}\left(\frac{1}{1 + \frac{{}^t H(1+\nu)}{E}}\right) \tag{4.37}$$

For a perfectly plastic material, ${}^{t}p_{ij} = 0$ and ${}^{t}H = 0$. For work-hardening materials, usually data from a simple tension test are known. Thus, in the case of linear hardening, if the strain-hardening modulus (tangential modulus) is available, ${}^{t}H$ can be derived from it, i.e.,

$$\frac{1}{{}^{t}H} = \frac{3}{2}\left(\frac{1}{{}^{t}E_T} - \frac{1}{E}\right) \tag{4.38}$$

in which ${}^{t}E_T$ is the strain-hardening modulus of the material.

Drucker-Prager Yield Condition

Using the Drucker-Prager yield criterion, the yield function is defined as [37]

$$F = 3\alpha\,{}^{t}\sigma_m + {}^{t}\bar{\sigma} - \sigma_y \tag{4.39}$$

where

$${}^{t}\bar{\sigma}^2 = 1/2\;{}^{t}s_{ij}\,{}^{t}s_{ij} \tag{4.40}$$

and α and σ_y are constant material properties derived from cohesion c and angle of friction θ. The following relations are used [37] [53]

$$\alpha = \frac{2\sin\theta}{\sqrt{3}(3-\sin\theta)} \tag{4.41}$$

$$\sigma_y = \frac{6c\cos\theta}{\sqrt{3}(3-\sin\theta)} \tag{4.42}$$

In general, c and θ may depend on a strain-hardening parameter. We consider the case of perfect plasticity, hence ${}^{t}p_{ij} = 0$. Furthermore, we have ${}^{t}q_{ij} = \alpha\delta_{ij} + \frac{1}{2\,{}^{t}\bar{\sigma}}\,{}^{t}s_{ij}$; i.e.

$${}^{t}q = \begin{bmatrix}\alpha\\ \alpha\\ 0\\ \alpha\end{bmatrix} + \frac{1}{2\,{}^{t}\bar{\sigma}}\begin{bmatrix}{}^{t}s_{11}\\ {}^{t}s_{22}\\ 2\,{}^{t}s_{12}\\ {}^{t}s_{33}\end{bmatrix} \tag{4.43}$$

Using $G = \frac{E}{2(1+\nu)}$ and $K = \frac{1}{3}\frac{E}{1-2\nu}$ we obtain

$$C^{EP} = \begin{pmatrix} K + 4/3G - (\beta_1 {}^t s_{11}+\beta_2)(\beta_1 {}^t s_{11}+\beta_2) & & & & \text{Symmetric} \\ K - 2/3G - (\beta_1 {}^t s_{11}+\beta_2)(\beta_1 {}^t s_{22}+\beta_2) & ; & K + 4/3G - (\beta_1 {}^t s_{22}+\beta_2)(\beta_1 {}^t s_{22}+\beta_2) & & \\ - (\beta_1 {}^t s_{11}+\beta_2)(\beta_1 {}^t s_{12}) & ; & - (\beta_1 {}^t s_{22}+\beta_2)(\beta_1 {}^t s_{12}) & ; & G - (\beta_1 {}^t s_{12})(\beta_1 {}^t s_{12}) \\ K - 2/3G - (\beta_1 {}^t s_{11}+\beta_2)(\beta_1 {}^t s_{33}+\beta_2) & ; & K - 2/3G - (\beta_1 {}^t s_{22}+\beta_2)(\beta_1 {}^t s_{33}+\beta_2) & ; & - (\beta_1 {}^t s_{12})(\beta_1 {}^t s_{33}+\beta_2) \\ & & K + 4/3G - (\beta_1 {}^t s_{33}+\beta_2)(\beta_1 {}^t s_{33}+\beta_2) & & \end{pmatrix} \quad (4.44)$$

in which $\beta_1 = \frac{G/{}^t\bar{\sigma}}{(G + 9K\alpha^2)^{\frac{1}{2}}}$; $\beta_2 = \frac{3K\alpha}{(G + 9K\alpha^2)^{\frac{1}{2}}}$

The computer implementation of the algorithm used in elastic-plastic analysis is given in Table 6. We should note that we are only concerned with the calculation of stress increments due to given strain increments, since the elastic-plastic stress-strain law is defined in terms of current total stresses.

T.L. Formulation

The material laws defined above can directly be employed in the T.L. formulation by using Green - Lagrange strain components and 2nd Piola - Kirchhoff stress components instead of infinitesimal strains and engineering stress components. For example, referring to Table 6, in the T.L. formulation, STRAIN are current total Green - Lagrange strains, EPS are the total Green - Lagrange strains available from the previous update, and DELEPS are increments in Green - Lagrange strains.

The ease of using the elastic-plastic analysis procedure already available from small displacement analysis in the T.L. formulation is apparent. However, the assumptions used should be noted, namely that all elastic-plasticity relations usually employed in small displacement analysis can also be used in the T.L. formulation [27].

U.L. Formulation

In the U.L. formulation we can use the procedure given in Eqs. (4.10) to (4.12), referred to as U.L. (T), or the procedure using the Jaumann stress rate, referred to as U.L. (J) and described in Eqs. (4.13) to (4.16).

Referring to Table 6, we have in both formulations Cauchy stresses stored in SIG. Also, we use linear strain increments referred to the configuration at time t, i.e. DELEPS contains linear strain increments in the same way as in small displacement analysis except that the incremental

strains are referred to the configuration established in the preceding solution. In the calculation of the yield function F and the value RATIO, we use the stress components defined in Eq. (4.11), in which ${}^{t+\Delta t}_{t}S_{ij}$ is understood to be an approximation to ${}^{t+\Delta t}\tau_{ij}$. Assuming that the yield function is defined in terms of Cauchy stresses, the above approximation is justifiable provided the incremental deformations are small enough. In order to be more exact it would be necessary to calculate Cauchy stresses whenever stress components are used.

In the U.L. (T) formulation the total final stress, which includes the stress increment due to DELEPS, is transformed to the new configuration using Eq. (4.12). In the U.L. (J) formulation this transformation is replaced using Eq. (4.13).

The main approximation in the analysis is the linearization of strains within each time step and the calculation of stress increments from the linear strain increments. This requires necessarily a small enough increment in stresses within each time step, and, therefore, the use of ${}^{t+\Delta t}_{t}S_{ij}$ as an approximation to ${}^{t+\Delta t}\tau_{ij}$ in the calculation of the yield condition appears justifiable (see above).

The effect of the linearization in the analysis of some problems is presented in Chapter 6.

TABLE 6. SOLUTION ALGORITHM FOR ELASTIC-PLASTIC STRESS CALCULATION

Given: STRAIN = total strains at time $t+\Delta t$

SIG = total stresses at time t

EPS = total strains at time t

The procedure below is used to calculate the total stresses TAU at time $t+\Delta t$. (We should note that the elastic-plastic incremental stress-strain law can be calculated, if the stresses are known.)

a. Calculate the strain increment DELEPS:

DELEPS = STRAIN - EPS

b. Calculate the stress increment DELSIG, assuming elastic behavior:

$DELSIG = C^{E} * DELEPS$

c. Calculate TAU:

TAU = SIG + DELSIG

d. With TAU as the state of stress, determine the value of the yield function F.

e. If $F(TAU) \leq 0$, elastic behavior assumption holds (loading elasticly or unloading).

Hence STRESS = TAU, and we return

If $F(TAU) > 0$ we continue

f. If the previous state of stress was plastic (as indicated by a flag) set RATIO = 0 and go to step (h). Otherwise, there is a transition from elastic to plastic, and RATIO, which is the portion of incremental strain taken elasticly, has to be

TABLE 6 (cont'd.)

determined. The variable RATIO is determined from the equation

$$F\{SIG + RATIO * DELSIG\} = 0$$

since at the stress SIG + RATIO * DELSIG the yield function F becomes equal to zero and yielding is initiated.

g. Redefine TAU as the stress at start of yield

$$TAU = SIG + RATIO * DELSIG$$

and calculate the elastic-plastic strain increment

$$DEPS = (1 - RATIO) * DELEPS$$

h. To obtain the final stresses, which include the effect of the complete strain increment DELEPS we need to add to TAU the stresses corresponding to the elastic-plastic strain increment DEPS. Since the material law is dependent on the current stresses, DEPS is divided into equal intervals and TAU is updated for each interval by the increments in stresses corresponding to the interval increments in elastic-plastic strains. In the calculations the stress-strain matrix corresponding to the latest available stress conditions are used.

4.4.5 Variable Tangent Moduli Model

The variable tangent moduli model was developed for the analysis of geological materials and is presented in detail in [38]. The model describes an isotropic hypoelastic material law, in which the bulk and shear moduli are functions of the stress and strain invariants. The functional relationships used replace an explicit yield condition.

Before presenting the model, it is convenient to define the notation adopted in this section. We consider in the following the analysis of small displacement problems. The use of the model in the T.L. and U.L. formulations is analogous to the use of the elastic-plastic models described in Section 4.4.4.

Notation used

$^{t}e_{ij}$ = total strains (the left superscript "t" always refers to time t)

e_{ij} = incremental strains

$^{t}e_{m} = {}^{t}e_{ii}/3$ = mean strain

$e_{m} = e_{ii}/3$ = incremental mean strain

$^{t}g_{ij} = {}^{t}e_{ij} - {}^{t}e_{m}\,\delta_{ij}$ = deviatoric strains

g_{ij} = incremental deviatoric strains

$^{t}\sigma_{ij}$ = total stresses

σ_{ij} = incremental stresses

$^{t}\sigma_{m} = {}^{t}\sigma_{ii}/3$ = mean stress

$\sigma_{m} = \sigma_{ii}/3$ = incremental mean stress

p_{min} = minimum mean stress ever reached

$^{t}s_{ij} = {}^{t}\sigma_{ij} - {}^{t}\sigma_{m}\ \delta_{ij}$ = deviatoric stresses

s_{ij} = incremental deviatoric stresses

$^{t}G,\ ^{t}K$ = shear and bulk moduli

$^{t}J_2 = \frac{1}{2}\ {}^{t}s_{ij}\ {}^{t}s_{ij}$ = 2nd invariant of stress deviator

The incremental stress-strain relations for the variable tangent moduli model are assumed to be

$$s_{ij} = 2\,{}^{t}G\ g_{ij} \tag{4.45}$$

and

$$\sigma_m = 3\,{}^{t}K\ e_m \tag{4.46}$$

where s_{ij} and g_{ij} are the incremental deviatoric stresses and strains, and σ_m and e_m are the incremental mean stress and strain. The instantaneous bulk and shear moduli, ^{t}G and ^{t}K, respectively, are functions of the loading conditions (loading or unloading), the mean strain $^{t}e_m$, the mean stress $^{t}\sigma_m$ and the second invariant of the stress deviator, $^{t}J_2$.

For the bulk modulus we have the condition of loading if $^{t}\sigma_m \leq p_{min}$, and the condition of unloading if $^{t}\sigma_m > p_{min}$, where p_{min} is the minimum mean stress ever reached during the history of solution, i.e.,

$$^{t}K = \begin{cases} {}^{t}K_{LD} & \text{when } {}^{t}\sigma_m \leq p_{min} \\ {}^{t}K_{UN} & \text{when } {}^{t}\sigma_m > p_{min} \end{cases} \tag{4.47}$$

We should note that as long as $^{t}\sigma_m > p_{min}$, K_{UN} is effective even though $^{t}\sigma_m$ may be decreasing, i.e. $^{t}\sigma_m < {}^{t-\Delta t}\sigma_m$. The loading and unloading bulk

moduli are calculated using

$$ {}^{t}K_{LD} = K_0 - K_1 \, {}^{t}e_m + K_2 \, {}^{t}e_m^2 \tag{4.48} $$

$$ {}^{t}K_{UN} = \text{constant} \tag{4.49} $$

in which K_0, K_1 and K_2 are constants.

For the shear behavior we have

$$ {}^{t}G = {}^{t}G_{LD} \quad \text{when} \quad {}^{t}J_2 > {}^{t-\Delta t}J_2 \tag{4.50} $$

$$ {}^{t}G = {}^{t}G_{UN} \quad \text{when} \quad {}^{t}J_2 \leq {}^{t-\Delta t}J_2 \tag{4.51} $$

in which the loading and unloading shear moduli are defined as

$$ {}^{t}G_{LD} = G_0 - \gamma_1 \, {}^{t}\sigma_m + \bar{\gamma}_1 \sqrt{{}^{t}J_2} \tag{4.52} $$

$$ {}^{t}G_{UN} = G_0 - \gamma_1 \, {}^{t}\sigma_m \tag{4.53} $$

where γ_1 and $\bar{\gamma}$ are constants. The material constants K_0, K_1, K_2, γ_1 and $\bar{\gamma}$, are determined by experiments, and have to fulfil certain conditions to admit only physically permissible states of stress and strain [38].

For the numerical solution Eqs. (4.45) and (4.46) are approximated at time t as follows:

$$ {}^{t+\Delta t}\sigma_m = 3 \, {}^{t}K \, ({}^{t+\Delta t}e_m - {}^{t}e_m) + {}^{t}\sigma_m \tag{4.54} $$

$$ {}^{t+\Delta t}s_{ij} = 2 \, {}^{t}G \, ({}^{t+\Delta t}g_{ij} - {}^{t}g_{ij}) + {}^{t}s_{ij} \tag{4.55} $$

To obtain ${}^{t}K$ and ${}^{t}G$ we need to know whether the loading or unloading conditions are active, and we need to have stored ${}^{t}e_m$, ${}^{t}\sigma_m$ and ${}^{t}J_2$ in order to be able to calculate the numerical values of ${}^{t}K$ and ${}^{t}G$. Assuming that the loading conditions at time 0 (with initial conditions on ${}^{0}e_m$, ${}^{0}\sigma_m$ and ${}^{0}J_2$) are known, we can use Eqs. (4.54) and (4.55) to perform the

incremental solution. It should be noted that the stresses at time $t+\Delta t$ are calculated using the material moduli pertaining to time t, which were also used in the calculation of the stiffness matrix at time t.

4.4.6 Curve Description Model

The curve description model is a simple incremental stress-strain law used to represent the response of geological materials. The model describes the instantaneous bulk and shear moduli as piecewise linear functions of the current volume strain (Fig. 4.3). An explicit yield condition is not used and whether the material is loading or unloading is determined by the history of the volume strain only.

The procedure of solution using the curve description model is essentially identical to the procedure using the variable tangent moduli model (see Section 4.4.5). We therefore adopt in this section the same notation as in Section 4.4.5. The difference between the curve description model and the variable tangent moduli model lies in the definition of the bulk and shear moduli and the loading and unloading criteria.

As in Section 4.4.5, we consider in this section only the analysis of small displacement problems. However, we should keep in mind that the implementation of the model in the T.L. and U.L. formulations would be analogous to the use of the elastic-plastic models in Section 4.4.4

The incremental stress-strain relations considered in the solution using the curve description model are those discussed already with the variable tangent moduli model, namely

$$s_{ij} = 2\,{}^{t}G\;g_{ij} \tag{4.56}$$

and

$$\sigma_m = 3\,{}^{t}K\;e_m \tag{4.57}$$

where s_{ij} and g_{ij} are incremental deviatoric stresses and strains, and σ_m and e_m are the incremental mean stress and strain. The instantaneous

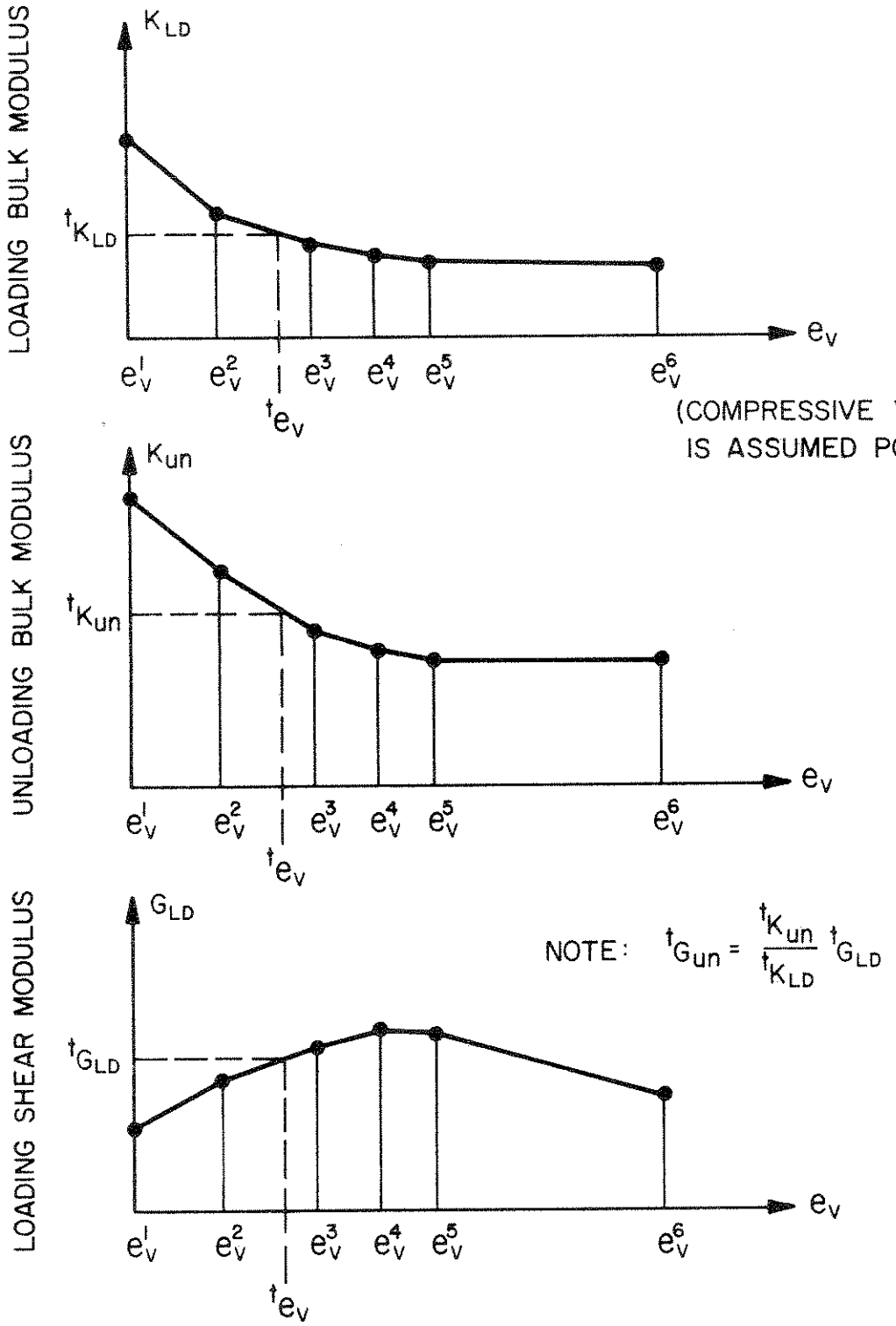

FIGURE 4.3 MODULI VERSUS VOLUME STRAIN FOR THE CURVE DESCRIPTION MODEL

bulk and shear moduli, ${}^{t}K$ and ${}^{t}G$, are functions of the loading condition and the volume strain ${}^{t}e_{v}$ is defined as

$$ {}^{t}e_{v} = e_{grav} + (-3\,{}^{t}e_{m}) \tag{4.58} $$

where e_{grav} is the volume strain (taken positive) due to gravity pressure and ${}^{t}e_{m}$ is the mean strain at time t. Defining e_{min} as the minimum mean strain ever reached during the solution, we have that the material is loading if ${}^{t}e_{m} \leq e_{min}$ and the material is unloading if ${}^{t}e_{m} > e_{min}$, i.e.

$$ {}^{t}K = \begin{cases} {}^{t}K_{LD} & \text{when } {}^{t}e_{m} \leq e_{min} \\ {}^{t}K_{UN} & \text{when } {}^{t}e_{m} > e_{min} \end{cases} \tag{4.59} $$

and

$$ {}^{t}G = \begin{cases} {}^{t}G_{LD} & \text{when } {}^{t}e_{m} \leq e_{min} \\ {}^{t}G_{UN} & \text{when } {}^{t}e_{m} > e_{min} \end{cases} \tag{4.60} $$

We should note that the loading conditions for both the bulk and the shear moduli are determined by the history of ${}^{t}e_{m}$ only. The values of ${}^{t}K_{LD}$, ${}^{t}K_{UN}$ and ${}^{t}G_{LD}$ are obtained using the curves in Fig. 4.3, and the modulus ${}^{t}G_{UN} = {}^{t}G_{LD} \, (\, {}^{t}K_{UN} / {}^{t}K_{LD} \,)$.

Once the calculation of the material moduli has been carried out, the solution using the curve description model proceeds in the same way as the incremental solution using the variable tangent moduli model. However, one important additional option is available, namely the material may weaken (crack) under loading conditions if tensile stresses exceed preassigned values.

Since the curve description model has been developed primarily for the analysis of geological materials, tension cut-off is assumed to occur once the principal tensile stresses due to the applied loading exceed the compressive stresses (taken positive) due to gravity pressure, i.e. the material is assumed not to be able to develop net tensile stresses (no-tension material). To model this material weakening the following assumptions are used:

(1) Once the principal tensile stress is equal to the gravity in-situ compressive stress, the material is treated as being orthotropic with the moduli corresponding to the direction of the principal tensile stress being reduced by a factor (usually 10^4). A factor may also be applied to reduce the shear stiffness.

(2) In successive load steps only tension cut-off in the direction determined in (1) and/or another one perpendicular to it may be active, i.e. no change in tension cut-off direction is considered. The decision if tension cut-off is active depends on if the tensile stress exceeds or does not exceed the virgin gravity compressive stress.

It should be noted that the curve description model with tension cut-off has essentially been developed for loading conditions only. The model may be understood to simulate "cracking" of the material as soon as net tensile stresses develop, i.e. the tensile stresses due to external loading are larger than the in-situ gravity pressure. The crack directions are perpendicular to the principal tensile stresses caused by the loading.

An application of the model including tension cut-off is presented in Chapter 6.

4.5 Three-Dimensional Element Models

It is apparent that all two-dimensional element models presented, with the exception of the hyperelastic model, could be extended for use in three-dimensional analysis. However, at this stage only the linear elastic isotropic and the curve description models have been implemented for the three-dimensional elements. Also, as pointed out in Section 3.3, only small displacement analyses can be considered.

4.5.1 Linear Elastic Isotropic Model

This model is a simple extension of the corresponding model used in two-dimensional analysis (see Section 4.4.1). In three-dimensional analysis the material matrix is

$$C = \begin{bmatrix} c_1 & c_2 & c_2 & 0 & 0 & 0 \\ & c_1 & c_2 & 0 & 0 & 0 \\ & & c_1 & 0 & 0 & 0 \\ & & & c_3 & 0 & 0 \\ & \text{symmetric} & & & c_3 & 0 \\ & & & & & c_3 \end{bmatrix} \tag{4.61}$$

where $c_1 = E(1-\nu)/((1+\nu)(1-2\nu))$; $c_2 = E\nu/((1+\nu)(1-2\nu))$; $c_3 = E/(2(1+\nu))$; E is Young's Modulus and ν is Poisson's ratio of the material. The stress and strain vectors in small displacement analysis, corresponding to the material matrix in Eq. (4.61), are

$$\begin{bmatrix} {}^{t}\sigma_{11} \\ {}^{t}\sigma_{22} \\ {}^{t}\sigma_{33} \\ {}^{t}\sigma_{12} \\ {}^{t}\sigma_{13} \\ {}^{t}\sigma_{23} \end{bmatrix} \quad ; \quad \begin{bmatrix} {}^{t}e_{11} \\ {}^{t}e_{22} \\ {}^{t}e_{33} \\ 2\,{}^{t}e_{12} \\ 2\,{}^{t}e_{13} \\ 2\,{}^{t}e_{23} \end{bmatrix}$$

respectively.

We should note again that the material matrix in Eq. 4.61) would also be used in the T.L. and U.L. formulations.

4.5.2 Curve Description Model

The curve description model in three-dimensional analysis is a simple extension of the corresponding two-dimensional model. The equations and procedures used are as described in Section 4.4.6, where now all six stress and strain components measured in three-dimensional analysis need be considered.

The capability of material weakening (cracking) has not yet been included in the three-dimensional curve description model.

5. STEP-BY-STEP SOLUTION

In the previous chapters we derived the matrices needed for the calculation of the element stiffness matrices, mass matrices and force vectors. Once the required element matrices have been calculated, we obtain the matrices corresponding to a system of elements using standard assemblage techniques [8] [53]. Including the effect of velocity dependent damping forces, the equilibrium equations for time $t+\Delta t$ are

$$M\ {}^{t+\Delta t}\ddot{u} + C\ {}^{t+\Delta t}\dot{u} + {}^{t}K\ u = {}^{t+\Delta t}R - {}^{t}F \qquad (5.1)$$

in which for the element assemblage

M = mass matrix

C = damping matrix

${}^{t}K$ = tangent stiffness matrix at time t which includes the linear and nonlinear strain stiffness matrices

${}^{t+\Delta t}R$ = vector of externally applied forces at time $t+\Delta t$

${}^{t}F$ = vector of nodal point forces equivalent to the stresses of the elements at time t

${}^{t+\Delta t}\ddot{u}$, ${}^{t+\Delta t}\dot{u}$ = vector of nodal point accelerations and velocities at time $t+\Delta t$

u = increment in nodal point displacements from time t to time $t+\Delta t$, i.e. $u = {}^{t+\Delta t}u - {}^{t}u$

In static analysis mass and damping effects are, of course, not included in Eq. (5.1). We should note that Eq. (5.1) may correspond to any one of Eqs. (3.7) to (3.10), which have been written for a single element. For this reason, additional subscripts and superscripts, as in Eq. (3.9) and (3.10), are not used to denote the stiffness matrix ${}^{t}K$ and the vector of nodal point forces ${}^{t}F$. Moreover, in program NONSAP the

total number of elements of an assemblage can be divided into elements which behave linearly (i.e. Eq. (3.7) is the governing equilibrium equation) and elements which are nonlinear. The nonlinear elements can again be subdivided into elements whose response is described using the T.L. or U.L. formulations, and elements with material nonlinearities only. Therefore, the tangent stiffness matrix ${}^{t}K$ and the vector of nodal point forces ${}^{t}F$ are the sum of contributions from elements governed by the equilibrium equations (3.7) to (3.10).

5.1 Numerical Time Integration

Equation (5.1) represents the incremental equilibrium equations to be solved in each time step using a numerical integration scheme. The accuracy of the step-by-step solution will naturally depend on the scheme used to solve Eq. (5.1) recursively. Various integration operators are currently used in practice. Although the properties of the operators have strictly only been established for the analysis of linear systems, many solutions in nonlinear analysis have been obtained. In NONSAP the Wilson θ - method and Newmark method can be used [6].

In the θ - method a linear variation of acceleration is assumed over the time increment $\tau = \theta \Delta t$, where (for unconditional stability in the analysis of linear systems) $\theta \geq 1.37$, and the equilibrium equations, Eq. (5.1), are considered at time $t + \tau$,

$$M\ {}^{t+\tau}\ddot{u} + C\ {}^{t+\tau}\dot{u} + {}^{t}K\ u = {}^{t+\tau}R - {}^{t}F \qquad (5.2)$$

where ${}^{t+\tau}R = {}^{t}R = \theta\ ({}^{t+\Delta t}R - {}^{t}R)$, and u is the change in displacement vector during the time interval t to $t+\tau$, i.e. $u = {}^{t+\tau}u - {}^{t}u$. Using the linear acceleration assumption it follows that

$${}^{t+\tau}\dot{u} = {}^{t}\dot{u} + \frac{\tau}{2}\ ({}^{t+\tau}\ddot{u} + {}^{t}\ddot{u}) \qquad (5.3)$$

$${}^{t+\tau}u = {}^{t}u + \tau\ {}^{t}\dot{u} + \frac{\tau^2}{6}\ ({}^{t+\tau}\ddot{u} + 2\,{}^{t}\ddot{u}) \qquad (5.4)$$

which gives

$${}^{t+\tau}\ddot{u} = \frac{6}{\tau^2}\ u - \frac{6}{\tau}\ {}^{t}\dot{u} - 2\,{}^{t}\ddot{u} \qquad (5.5)$$

and

$$ {}^{t+\tau}\dot{u} = \frac{3}{\tau}\, u - 2\,{}^{t}\dot{u} - \frac{\tau}{2}\,{}^{t}\ddot{u} \qquad (5.6) $$

Substituting the relations (5.5) and (5.6) into Eq. (5.2), an equation with u as the only unknown is obtained. Solving for u and using the linear acceleration assumption, the required displacement, velocity and acceleration vectors are obtained,

$$ {}^{t+\Delta t}\ddot{u} = \left(1 - \frac{1}{\theta}\right) {}^{t}\ddot{u} + \frac{1}{\theta}\,{}^{t+\tau}\ddot{u} \qquad (5.7) $$

$$ {}^{t+\Delta t}\dot{u} = {}^{t}\dot{u} + \frac{\Delta t}{2}\left({}^{t}\ddot{u} + {}^{t+\Delta t}\ddot{u}\right) \qquad (5.8) $$

$$ {}^{t+\Delta t}u = {}^{t}u + \Delta t\,{}^{t}\dot{u} + \frac{\Delta t^2}{6}\left({}^{t+\Delta t}\ddot{u} + 2\,{}^{t}\ddot{u}\right) \qquad (5.9) $$

In the Newmark method, the following assumptions are made [6] [39],

$$ {}^{t+\Delta t}u = {}^{t}u + \Delta t\,{}^{t}\dot{u} + \frac{\Delta t^2}{2}\,{}^{t}\ddot{u} + \alpha\,\Delta t^2\left({}^{t+\Delta t}\ddot{u} - {}^{t}\ddot{u}\right) \qquad (5.10) $$

$$ {}^{t+\Delta t}\dot{u} = {}^{t}\dot{u} + \Delta t\,{}^{t}\ddot{u} + \delta\,\Delta t\left({}^{t+\Delta t}\ddot{u} - {}^{t}\ddot{u}\right) \qquad (5.11) $$

where, in linear analysis, for unconditional stability $\delta \geq \frac{1}{2}$ and $\alpha \geq \frac{1}{4}\,(\gamma + \frac{1}{2})^2$. Using Eqs. (5.1), (5.10) and (5.11) we can solve for the displacements, velocities and accelerations at time $t+\Delta t$ by simple elimination.

5.2 Equilibrium Iteration

It is important to realize that in nonlinear analysis Eq. (5.1) is only an approximation to the actual equation to be solved in each time step, which is Eq. (2.1). Equation (5.1) was obtained by linearizing the equations of motion as shown in Tables 1 and 2. Depending on the nonlinearities in the system and the magnitude of the time step Δt, the linearization may introduce serious errors and, indeed, solution instability. It should be noted that the step-by-step solution may become unstable although an integration operator is used which is unconditionally stable in linear analysis.

A common observation is that the errors introduced as a consequence of the linearization cause the calculated solution to "drift away" from the exact solution. This is much more serious in dynamic analysis than in static analysis, since, in dynamic analysis, the solution for any prescribed load at a specific time is always dependent on the history of solution.

In order to avoid large integration errors we may choose to iterate in each load step until, within the necessary assumptions on the variation of the material constants and the numerical time integration scheme used, Eq. 2.1) is satisfied within a required tolerance. The equations solved in the iteration depend on the nonlinear finite element formulation used, and are extensions of the incremental equations derived in Chapter 3. Considering as before a single finite element, in the T.L. formulation the equation used for iteration is obtained from Eq. (3.9), and is written as

$$\left({}^{t}_{0}K_{L} + {}^{t}_{0}K_{NL} \right) \Delta u^{(i)} = {}^{t+\Delta t}R - {}^{t+\Delta t}_{0}F^{(i-1)} - M \, {}^{t+\Delta t}\ddot{u}^{(i)} \qquad (5.12)$$

$$i = 1,2,3 \ldots$$

where ${}^{t+\Delta t}u^{(i)} = {}^{t+\Delta t}u^{(i-1)} + \Delta u^{(i)}$.

It should be noted that for i = 1 Eq. (5.12) corresponds to Eq. (3.9), i.e. $\Delta u^{(1)} = u$, ${}^{t+\Delta t}\ddot{u}^{(1)} = {}^{t+\Delta t}\ddot{u}$, ${}^{t+\Delta t}u^{(0)} = {}^{t}u$ and ${}^{t+\Delta t}_{0}F^{(0)} = {}^{t}_{0}F$.

The calculation of the acceleration approximation ${}^{t+\Delta t}\ddot{u}^{(i)}$ depends on the time integration scheme used.

The vector of internal resisting forces ${}^{t+\Delta t}_{0}F^{(i)}$ is the finite element evaluation of $\int_{0V}^{t+\Delta t} {}_{0}S_{ij}^{(i)} \; \delta \, {}^{t+\Delta t}_{0}\epsilon_{ij}^{(i)} \; {}^{0}dv$, where the superscript (i) shows that stresses and strains are evaluated using ${}^{t+\Delta t}u^{(i)}$. Since

$$\delta \, {}^{t+\Delta t}_{0}\epsilon_{ij} = \tfrac{1}{2} \left(\delta {}_{0}u_{i,j} + \delta {}_{0}u_{j,i} + {}^{t+\Delta t}_{0}u_{k,i} \, \delta {}_{0}u_{k,j} + {}^{t+\Delta t}_{0}u_{k,j} \, \delta {}_{0}u_{k,i} \right)$$

we have

$${}^{t+\Delta t}_{0}F^{(i)} = \int_{0V}^{t+\Delta t} {}_{0}B_{L}^{(i)T} \; {}^{t+\Delta t}_{0}\hat{S}^{(i)} \; {}^{0}dv \qquad (5.13)$$

where the matrices ${}^{t+\Delta t}_{0}B_{L}^{(i)}$ and ${}^{t+\Delta t}_{0}\hat{S}^{(i)}$ correspond to the matrices ${}^{t}_{0}B_{L}$ and ${}^{t}_{0}\hat{S}$ in Table 4A, respectively.

In the U.L. formulation the equation used for a single element with equilibrium iteration is

$$\left({}^{t}_{t}K_{L} + {}^{t}_{t}K_{NL} \right) \Delta u^{(i)} = {}^{t+\Delta t}R - {}^{t+\Delta t}_{t+\Delta t}F^{(i-1)} - M \, {}^{t+\Delta t}\ddot{u}^{(i)} \qquad (5.14)$$

$$i = 1,2,3 \ldots$$

---

in which the i'th displacement and acceleration approximations are calculated as above and ${}^{t+\Delta t}_{t+\Delta t}F^{(i)}$ is the finite element evaluation of

$$\int_{t+\Delta t_V(i)}^{t+\Delta t_\tau(i)} {}_{t+\Delta t}\delta e_{ij}^{(i)} \; {}^{t+\Delta t}_{dv}(i) \quad ; \quad \text{i.e.}$$

$$ {}^{t+\Delta t}_{t+\Delta t}F(i) = \int_{t+\Delta t_V(i)}^{t+\Delta t_{B_L}(i)T} {}^{t+\Delta t}_{t+\Delta t}\hat{\tau}(i) \; {}^{t+\Delta t}_{dv}(i) \qquad (5.15)$$

where the matrices ${}^{t+\Delta t}_{t+\Delta t}B_L(i)$ and ${}^{t+\Delta t}_{t+\Delta t}\hat{\tau}(i)$ correspond to the matrices ${}^{t}_{t}B_L$ and ${}^{t}_{t}\hat{\tau}$ in Table 4B, respectively.

The equation used in analysis with material nonlinearities only is obtained from Eq. (5.12), or Eq. (5.15), by assuming that the configuration of the element does not change and that all strains are small, i.e. products of displacement derivatives in the strain calculations can be neglected. In this case we obtain with the previously used notation,

$$ {}^{t}K \; \Delta u^{(i)} = {}^{t+\Delta t}R - {}^{t+\Delta t}F(i-1) - M \; {}^{t+\Delta t}\ddot{u}(i) \qquad (5.16)$$

$$i = 1,2,3 \ldots$$

where ${}^{t+\Delta t}F(i)$ is the finite element evaluation of $\int_{0_V}^{t+\Delta t} {}^{(i)}_{ij} \; \delta e_{ij}^{(i)} \; {}^{0}dv$, i.e.,

$$ {}^{t+\Delta t}F(i) = \int_{0_V} B_L^T \; {}^{t+\Delta t}_{\Sigma}\hat{}(i) \; {}^{0}dv. \qquad (5.17)$$

For an assemblage of elements which are described as linear, materially nonlinear only, by the T.L. or the U.L. formulations, we have corresponding to Eq. (5.1) the following equilibrium iteration,

$$ {}^{t}K \; \Delta u^{(i)} = {}^{t+\Delta t}R - {}^{t+\Delta t}F(i-1) - M \; {}^{t+\Delta t}\ddot{u}(i) - C \; {}^{t+\Delta t}\dot{u}(i) \qquad (5.18)$$

$$i = 1,2,3 \ldots$$

in which the iteration vectors are now defined for the element assemblage, and an appropriate convergence measure need be employed [40]. Equation (5.18) is used in the Newmark integration scheme, whereas using the Wilson θ-method, the equilibrium iteration is performed for time $t + \tau$.

The equilibrium iteration in Eq. (5.18) (and Eqs. (5.12), (5.14) and (5.16)) corresponds to a Newton iteration with a constant stiffness matrix [40]. It should be noted that provided convergence occurs, and the material description used is not path dependent, i.e. the material is elastic or hyperelastic, the "exact" solution within the assumption of the time integration operator and the convergence tolerance is obtained. It follows also that in the dynamic analysis of geometrically nonlinear systems with elastic or hyperelastic materials, we do not need to form a new stiffness matrix in each time step, but can assure solution accuracy using equilibrium iteration. In the analysis of systems with path dependent material properties, however, the solution path is determined by the tangent stiffness matrix and sufficiently small load steps are required for solution accuracy.

In program NONSAP we can specify an interval of time steps for formation of a new tangent stiffness matrix, and a second interval of time steps in which equilibrium iterations are to be performed. Table 7 gives the step-by-step time integration scheme used in the program. It is noted that the same constants are defined for the Wilson θ-method and the Newmark method in order to have one computer algorithm for both integration schemes. In the iteration the convergence tolerance used is the ratio of the Euclidian norms of incremental displacements and total displacements.

TABLE 7 SUMMARY OF STEP-BY-STEP INTEGRATION

- - INITIAL CALCULATIONS - - -

1. Form linear stiffness matrix K, mass matrix M and damping matrix C; initialize ${}^0u$, ${}^0\dot{u}$, ${}^0\ddot{u}$

2. Calculate the following constants:

   tol ≤ 0.01 ; nitem ≥ 3 ; in static analysis $\theta = 1$ and go to 3.

   Wilson θ-method : $\theta \geq 1.37$, usually $\theta = 1.4$, $\tau = \theta\Delta t$

   $a_0 = 6/\tau^2$ $a_1 = 3/\tau$ $a_2 = 2a_1$ $a_3 = 2$

   $a_4 = 2$ $a_5 = \tau/2$ $a_6 = a_0/\theta$ $a_7 = -a_2/\theta$

   $a_8 = 1 - 3/\theta$ $a_9 = \Delta t/2$ $a_{10} = \Delta t^2/6$

   Newmark method: $\theta = 1.0$, $\delta \geq 0.50$, $\alpha \geq 0.25\ (0.5 + \delta)^2$, $\tau = \Delta t$

   $a_0 = 1/(\alpha\Delta t^2)$ $a_1 = \delta/(\alpha\Delta t)$ $a_2 = 1/(\alpha\Delta t)$ $a_3 = 1/(2\alpha) - 1$

   $a_4 = \delta/\alpha - 1$ $a_5 = \Delta t(\delta/\alpha - 2)/2$ $a_6 = a_0$ $a_7 = -a_2$

   $a_8 = -a_3$ $a_9 = \Delta t(1 - \delta)$ $a_{10} = \delta\Delta t$

3. Form effective linear stiffness matrix: $\hat{K} = K + a_0M + a_1C$

4. In linear analysis triangularize $\hat{K}$

TABLE 7 (cont'd.)

- - FOR EACH TIMESTEP - - -

A. IN LINEAR ANALYSIS

(i) Form effective loadvector:

$$^{t+\tau}\hat{R} = {}^{t}R + \theta({}^{t+\Delta t}R - {}^{t}R) + M(a_0\,{}^{t}u + a_2\,{}^{t}\dot{u} + a_3\,{}^{t}\ddot{u}) + C(a_1\,{}^{t}u + a_4\,{}^{t}\dot{u} + a_5\,{}^{t}\ddot{u})$$

(ii) Solve for displacement increments:

$$\hat{K}\,{}^{t+\tau}u = {}^{t+\tau}\hat{R} \quad ; \quad u = {}^{t+\tau}u - {}^{t}u$$

(iii) Go to C.

B. IN NONLINEAR ANALYSIS

(i) If a new stiffness matrix is to be formed, update $\hat{K}$ for nonlinear stiffness effects to obtain $^{t}\hat{K}$; triangularize $^{t}\hat{K}$:

$$^{t}\hat{K} = LDL^{T}$$

(ii) Form effective load vector:

$$^{t+\tau}\hat{R} = {}^{t}R + \theta({}^{t+\Delta t}R - {}^{t}R) + M\,(a_2\,{}^{t}\dot{u} + a_3\,{}^{t}\ddot{u}) + C\,(a_4\,{}^{t}\dot{u} + a_5\,{}^{t}\ddot{u}) - {}^{t}F$$

(iii) Solve for displacement increments using latest D,L factors:

$$LDL^{T}\,u = {}^{t+\tau}\hat{R}$$

TABLE 7 (cont'd.)

B. IN NONLINEAR ANALYSIS (cont'd.)

(iv) If required, iterate for dynamic equilibrium; then initialize $u^{(0)} = u$, $i = 0$

(a) $i = i + 1$

(b) Calculate (i-1)st approximation to accelerations, velocities, and displacements:

$$ {}^{t+\tau}\ddot{u}^{(i-1)} = a_0 u^{(i-1)} - a_2 {}^{t}\dot{u} - a_3 {}^{t}\ddot{u} \; ; \quad {}^{t+\tau}\dot{u}^{(i-1)} = a_1 u^{(i-1)} - a_4 {}^{t}\dot{u} - a_5 {}^{t}\ddot{u} \; ; $$

$$ {}^{t+\tau}u^{(i-1)} = {}^{t}u + u^{(i-1)} $$

(c) Calculate (i-1)st effective out-of-balance loads:

$$ {}^{t+\tau}\hat{R}^{(i-1)} = {}^{t}R + \theta({}^{t+\Delta t}R - {}^{t}R) - M\,{}^{t+\tau}\ddot{u}^{(i-1)} - C\,{}^{t+\tau}\dot{u}^{(i-1)} - {}^{t+\tau}F^{(i-1)} $$

(d) Solve for i'th correction to displacement increments:

$$ LDL^{T}\,\Delta u^{(i)} = {}^{t+\tau}\hat{R}^{(i-1)} $$

(e) Calculate new displacement increments:

$$ u^{(i)} = u^{(i-1)} + \Delta u^{(i)} $$

TABLE 7 (cont'd.)

B. IN NONLINEAR ANALYSIS (cont'd.)

(iv) If required, iterate for dynamic equilibrium; then initialize $u^{(0)} = u$, $i = 0$ (cont'd.)

(f) Iteration convergence if $\|\Delta u^{(i)}\|_2 / \|u^{(i)} + {}^t u\|_2 < tol$

If convergence: $u = u^{(i)}$ and go to C;

If no convergence and $i <$ nitem: go to (a); otherwise restart using new stiffness matrix and/or a smaller time step size.

C. CALCULATE NEW ACCELERATIONS, VELOCITIES, AND DISPLACEMENTS

Wilson θ-method:

$$
\begin{aligned}
{}^{t+\Delta t}\ddot{u} &= a_6 u + a_7 {}^t\dot{u} + a_8 {}^t\ddot{u} \\
{}^{t+\Delta t}\dot{u} &= {}^t\dot{u} + a_9 ({}^{t+\Delta t}\ddot{u} + {}^t\ddot{u}) \\
{}^{t+\Delta t}u &= {}^t u + \Delta t {}^t\dot{u} + a_{10} ({}^{t+\Delta t}\ddot{u} + 2 {}^t\ddot{u})
\end{aligned}
$$

Newmark method:

$$
\begin{aligned}
{}^{t+\Delta t}\ddot{u} &= a_6 u + a_7 {}^t\dot{u} + a_8 {}^t\ddot{u} \\
{}^{t+\Delta t}\dot{u} &= {}^t\dot{u} + a_9 {}^t\ddot{u} + a_{10} {}^{t+\Delta t}\ddot{u} \\
{}^{t+\Delta t}u &= {}^t u + u
\end{aligned}
$$

The importance of equilibrium iteration depends on the problem considered, and is more pronounced in problems which allow relatively large load steps, i.e. the solution is not highly path dependent. If equilibrium iteration is to be allowed, the subroutine calculating the material law and stress components has to be programmed accordingly. In program NONSAP, the curve description model and the variable tangent moduli model have not been prepared to allow for equilibrium iteration, since solutions using these models would probably always require small load steps. The effect of equilibrium iteration in the analysis of some problems using the other material models is demonstrated in the next chapter.

6. SAMPLE SOLUTIONS

The sample analyses presented in this chapter have been selected with some main objectives. The first aim was to present solutions which demonstrate some of the analysis capabilities of program NONSAP. Therefore, linear, geometrically nonlinear and materially nonlinear analyses are presented, using the different formulations, elements and material models available in the program.

A further objective was to study the accuracy and stability of the solutions. Therefore, comparisons with the structural response predicted by other researchers are given. In this context, the importance of equilibrium iteration in some analyses was investigated.

Since various nonlinear formulations have been tested in the program, the important differences had to be studied that are obtained using the materially nonlinear only formulation, the T.L., U.L., U.L.(T) and U.L.(J) formulations.

Throughout this chapter reference is made to the theory presented in the preceding chapters. The solutions have been obtained using the algorithm presented in Table 7, in which the selected parameters were tol = 0.001, nitem = 15, $\theta = 1.4$, $\delta = 0.50$ and $\alpha = 0.25$. Therefore, the Newmark constant average acceleration method and the Wilson θ-method have been used with a maximum number of 15 equilibrium iterations and a tolerance for three digit accuracy on the displacement vectors.

In the dynamic analyses nearly always one or two equilibrium iterations were sufficient in each time step. In the static analyses the number of iterations was dependent on the magnitude of the load steps

used. An important problem is the optimization of the load steps in nonlinear analyses. However, in this work, no specific attention has so far been given to this problem; and no attempt was made in the static response calculations to optimize the solution times (see Chapter 7). But it should be noted that the order of all systems considered in this report was small and the computer time used rather negligible.

In the sample solutions the time step used in an analysis is denoted by Δt and has been selected as a reasonable fraction of the fundamental period, T_f, at time 0 of the structure considered. In all dynamic analyses zero initial conditions on the displacements, velocities and accelerations have been assumed.

6.1 Static Collapse Analysis of a Simple Truss

The simple truss structure shown in Fig. 6.1 was analyzed for load deflection response including material yielding and large displacement effects. Since the loading was monotonically increased, the nonlinear elastic stress-strain model could be used to simulate the elastic-plastic material behavior with strain hardening.

Figure 6.1 shows the elastic-plastic displacement response of the truss. As can readily be verified, since large displacement effects are initially negligible, yielding of the diagonal truss bar occurs at the load P = 18 kip, after which the displacements increase rapidly with increasing load.

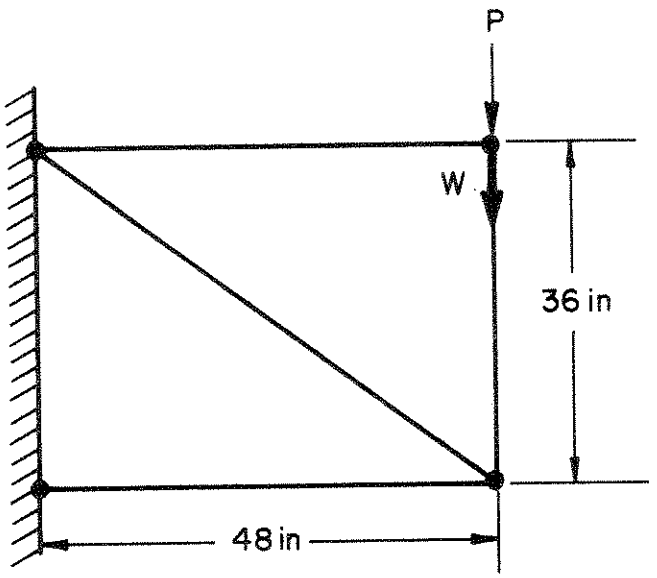

$A = 1\ in^2$
$E = 3 \times 10^4\ kip/in^2$
$\sigma_y = 30\ kip/in^2$
$E_T = 300\ kip/in^2$

SIMPLE TRUSS STRUCTURE

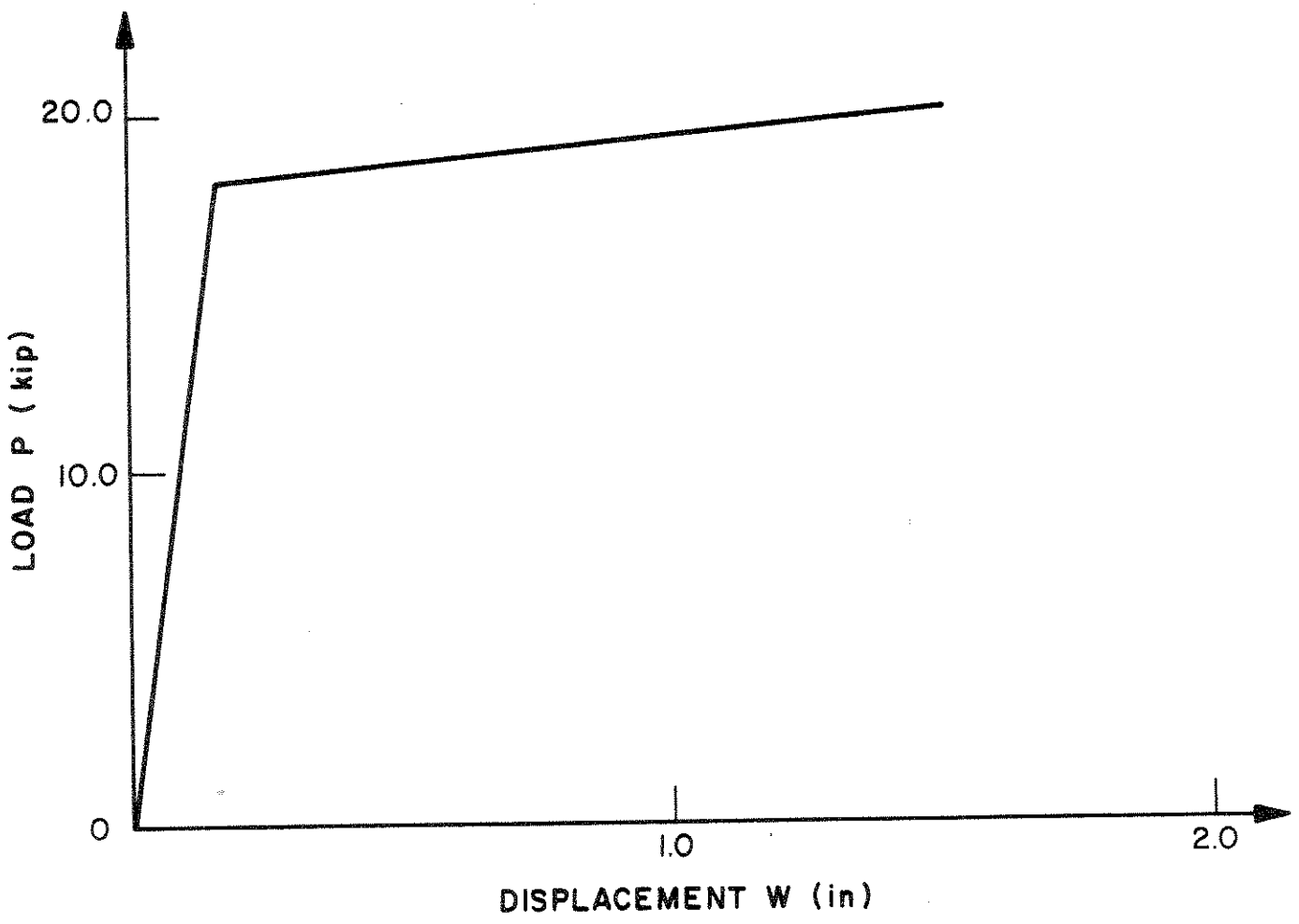

FIGURE 6.1 LOAD DEFLECTION RESPONSE OF SIMPLE TRUSS

6.2 Static and Frequency Analysis of a Tower Cable

The cable stretched between a ground anchor point and a tower attach point shown in Fig. 6.2 was analyzed for static displacements and frequencies of vibration. The cable was modelled using 12 truss elements of linear elastic material as shown in Fig. 6.2 . The initial tension in the cable was 7520.00 lb. Insulators weighing 510 lb each were located at nodes 2, 4 and 6, and a cluster of 6 insulators totaling 3060 lb was located at node 8. Nodes 3, 5, 7 and 9 through 12 are intermediate nodes located along the cable without insulators. The total vertical load acting on the cable nodes was 5677.83 lb which includes the insulator weights and the cable self-weight.

Figure 6.2 shows the cable in the static equilibrium configuration with the total load applied. The nonlinear displacement response of node 8 is shown in Fig. 6.3 . Twenty equal load steps with a new stiffness matrix being calculated in every second step were used to reach the final cable configuration, and an average of four equilibrium iterations were performed in each load step.

For the frequency analysis a lumped mass matrix of the cable has been assumed to which the masses of insulators have been added. The periods of vibration of the cable about the static equilibrium configuration are given in Table 8.

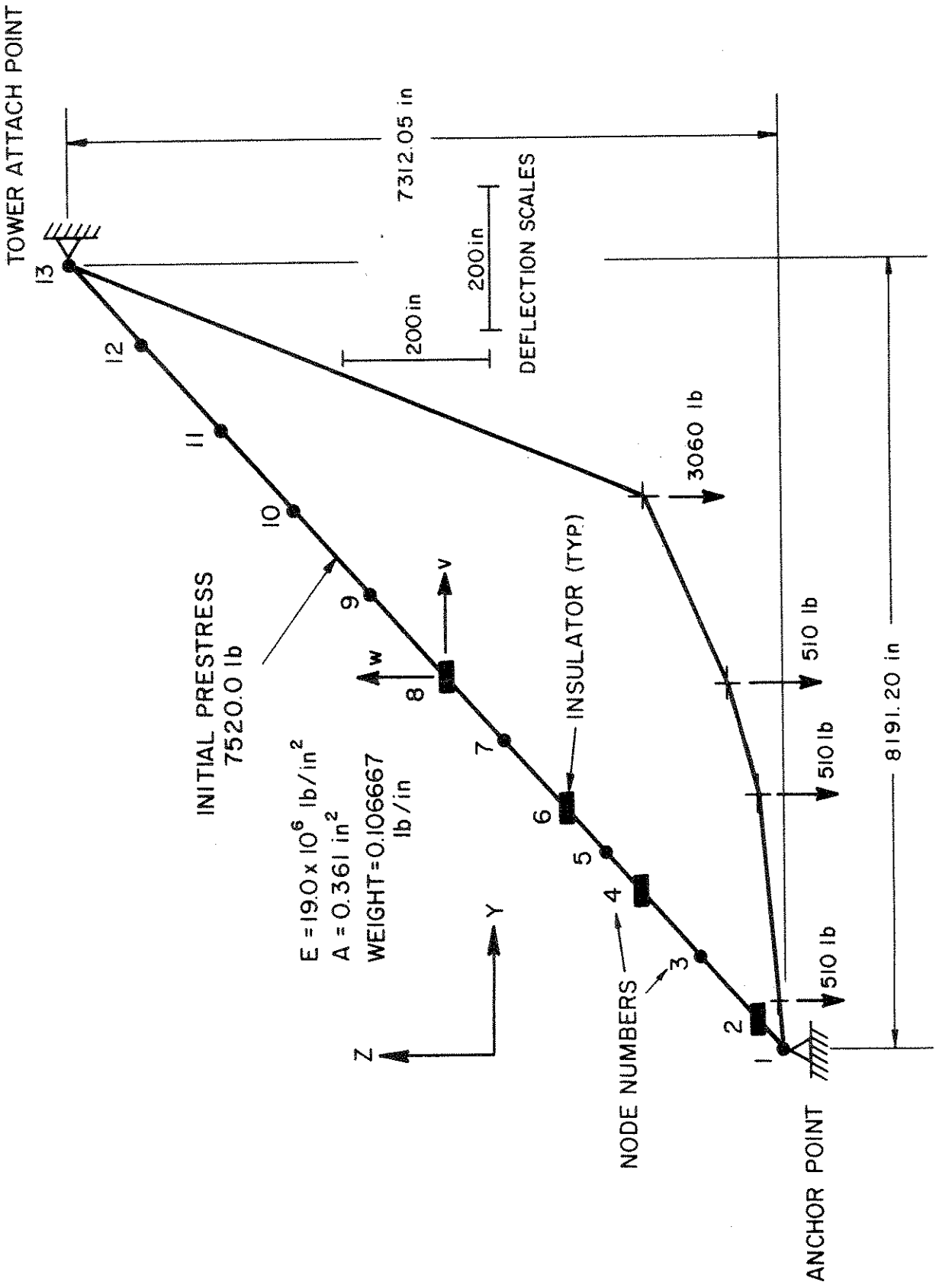

FIGURE 6.2 STATIC CONFIGURATION OF TOWER CABLE

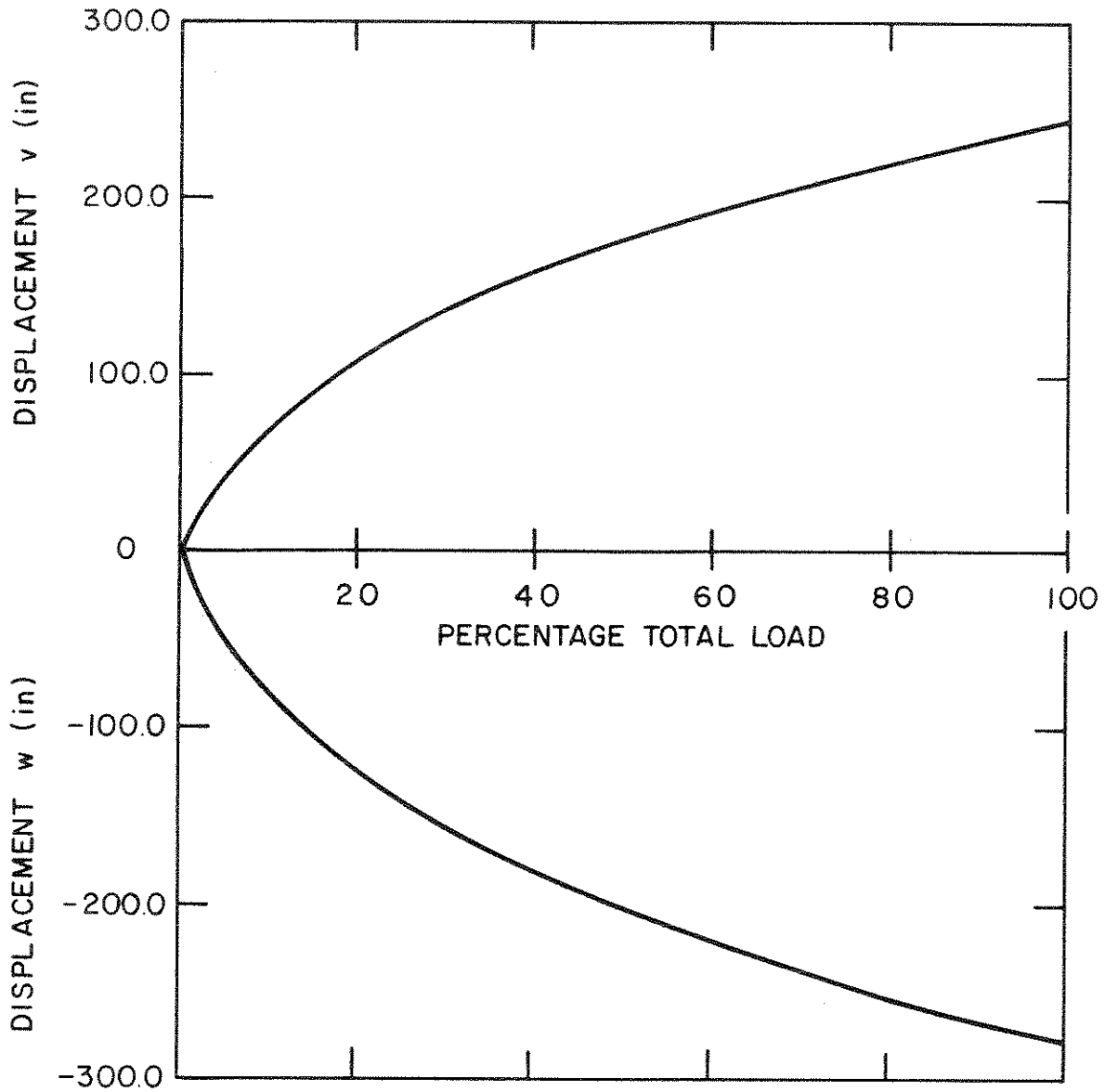

FIGURE 6.3 LOAD DEFLECTION CURVE OF TOWER CABLE

Table 8 . Vibration Periods of Cable in Static Equilibrium Configuration.

MODE NUMBER	PERIOD (SEC)
1	3.693
2	1.654
3	0.8571
4	0.8298
5	0.6660

6.3 Static and Dynamic Large Displacement Analysis of a Cantilever

The cantilever in Fig. 6.4 under uniformly distributed load was analyzed using a finite element idealization of five 8-node plane stress elements. The material of the cantilever was assumed to be isotropic linear elastic (see Section 4.4.1).

The first purpose of the static analysis was to compare the results obtained using the T.L., U.L., U.L.(T), and U.L.(J) formulations in a large displacement problem. In the U.L.(T) and U.L.(J) formulations the stress and material law calculations have been carried out as described in Section 4.4.4, where it should be noted that to prevent plastic response the yield stress of the material was selected sufficiently high.

The purpose of the dynamic analysis was to test the Wilson θ and Newmark integration schemes. The importance of equilibrium iterations was also investigated.

The static solution of the cantilever using the four available formulations and a total of 100 equal load steps is shown in Fig. 6.5 and compared with an analytical solution obtained by Holden [20]. Excellent agreement between all solutions is observed. It should be noted that the linearization inherent in the U.L.(T) and U.L.(J) formulations, and the use of the same material constants E and ν in all formulations have in this analysis negligible effect.

The static solutions employing the four formulations have also been obtained using only 5 equal load steps to reach the final configuration of the beam. Figure 6.6 shows the different response curves calculated, where it is seen that the U.L.(T) and U.L.(J) formulations give in this analysis a much better solution than the T.L. and U.L. formulations.

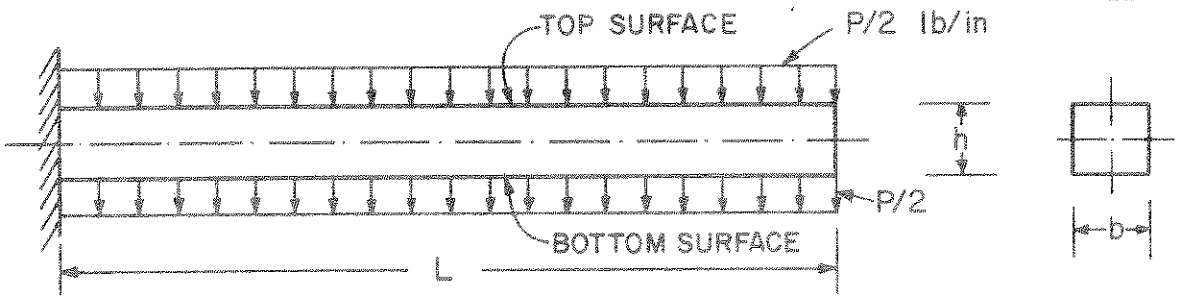

$L = 10$ in $\quad E = 1.2 \times 10^4$ lb/in^2

$h = 1$ in $\quad \nu = 0.2$

$b = 1$ in

FIGURE 6.4 CANTILEVER UNDER UNIFORMLY DISTRIBUTED LOAD

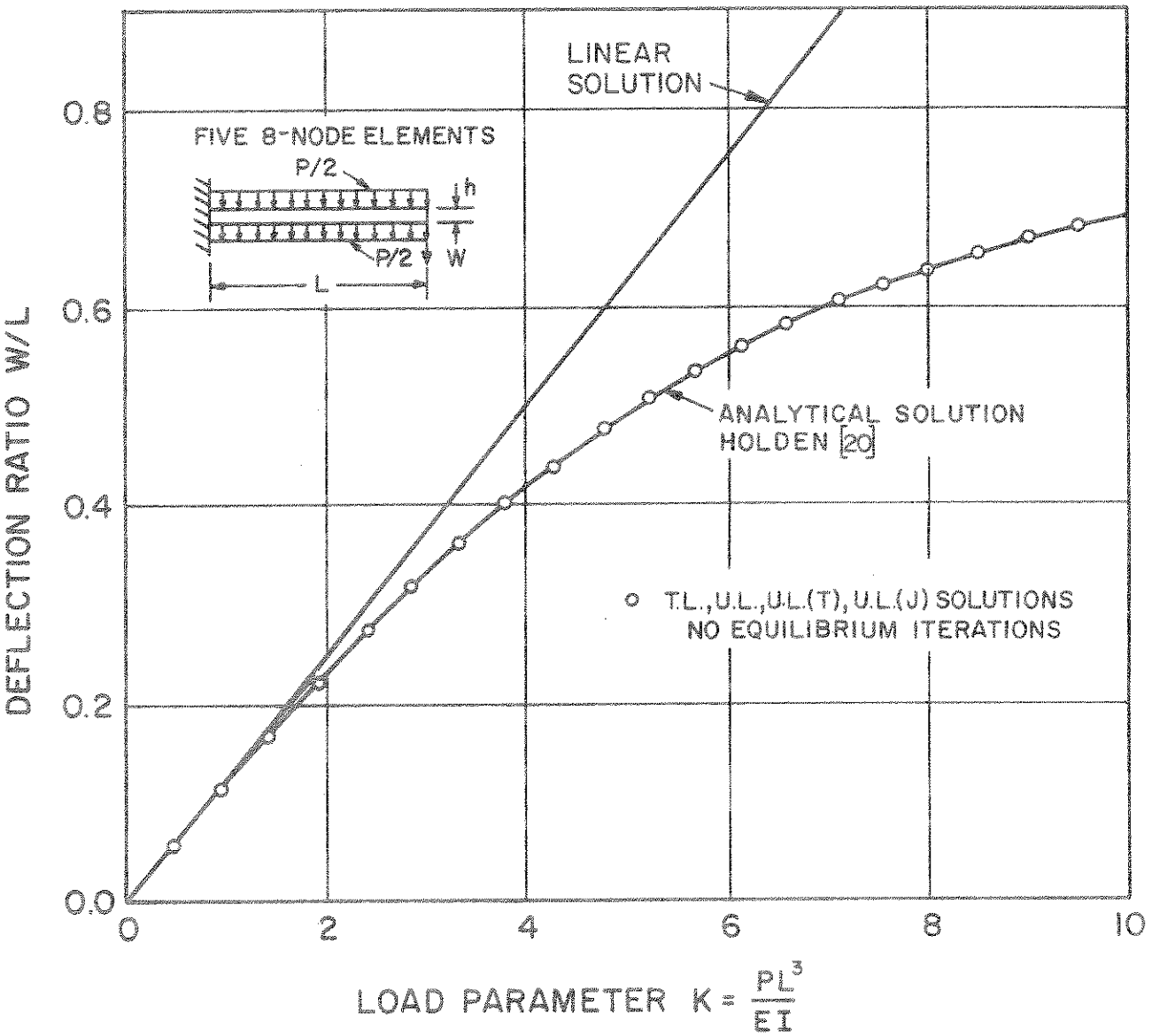

FIGURE 6.5 LARGE DEFLECTION ANALYSIS OF CANTILEVER UNDER UNIFORMLY DISTRIBUTED LOAD

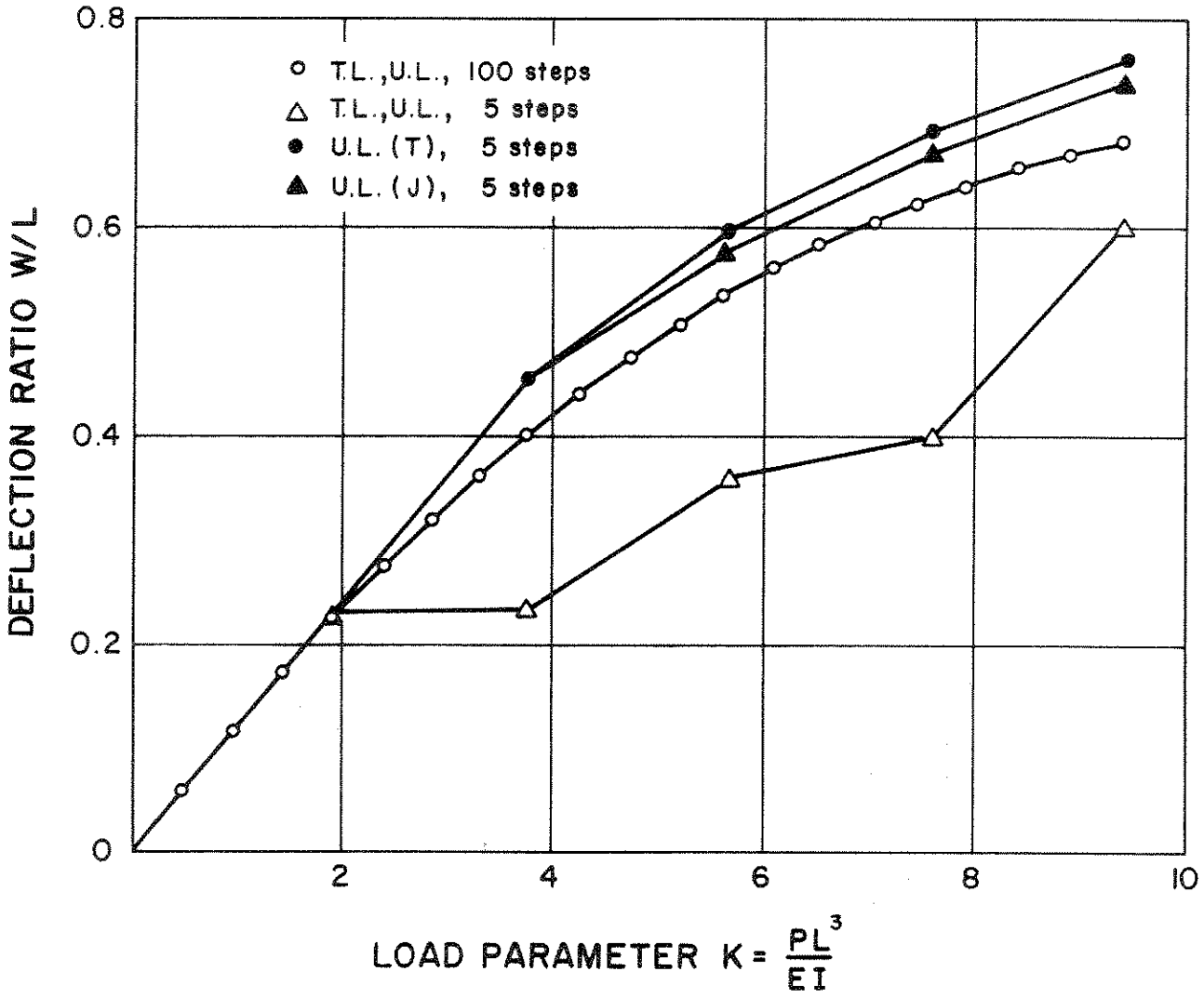

FIGURE 6.6 LARGE DEFLECTION ANALYSIS OF CANTILEVER, COMPARISON OF NONLINEAR FORMULATIONS

For the dynamic analysis the T.L. formulation was selected. Figures 6.7 and 6.8 show the results obtained using the Wilson θ and Newmark integration schemes. It is seen that for a time step $\Delta t \cong T_f/126$, where T_f is the fundamental period of the cantilever, the solutions using the two integration methods give practically the same results. However, if $\Delta t \cong T_f/42$ the equilibrium iteration in the Newmark integration scheme improves the solution a great deal, as shown in Fig. 6.8 . In this analysis an average of 4 iterations were required. Using the Wilson θ integration method with $\Delta t \cong T_f/42$ the same improvement in accuracy could not be obtained, since shortly before the occurrence of the peak response, the equilibrium iteration failed to converge.

It should be noted that a main characteristic of the cantilever is that the structure stiffens with increasing displacement, which, as shown in Figs. 6.7 and 6.8 , results in a substantial decrease in amplitude and effective period of vibration. It is the stiffening of the structure that can result in convergence difficulties in equilibrium iteration [40].

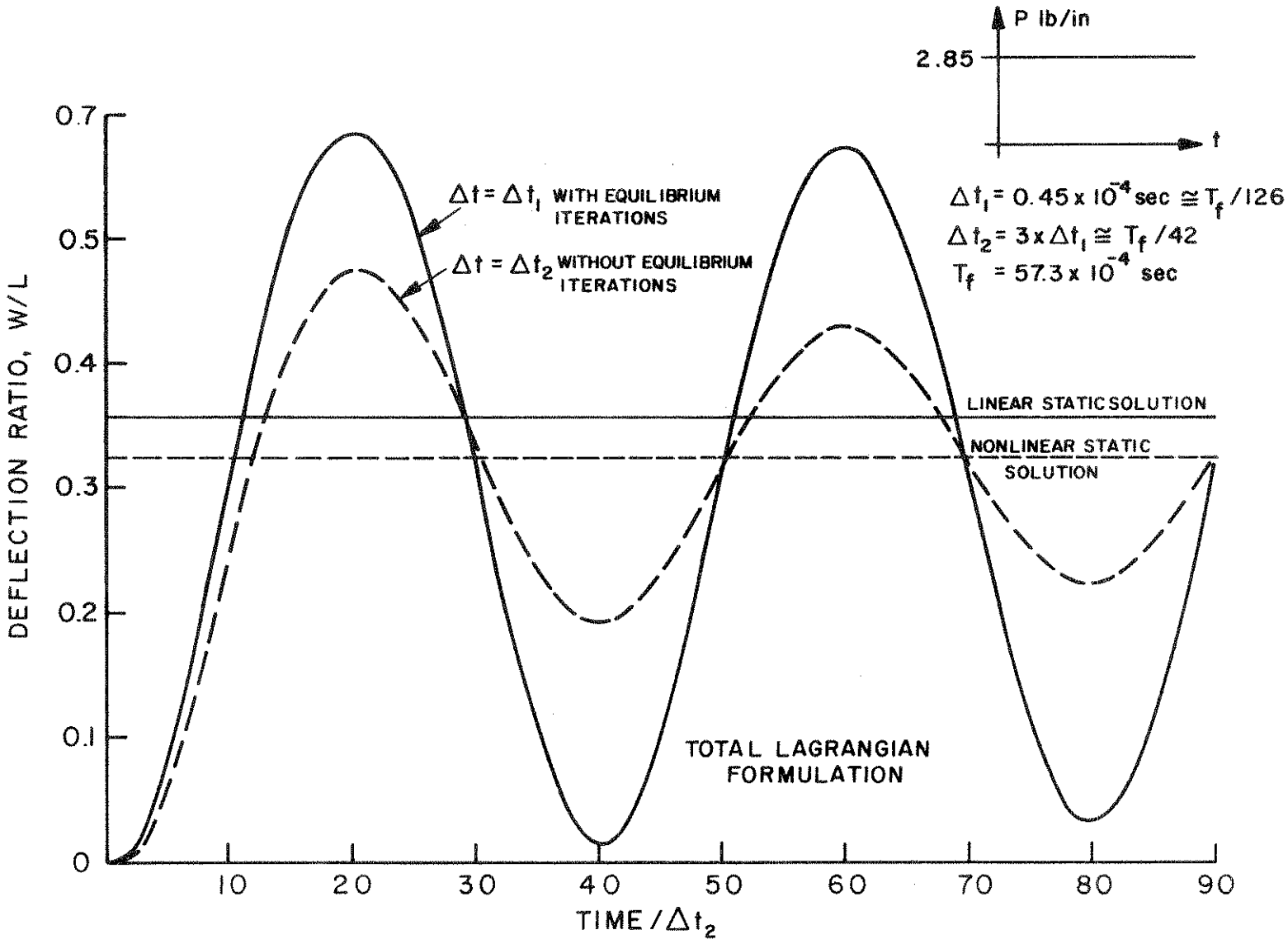

FIGURE 6.7 LARGE DISPLACEMENT DYNAMIC RESPONSE OF CANTILEVER UNDER UNIFORMLY DISTRIBUTED LOAD, WILSON θ-METHOD, $\theta = 1.4$

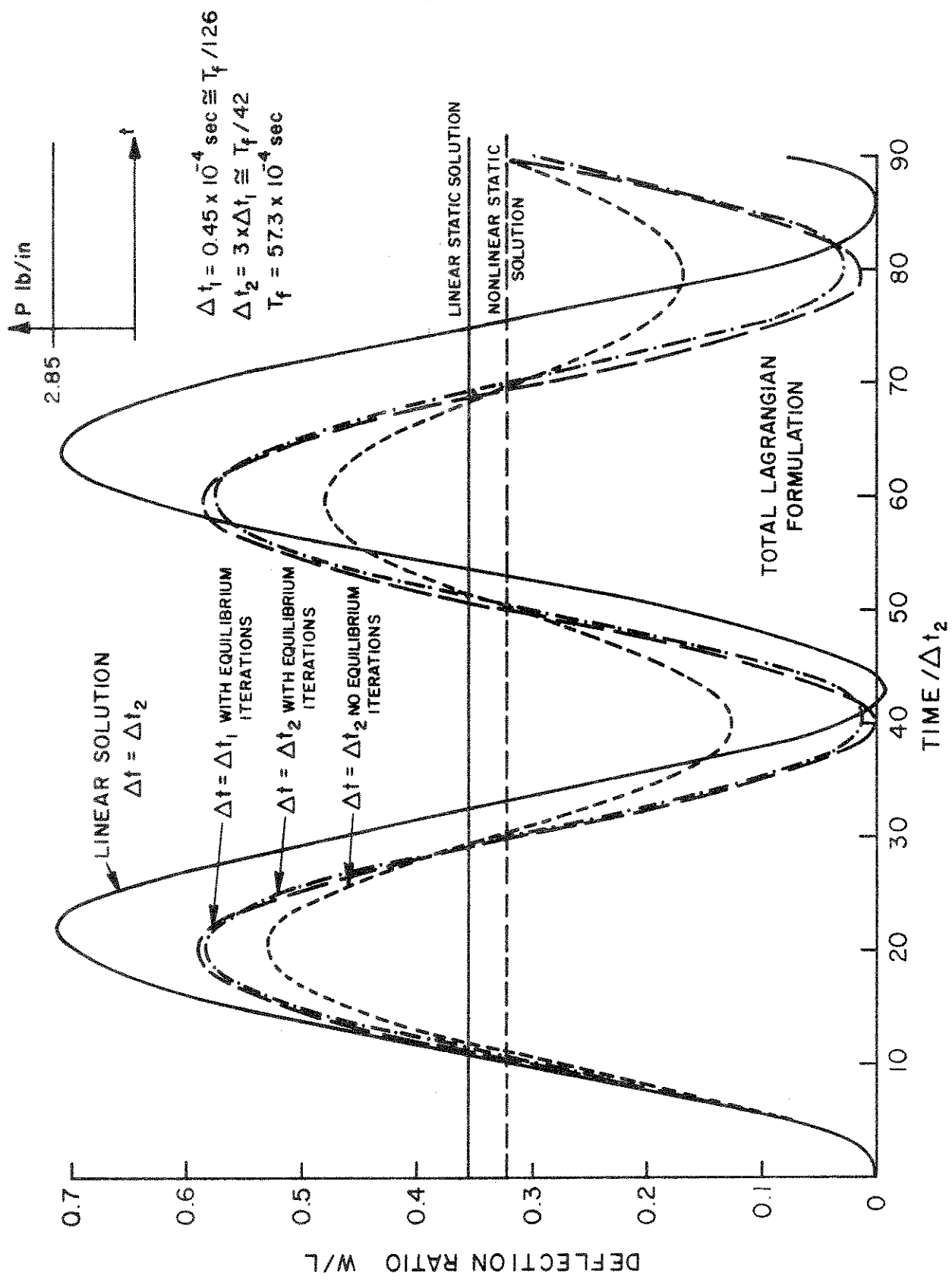

FIGURE 6.8 LARGE DISPLACEMENT DYNAMIC RESPONSE OF CANTILEVER UNDER UNIFORMLY DISTRIBUTED LOAD, NEWMARK METHOD $\delta = 0.50$, $\alpha = 0.25$

6.4 Large Displacement Static Buckling Analysis of an Arch

The clamped circular arch shown in Fig. 6.9 was analyzed for buckling due to a single static load using the T.L. and U.L. formulations with equilibrium iterations [4]. The material of the arch was assumed to be isotropic linear elastic (see Section 4.4.1). Considering the symmetry of the structure and loading, half of the arch was idealized by twelve 8-node plane stress elements.

The purpose of this analysis was to assess the accuracy that can be obtained with the static solution schemes used in NONSAP.

Figure 6.9 shows the calculated load-deflection curve of the arch. The differences in the displacements calculated using the U.L. and T.L. formulations were less than 2 percent.

The same arch was also analyzed by Mallet and Berke, who used four "equilibrium-based" elements [29]. Dupuis et al. analyzed the arch with curved beam elements, and used this example to demonstrate the convergence of their Lagrangian and "updated" formulations [11]. In the latter formulation only the nodal points were updated, but not the geometry within the elements. As shown in Fig. 6.9 , the results are very sensitive to the number of elements used and are not satisfactory. Dupuis et al. also compared the calculated results with experimental results by Gjelsvik and Bodner [15], whose predicted buckling load is about ten percent lower than calculated by Mallet. However, it need be realized that an arch with a parameter $\lambda = 11.6$ is already influenced by antisymmetric buckling modes, which, although possible in the experiment, have not been taken account of in the analyses. The results obtained using NONSAP are therefore satisfactory.

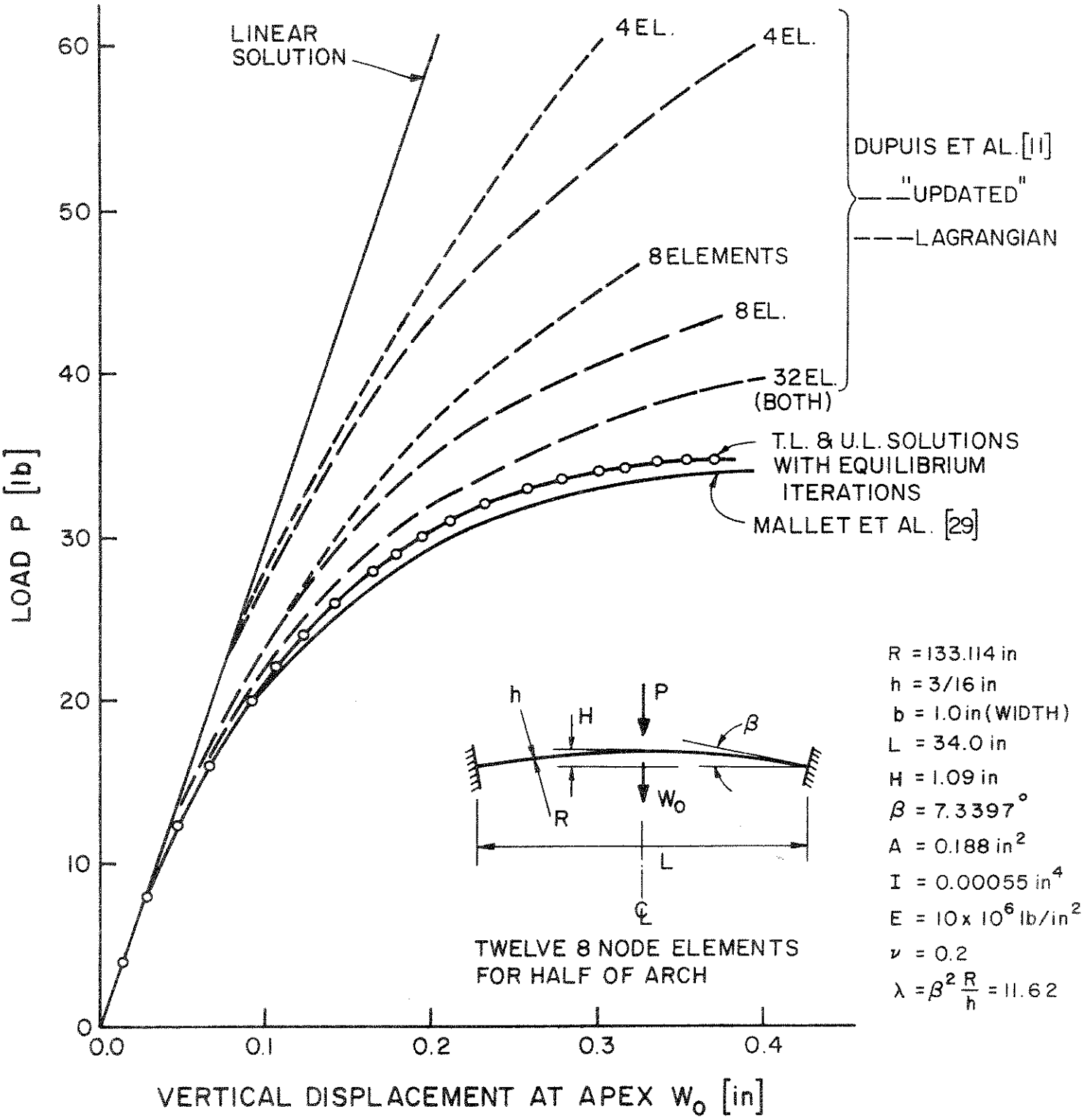

FIGURE 6.9 LOAD-DEFLECTION CURVE FOR A SHALLOW ARCH UNDER CONCENTRATED LOAD

6.5 Static Large Displacement Analysis of a Spherical Shell

The clamped shallow spherical shell in Fig. 6.10 subjected to uniform pressure was analyzed using a finite element idealization of eight 8-node elements [4]. The material was assumed to be isotropic linear elastic (see Section 4.4.1).

The purpose of this analysis was to test the accuracy of the static solution schemes used in NONSAP.

Figure 6.10 shows the load defection curve predicted by NONSAP using the T.L. formulation. The results are compared with an analytical solution of Kornishin and Isanbaeva [26], and a finite element solution of Yeh [52]. As shown, good agreement between the different solutions has been obtained. Since equilibrium iterations were performed in NONSAP, the oscillating behavior at the beginning of the post-buckling range in Yeh's solution was not obtained.

The U.L. formulation gave almost indistinguishable results to those of the T.L. formulation.

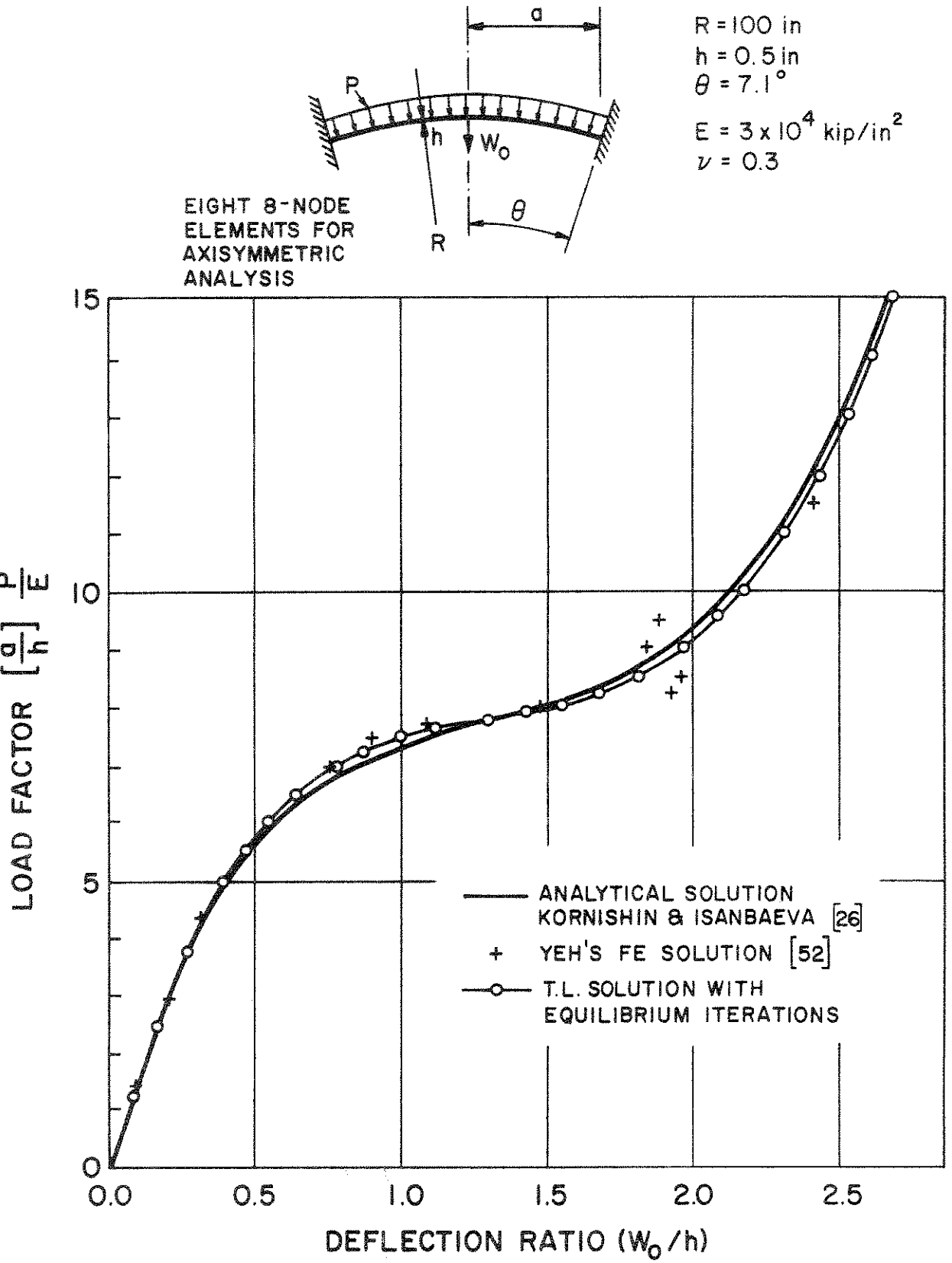

FIGURE 6.10 LOAD-DEFLECTION CURVE FOR A SHALLOW SPHERICAL SHELL

6.6 Static and Dynamic Large Displacement Analysis of a Spherical Shell

The elastic spherical shell subjected to a concentrated apex load shown in Fig. 6.11 was analyzed for static and dynamic response. The purpose of the static analysis was to compare the NONSAP solutions using the different formulations available with the solutions reported by Stricklin [47] and Mescall [34]. The aim in the dynamic analysis was to study the response predicted using the Wilson-θ and the Newmark integration schemes.

Figure 6.11 shows the static load-deflection response predicted by NONSAP, Stricklin [47], and Mescall [34]. Good agreement between the different solutions has been obtained. In the NONSAP solutions, the T.L. and U.L. formulations were used and no equilibrium iterations have been performed. In addition, to assess the accuracy that may be obtained in elastic-plastic analysis, the U.L.(T) and U.L.(J) formulations have been used as in the analysis of the cantilever (see Section 6.3). Figure 6.12 compares the T.L. response predictions with two U.L.(T) and U.L.(J) solutions. It is seen that the U.L.(T) and U.L.(J) solutions approach the T.L. solution as the load steps become smaller. It should be noted that this solution behavior is somewhat different from the one obtained in the analysis of the cantilever (see Section 6.3).

The dynamic response calculated using the Wilson θ and Newmark integration methods when the apex load is applied as a step load is shown in Figs. 6.13 and 6.14. It is observed that for this problem the differences between the solutions using equilibrium iteration and not iterating for equilibrium are small. The much larger response and period predicted using nonlinear analysis is a result of the softening behavior of the structure with increasing load. It should be noted that in the analysis

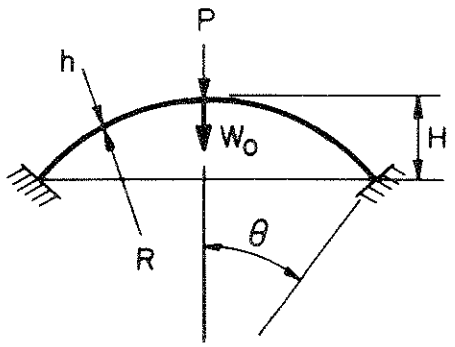

TEN 8 NODE ELEMENTS
FOR AXISYMMETRIC
ANALYSIS

R = 4.76 in
h = 0.01576 in
H = 0.0859 in
θ = 10.9°
λ = 6
E = 10×10^6 lb/in^2
ν = 0.3
ρ = 0.000245 lb-sec^2/in^4

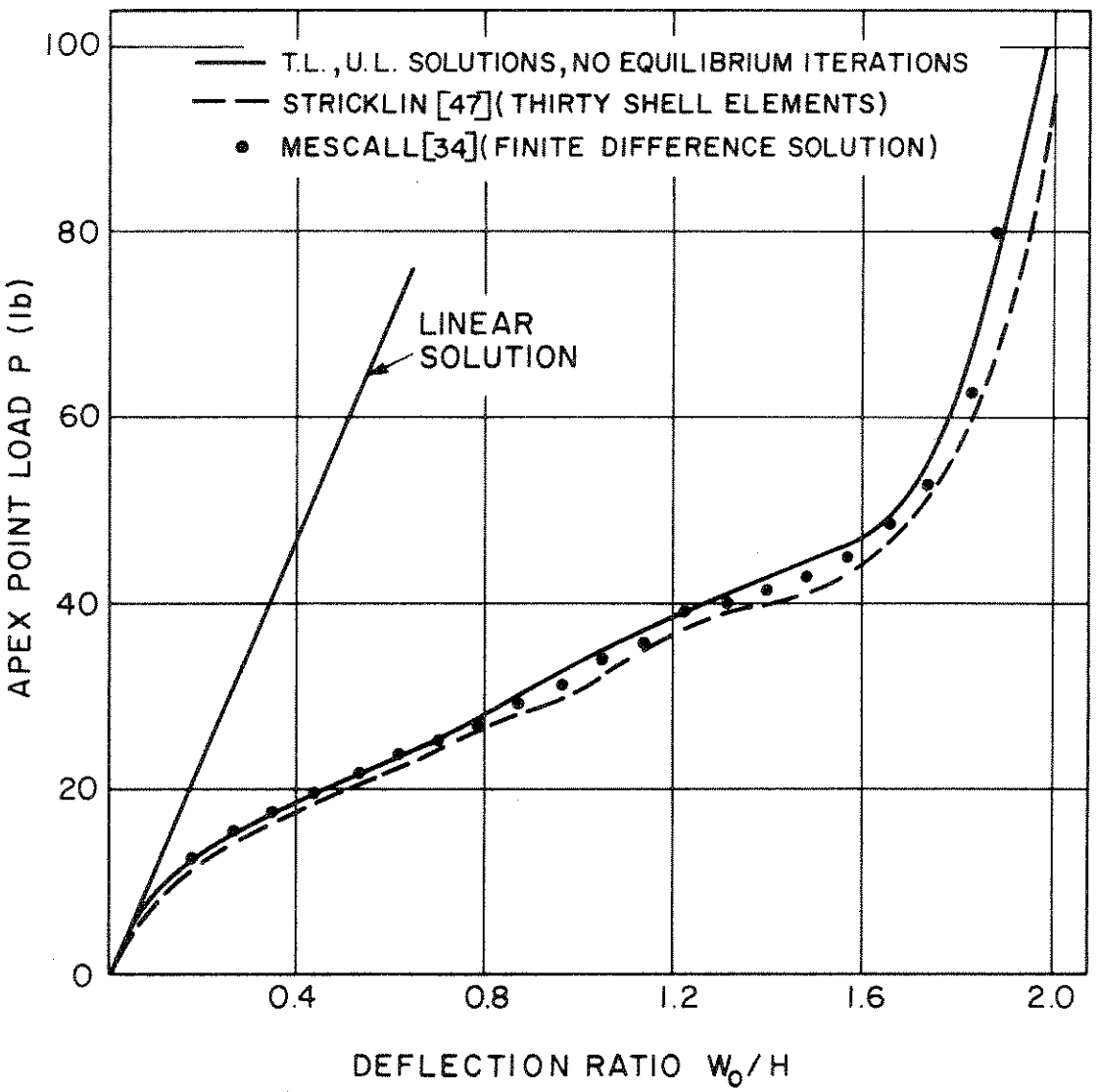

FIGURE 6.11 LOAD-DEFLECTION CURVES FOR SPHERICAL SHELL

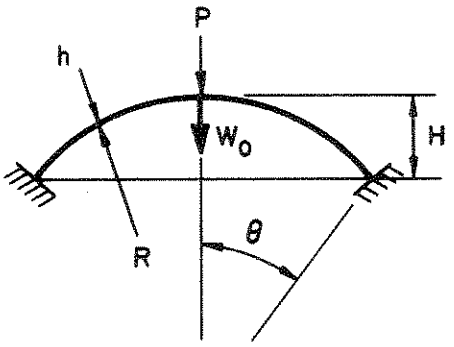

TEN 8 NODE ELEMENTS
FOR AXISYMMETRIC
ANALYSIS

R = 4.76 in
h = 0.01576 in
H = 0.0859 in
θ = 10.9°
λ = 6
E = 10 x 10^6 lb/in^2
ν = 0.3
ρ = 0.000245 lb-sec^2/in^4

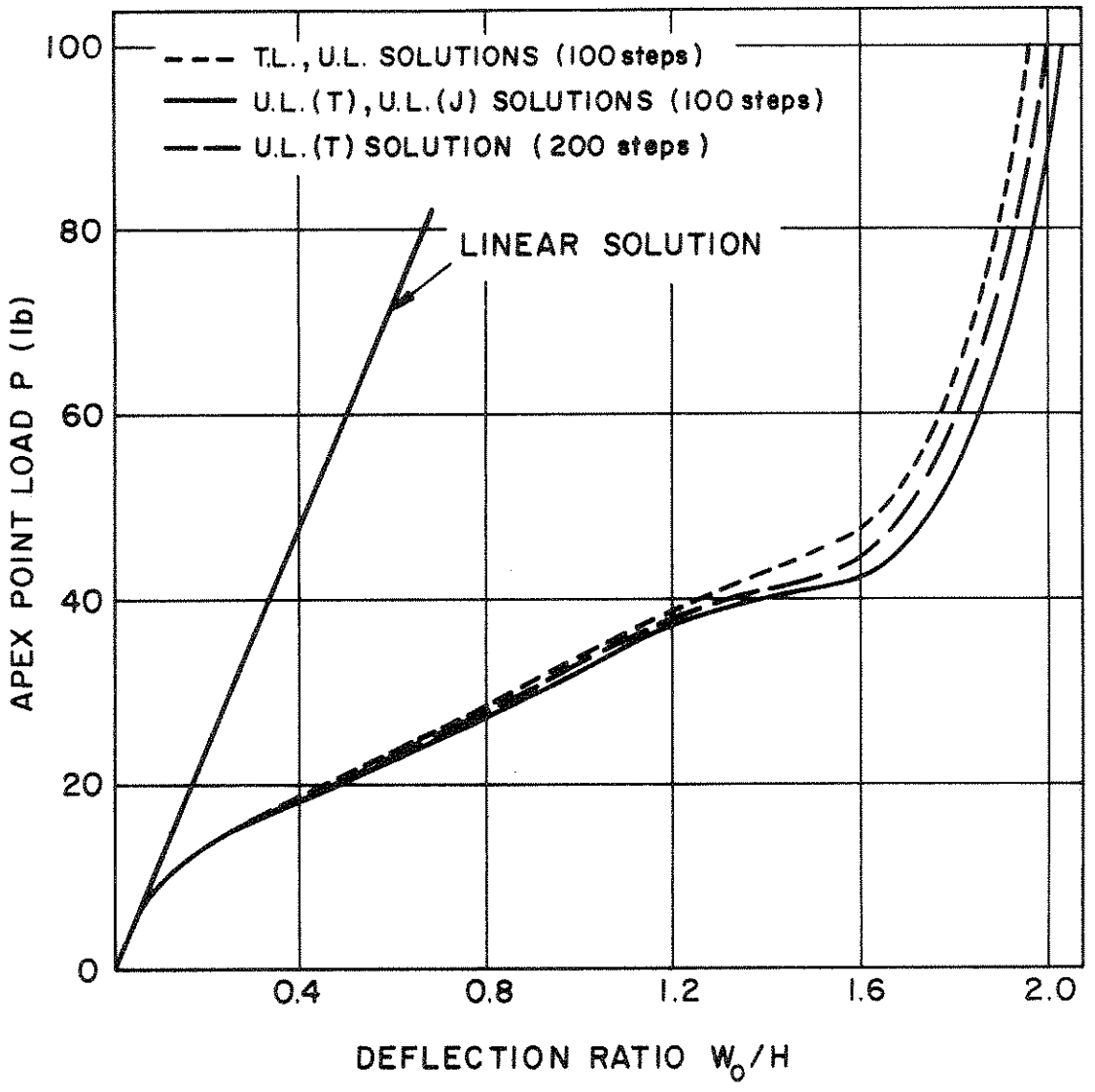

FIGURE 6.12 LOAD-DEFLECTION CURVES FOR SPHERICAL SHELL

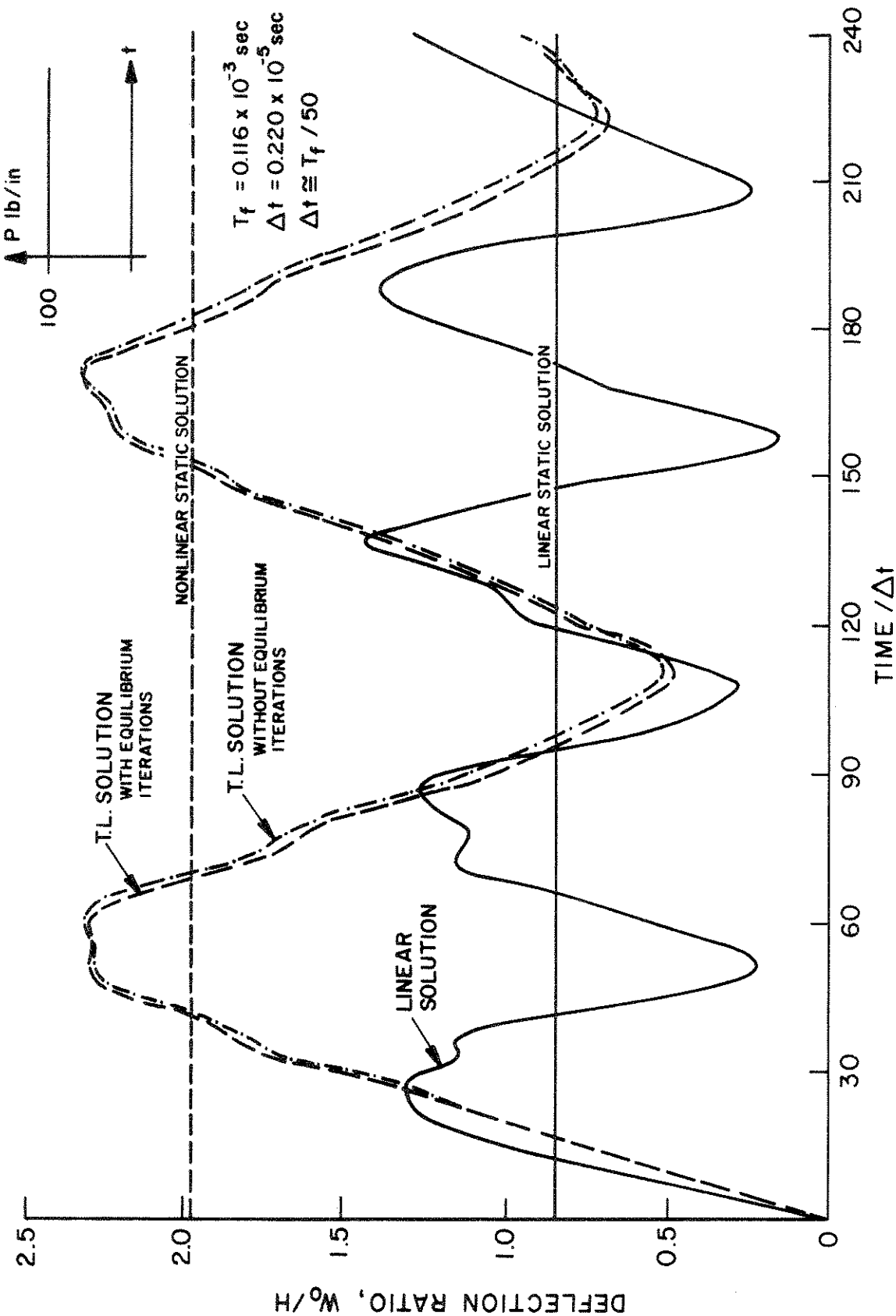

FIGURE6.13 NONLINEAR DYNAMIC RESPONSE OF SPHERICAL SHELL, WILSON θ-METHOD, $\theta = 1.4$

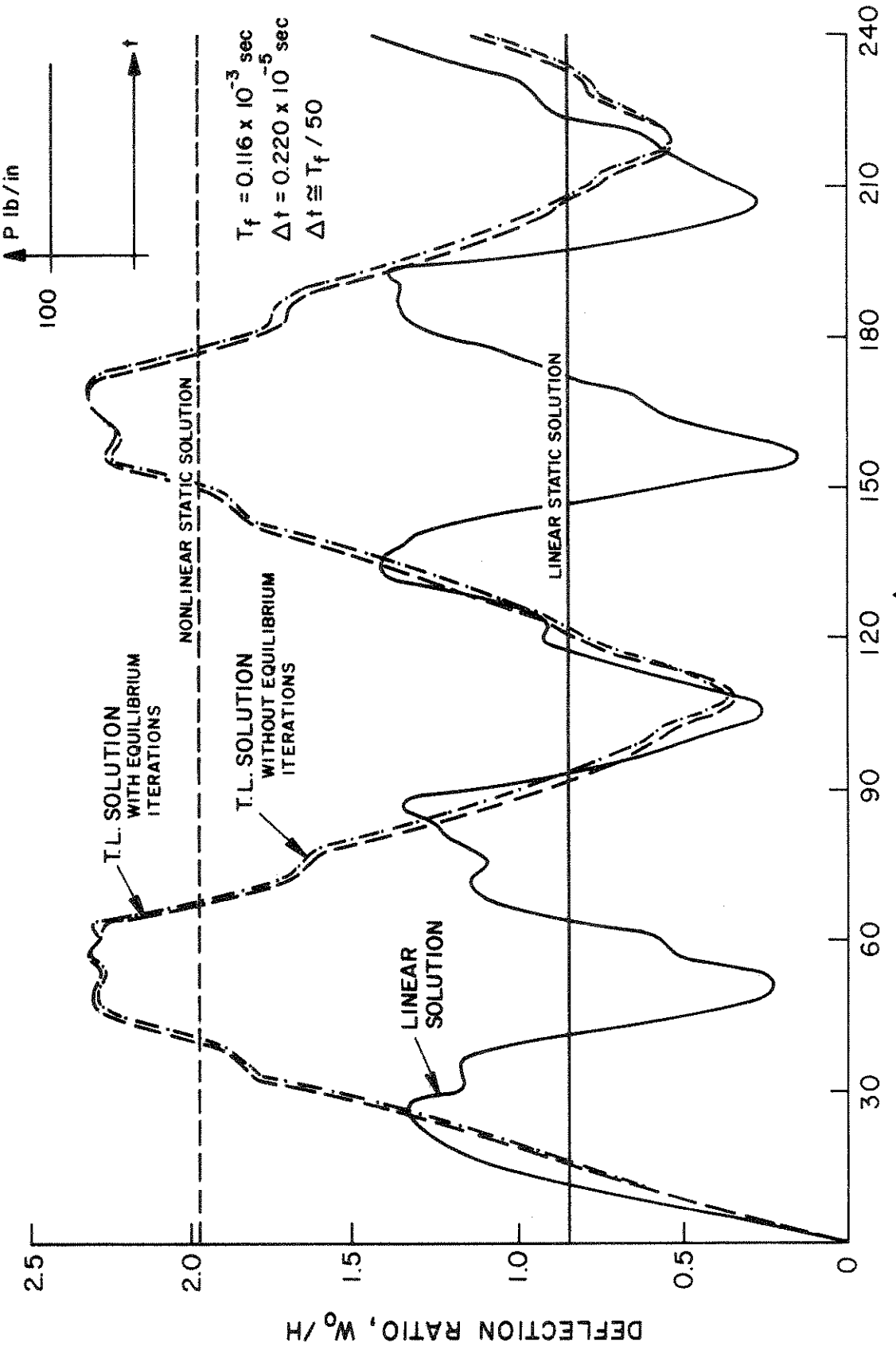

FIGURE 6.14 NONLINEAR DYNAMIC RESPONSE OF SPHERICAL SHELL, NEWMARK METHOD, $\delta = 0.50$, $\alpha = 0.25$

of this highly nonlinear shell no difficulties were encountered using the Wilson or the Newmark integration methods.

6.7 Elastic Dynamic Snap Buckling of a Shallow Circular Arch

A dynamic buckling analysis of the circular arch shown in Fig. 6.15 was carried out using six 8-node plane stress elements to idealize half of the symmetric structure [4]. The material of the arch was assumed to be isotropic linear elastic (see Section 4.4.1).

The purpose of this analysis was to assess the accuracy that could be obtained using the NONSAP dynamic solution algorithms.

In the analyses the T.L. formulation was used. The uniformly distributed pressure load was applied as a step load. The timestep Δt was selected equal to 3.315×10^{-5} sec, which is approximately 1/70th of the fundamental period of the structure. Physical damping was not considered.

The arch is an example of Humphrey's analytical and experimental investigation, who solved the governing differential equation using an analog computer [21]. Humphreys concluded that the buckling load of this arch is not influenced by antisymmetric modes.

Figure 6.16 shows the displacement response predicted by NONSAP using the Wilson θ integration scheme. The solution obtained by Humphreys is also shown. In the figure, the deflection ratio Δ defined as

$$\Delta = \frac{\text{average normal deflection } w}{\text{average rise of arch}=H/2}$$

is used. The dynamic buckling of the arch occurs at that load level at which a sudden increase in the deflection ratio Δ is measured. Figure 6.16 shows that at $p_0 = 0.190$ the arch oscillates about a position of approximately $\Delta = 0.25$, and that at $p_0 = 0.200$ the arch first snaps through, and then oscillates about a position of approximately $\Delta = 2.5$.

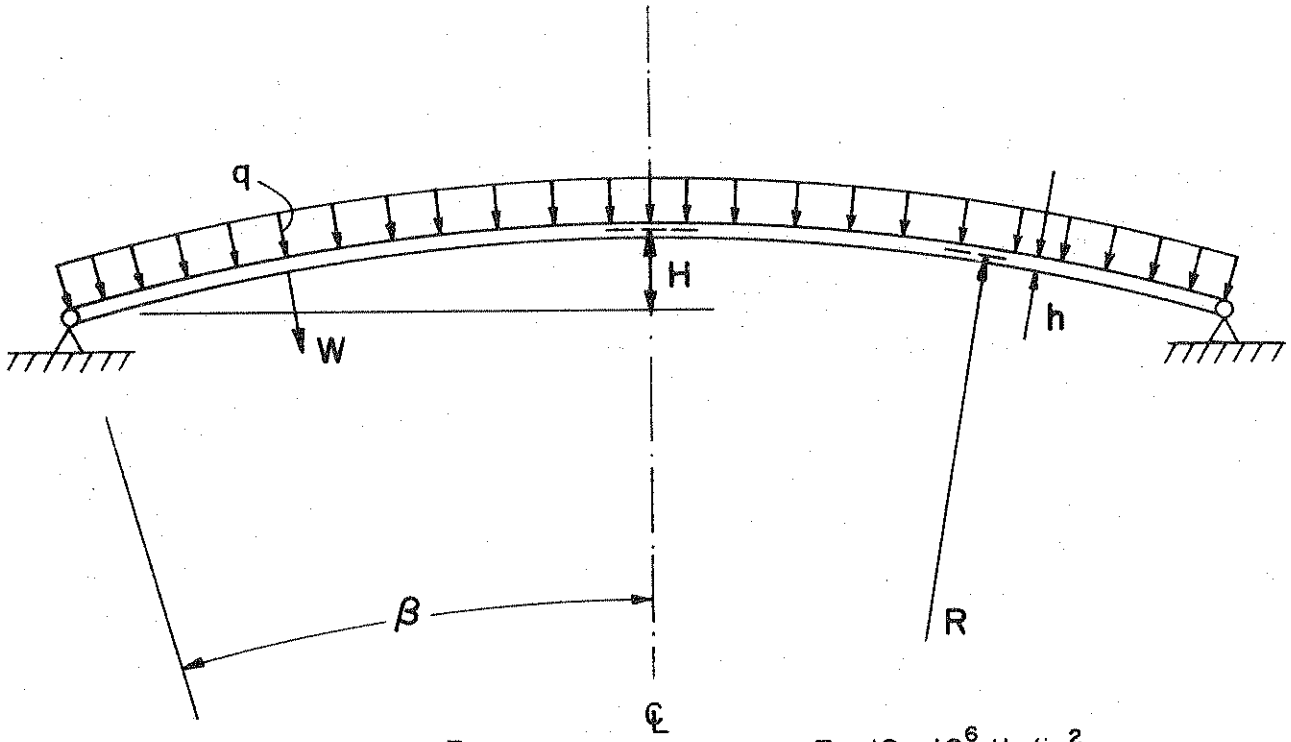

$R = 67.115$ in
$h = 1.0$ in
$b = 1.0$ in
$\beta = 15°$

$\gamma = \beta^2 \frac{R}{h} = 4.6$

$H = 2.287$ in

TIME PARAMETER

$\tau = \frac{C}{R} x t$

$E = 10 \times 10^6$ lb/in^2

$\nu = 0.2$

$\rho = 2.44 \times 10^{-4} \frac{\text{lb sec}^2}{\text{in}^4}$

$C = \sqrt{\frac{E}{\rho}} = 2.024 \times 10^5 \frac{\text{in}}{\text{sec}}$

LOAD PARAMETER

$P = (\frac{R}{h})^2 x \frac{q}{E}$

FIGURE 6.15 SIMPLY SUPPORTED SHALLOW ARCH

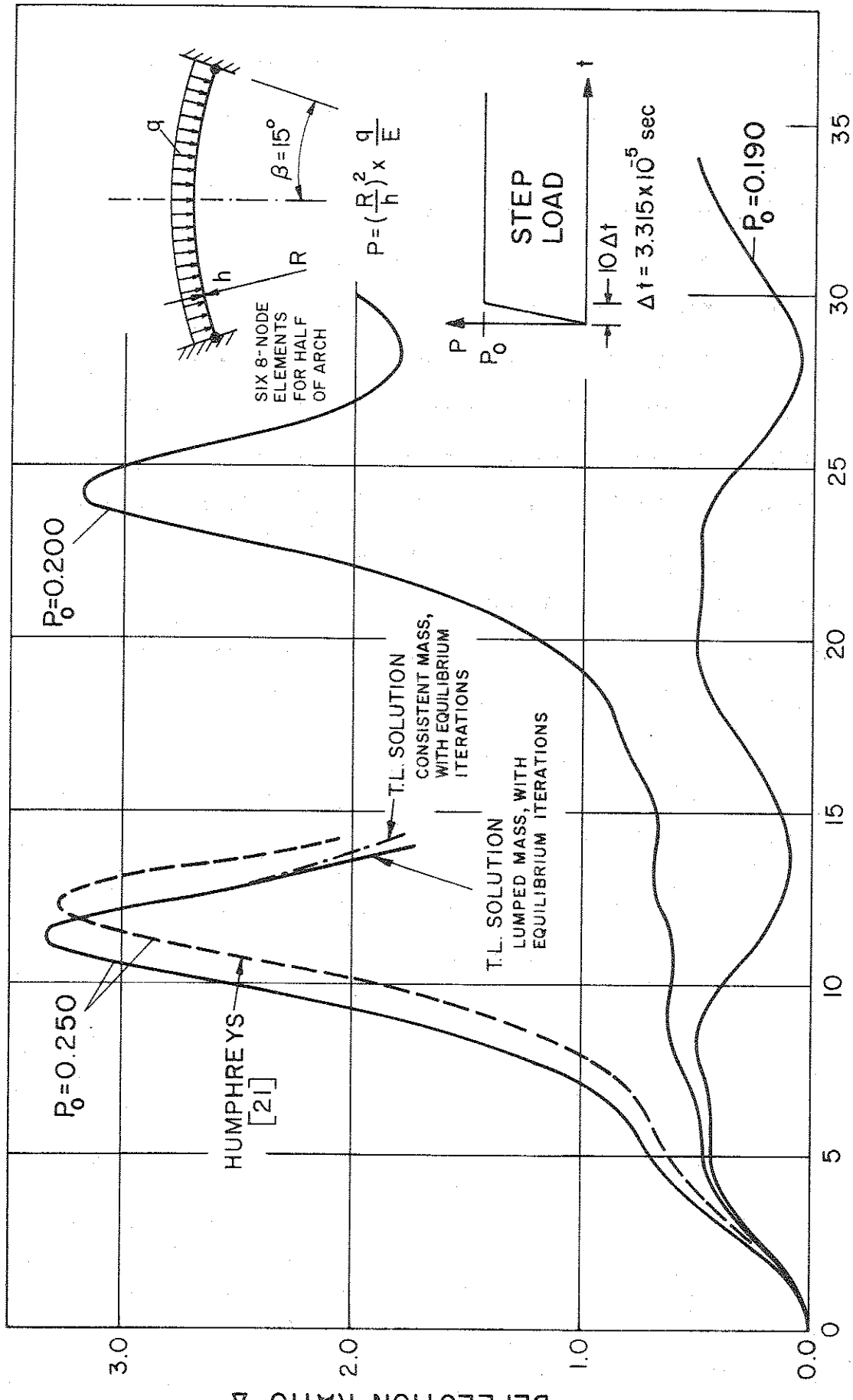

FIGURE 6.16 DYNAMIC SNAP-THROUGH OF A SHALLOW CIRCULAR ARCH
WILSON θ-METHOD, $\theta = 1.4$

Therefore, the buckling load predicted using NONSAP lies between p_0 = 0.190 and p_0 = 0.200, which is about five percent lower than predicted by Humphreys.

It should be noted that for a load larger than the buckling load, i.e. for p_0 = 0.25, the maximum response increases only little. The results using NONSAP for p_0 = 0.250 are in essential agreement with Humphreys' results, where the slightly larger response agrees with the observation that NONSAP predicted a smaller buckling load. The discrepancies in the results can arise from approximations in either analysis. Humphreys' series solution is based on the assumption of shallowness, i.e. q and w are measured vertically, and in the series solution only a finite number of terms have been included.

It is noted that in a practical analysis damping should be included and a longer time range may be considered as well.

6.8 Large Displacement and Large Strain Static Analysis of a Rubber Sheet

The rubber sheet shown in Figure 6.17 was analyzed for the uniform end loading indicated. The purpose of this analysis was to compare the NONSAP solution with experimental results of the static displacement response of the sheet obtained by Iding et al. [22] [23]. The material was assumed to be of the Mooney - Rivlin type, for which the experiments gave $C_1 = 21.605$ lb/in^2 , $C_2 = 15.747$ lb/in^2.

Figure 6.18 shows the static displacement response of the sheet. It is noted that the final displacement at the loaded end is of the order of the original length of the sheet, at which stage Green - Lagrange strains of 1.81 are measured. The final configuration of the sheet was reached in 4 equal load steps with an average of 5 equilibrium iterations in each step. Excellent agreement between the experimental results and those predicted by NONSAP has been obtained.

In order to show the large differences between the 2nd Piola - Kirchhoff and Cauchy stresses, the stress distributions at two sections at the application of the total load are given in Fig. 6.18. It should be recalled that the integration of the Cauchy stresses must equal the applied load, P; however, the sum of the 2nd Piola - Kirchhoff stresses does not equal P.

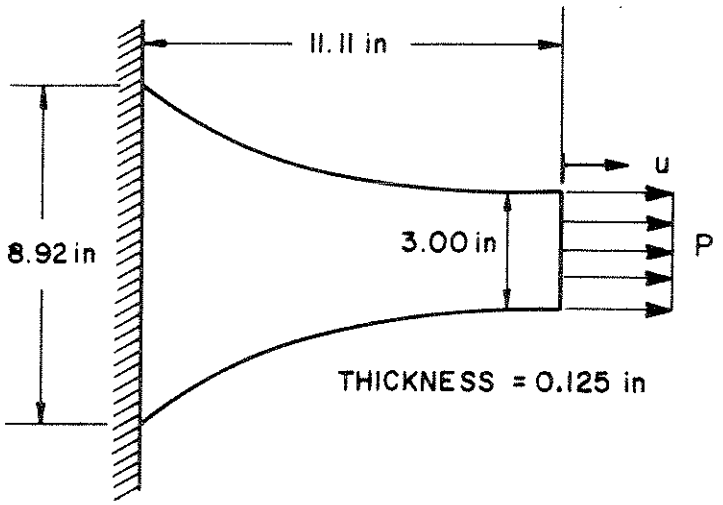

RUBBER SHEET

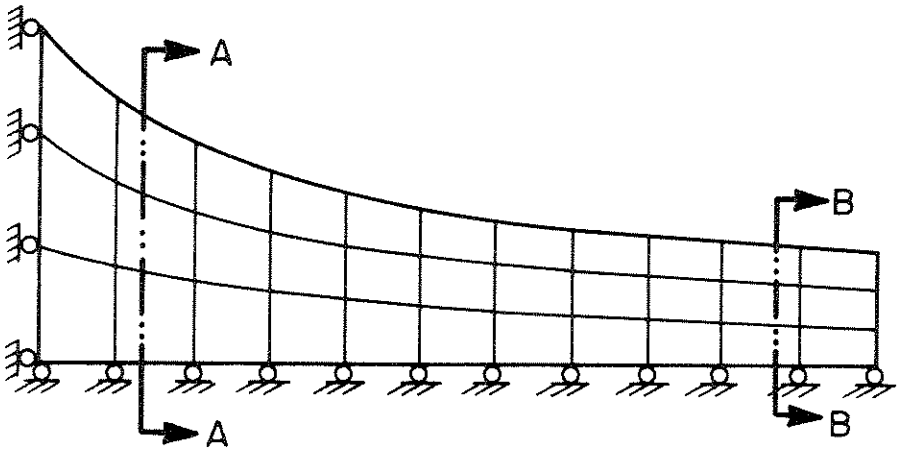

FINITE ELEMENT MESH (4 NODE ELEMENTS)

FIGURE 6.17 LARGE DISPLACEMENT AND LARGE STRAIN STATIC ANALYSIS OF A RUBBER SHEET

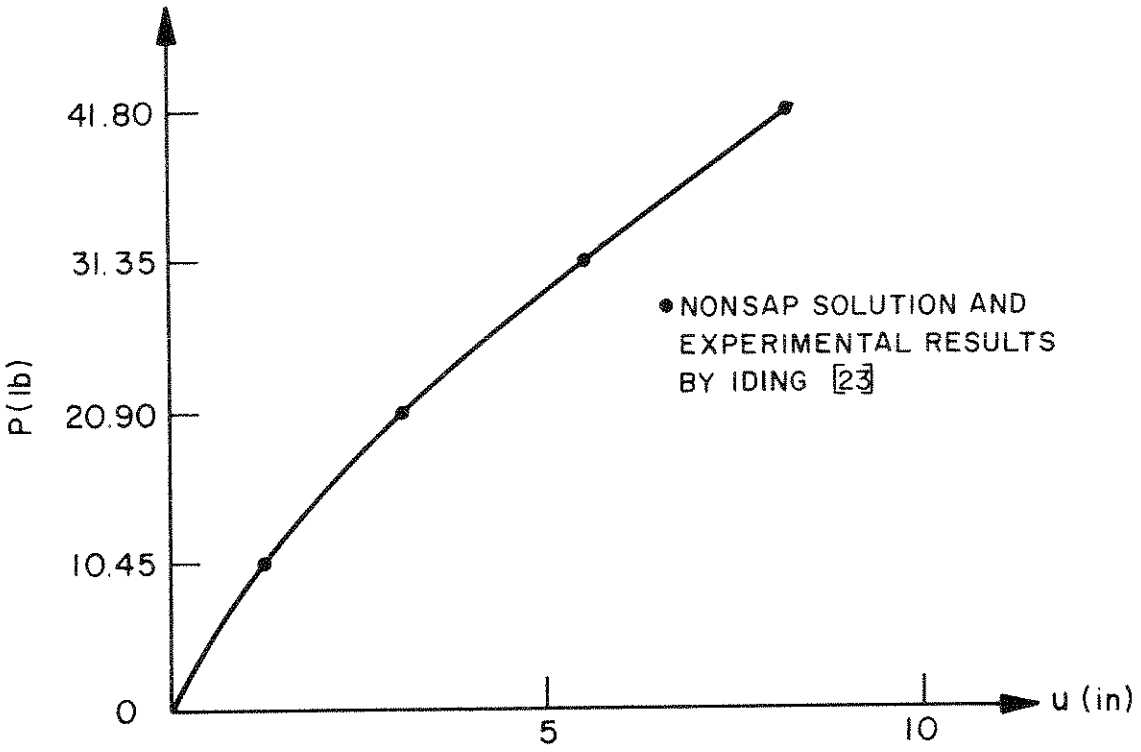

DEFLECTION AT LOADED END

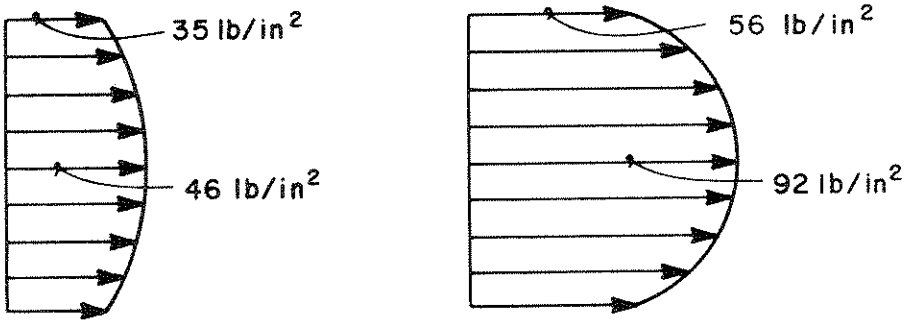

2ND PIOLA-KIRCHHOFF STRESS

CAUCHY STRESS

STRESS DISTRIBUTION ACROSS SECTION A-A AT P = 41.80 lb

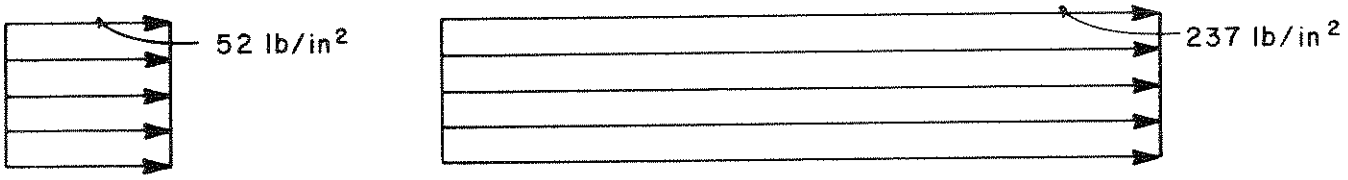

2ND PIOLA-KIRCHHOFF STRESS

CAUCHY STRESS

STRESS DISTRIBUTION ACROSS SECTION B-B AT P = 41.80 lb

FIGURE 6.18 DISPLACEMENT AND STRESS RESPONSE OF A RUBBER SHEET

6.9 Large Displacement and Large Strain Static and Dynamic Analysis of a Rubber Sheet with Hole

A plane stress analysis of the rubber sheet shown in Fig. 6.19 was carried out. The purpose of this analysis was to test the capability of program NONSAP to predict static and dynamic large strain response.

The material of the rubber sheet was assumed to be of Mooney - Rivlin type. The specific material constants used for the hyperelastic incompressible material were $C_1 = 25$ lb/in^2, $C_2 = 7$ lb/in^2. These constants are based on an analytical and experimental investigation of the rubber sheet by Iding [22]. The finite element mesh used in the analysis is presented in Fig. 6.19.

Figure 6.20 shows the static load-deflection curves for different points on the sheet. In one analysis only 5 equal load increments with an average of 4 equilibrium iterations have been used to reach the final load position with a displacement of more than 11 inches at point B. At this stage Green - Lagrange strains of more than 4.5 are measured. The results obtained are in excellent agreement with those of Iding. The results of Iding have been obtained with the computer program developed in [22], but are not given in the reference.

The dynamic analysis was performed for the step load shown in Fig. 6.21 using the Wilson θ and Newmark integration schemes. The selected time step Δt was 0.0015 sec, which is approximately 1/120 of the fundamental period T_f of the sheet, and no physical damping was considered.

Figure 6.21 compares the displacement response predicted by NONSAP using the two integration methods. As is seen, practically the same response was calculated using the Wilson θ and the Newmark methods. In addition, it should be noted that identical solutions have been obtained

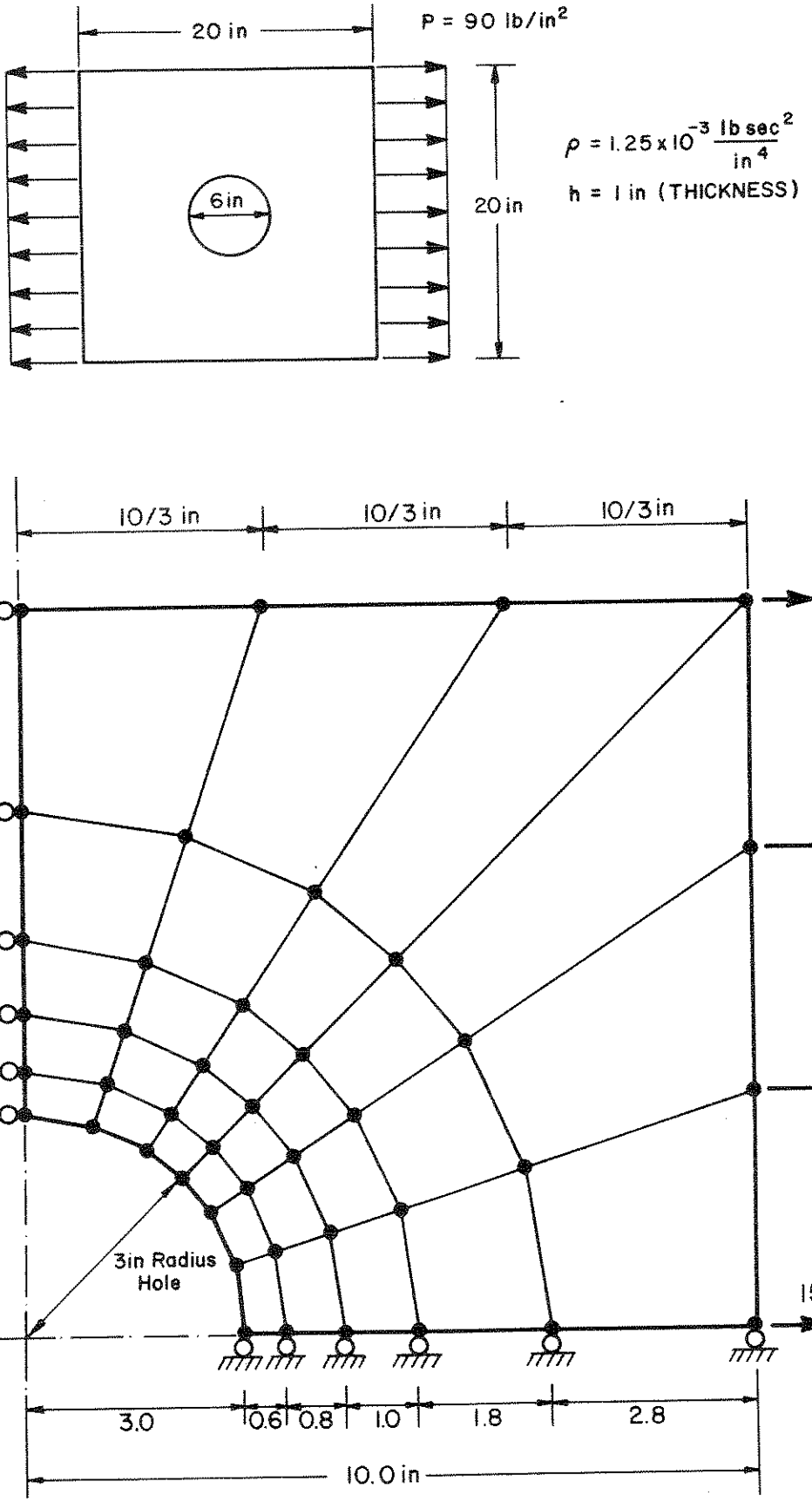

FIGURE 6.19 FINITE ELEMENT MESH OF RUBBER SHEET WITH HOLE

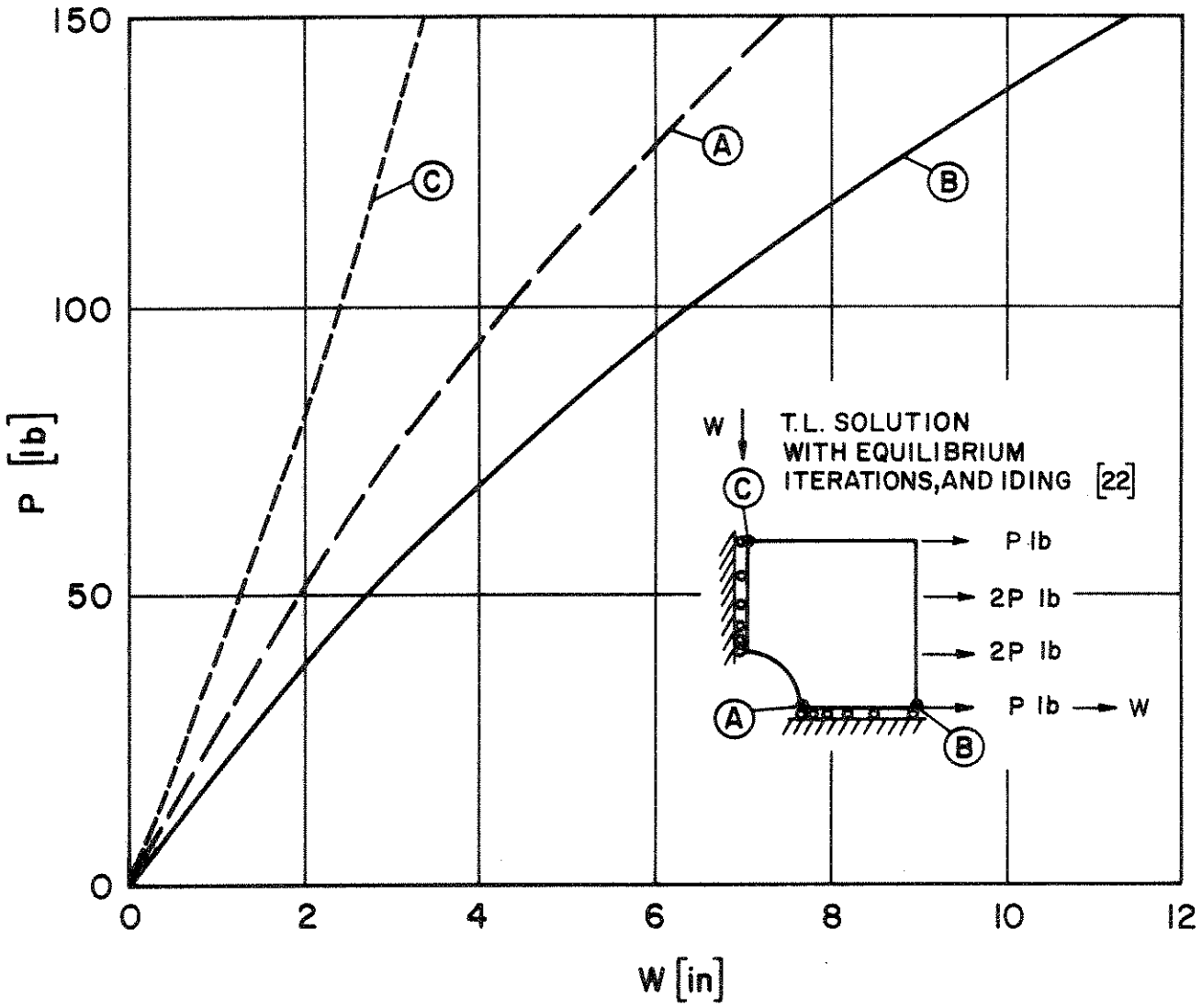

FIGURE 6.20 STATIC LOAD DEFLECTION CURVE FOR A RUBBER SHEET WITH HOLE

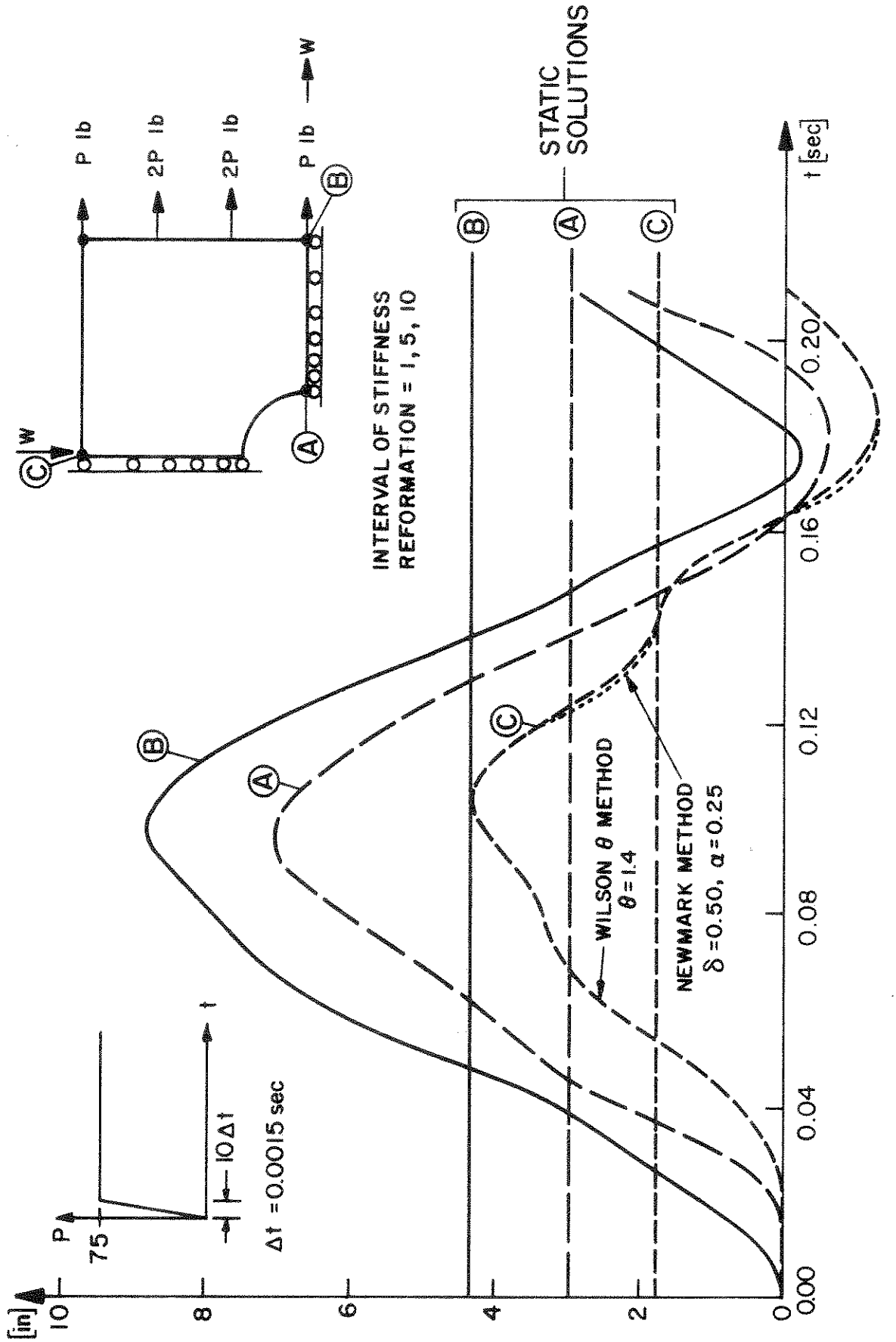

FIGURE 6.21 DISPLACEMENTS VS. TIME FOR RUBBER SHEET WITH HOLE
T.L. SOLUTION WITH EQUILIBRIUM ITERATIONS

using either integration scheme and an interval of stiffness reformation of 10, 5 or 1 time steps (see Table 7).

6.10 Elastic-Plastic Static Analysis of Thick-Walled Cylinder

The thick-walled cylinder in Fig. 6.22 subjected to internal pressure was analyzed using four 8-node axisymmetric elements. The purpose of the analysis was to study the accuracy that can be obtained in elastic-plastic analysis.

The material of the cylinder was assumed to obey the von Mises yield condition with elastic perfectly plastic response. The same analysis was also carried out using the Drucker-Prager yield condition with material variables corresponding to those used in the von Mises condition, and identical results have been obtained.

Since displacements and strains are small, the analysis of the cylinder was carried out using the materially nonlinear only formulation. Figure 6.23 shows the radial displacement response of the cylinder as a function of the applied load and Figure 6.24 gives the stress distribution through the wall of the cylinder at a given level of internal pressure. Excellent agreement with the solution given by Hodge and White has been obtained [19].

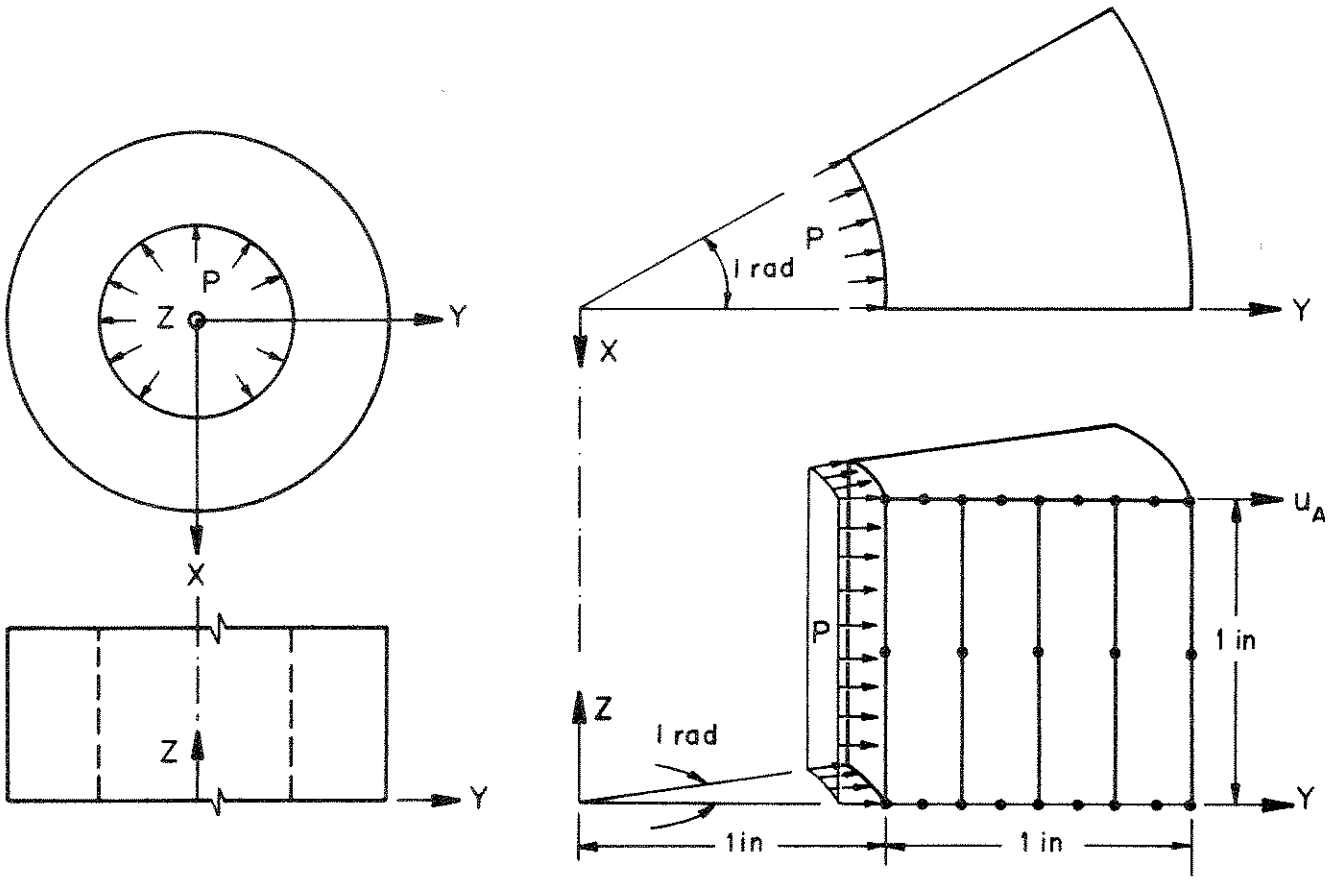

ELASTIC-PERFECTLY PLASTIC MATERIAL

VON MISES YIELD CONDITION

$G = 10^5/3$ lb/in^2

$\nu = 0.3$

$\sigma_y = 17.32$ lb/in^2

DRUCKER-PRAGER YIELD CONDITION

$G = 10^5/3$ lb/in^2

$\nu = 0.3$

ANGLE OF FRICTION = 0.0^0

COHESION = 8.66 lb/in^2

FIGURE 6.22 FINITE ELEMENT MESH OF THICK-WALLED CYLINDER

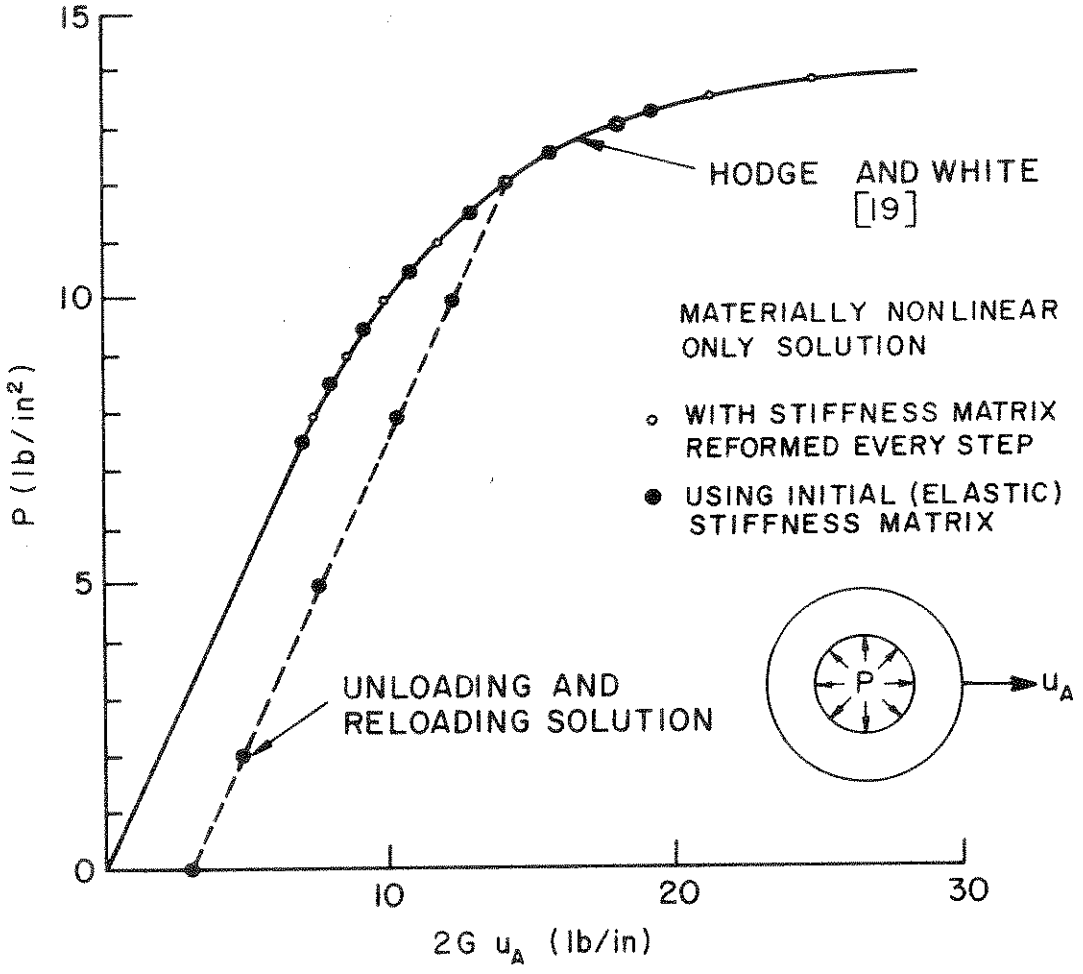

FIGURE 6.23 ELASTIC-PLASTIC DISPLACEMENT RESPONSE OF THICK-WALLED CYLINDER

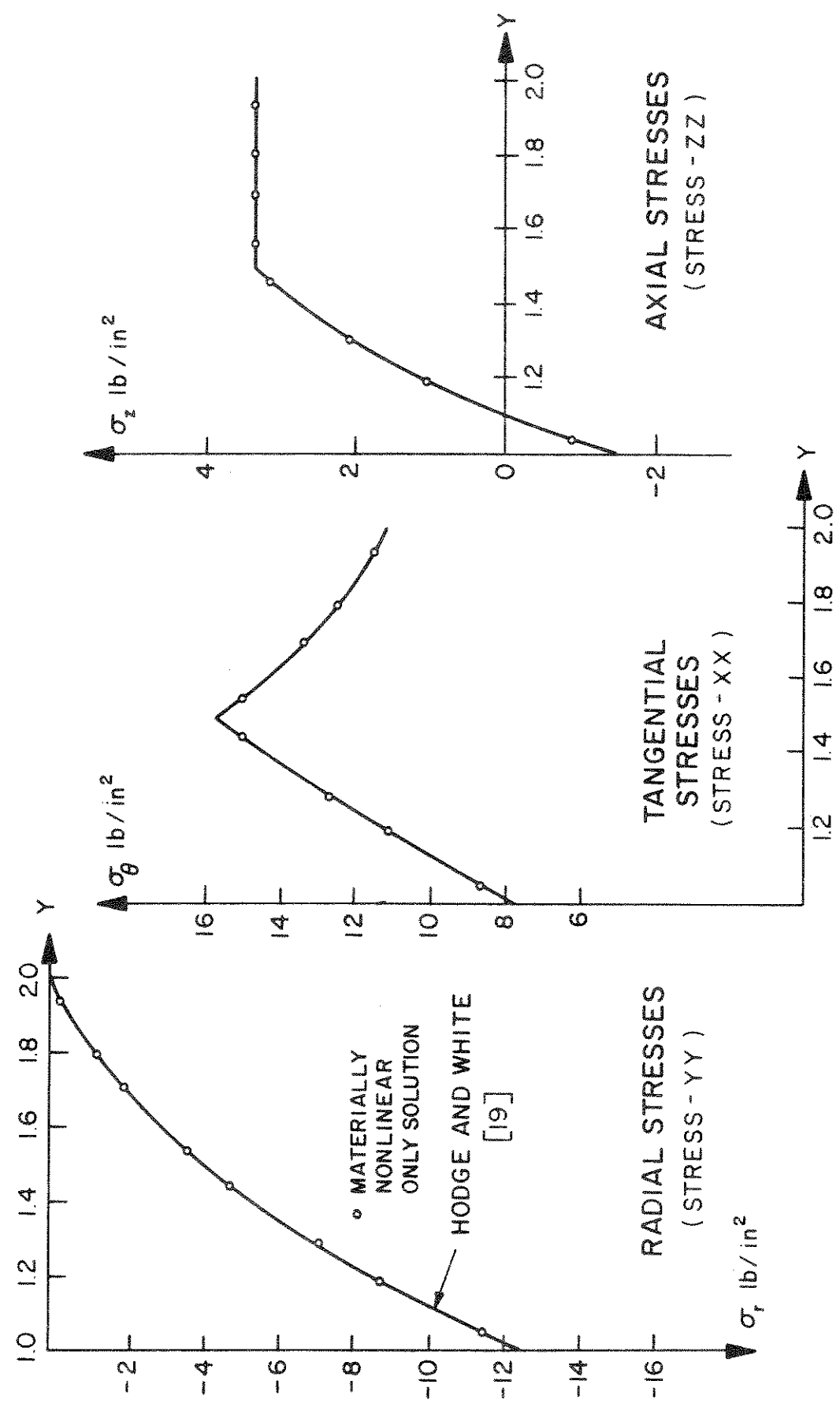

FIGURE 6.24 ELASTIC-PLASTIC STRESS DISTRIBUTION THROUGH THICKNESS OF THICK-WALLED CYLINDER AT p = 12.5 lb/in^2

6.11 Elastic-Plastic Static Analysis of Perforated Tension Strip

The perforated tension strip shown in Fig. 6.25 was analyzed for its elastic-plastic response. The material was assumed to obey the von Mises yield condition with isotropic (linear) hardening. In the finite element idealization, Fig. 6.25, four- and eight-node elements have been used. The purpose of this analysis was to test the accuracy that can be obtained using the elastic-plastic analysis options in NONSAP.

The analysis was carried out using the materially nonlinear only formulation. Figure 6.26 shows the strain response at the point of first yield as predicted by NONSAP and Zienkiewicz [53]. The results of Theocaris and Marketos have been obtained by experiment [49]. In the same figure, the final stress distribution across section A-B of the strip is also given.

Figure 6.26 shows that the experimental values for the maximum strain response of Theocaris and Marketos [49] are slightly above those calculated by NONSAP and by Zienkiewicz. This suggests that the actual value of the yield stress σ_y in the experiment was slightly larger than used in the analysis. However, good overall correspondence between the solutions is observed.

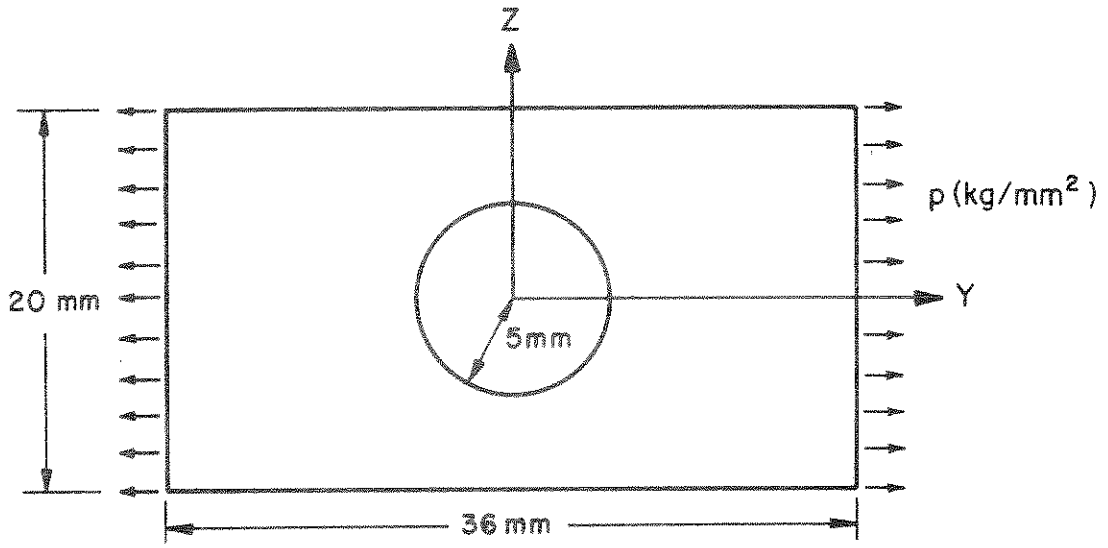

ELASTIC-PLASTIC ISOTROPIC HARDENING MATERIAL,
VON MISES YIELD CONDITION

$E = 7000\ kg/mm^2$

$\nu = 0.2$

$\sigma_y = 24.3\ kg/mm^2$

$E_T = 225\ kg/mm^2$

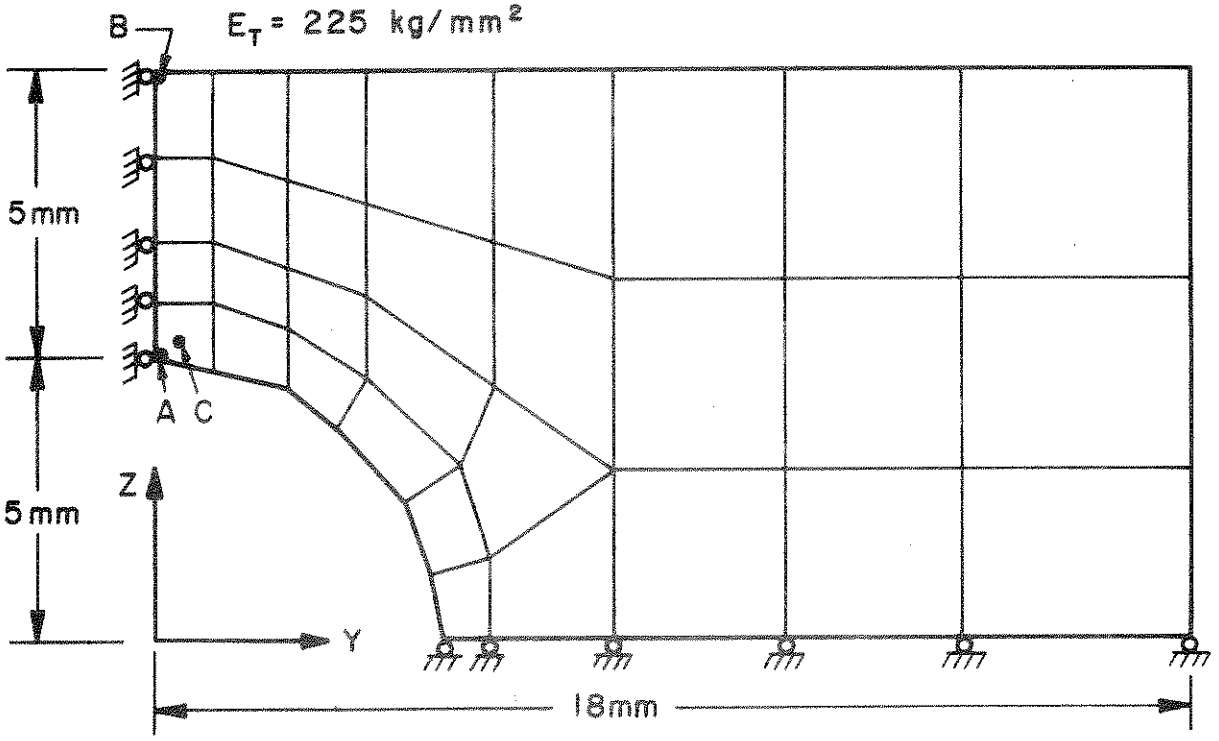

FIGURE 6.25 FINITE ELEMENT MESH OF PERFORATED TENSION STRIP

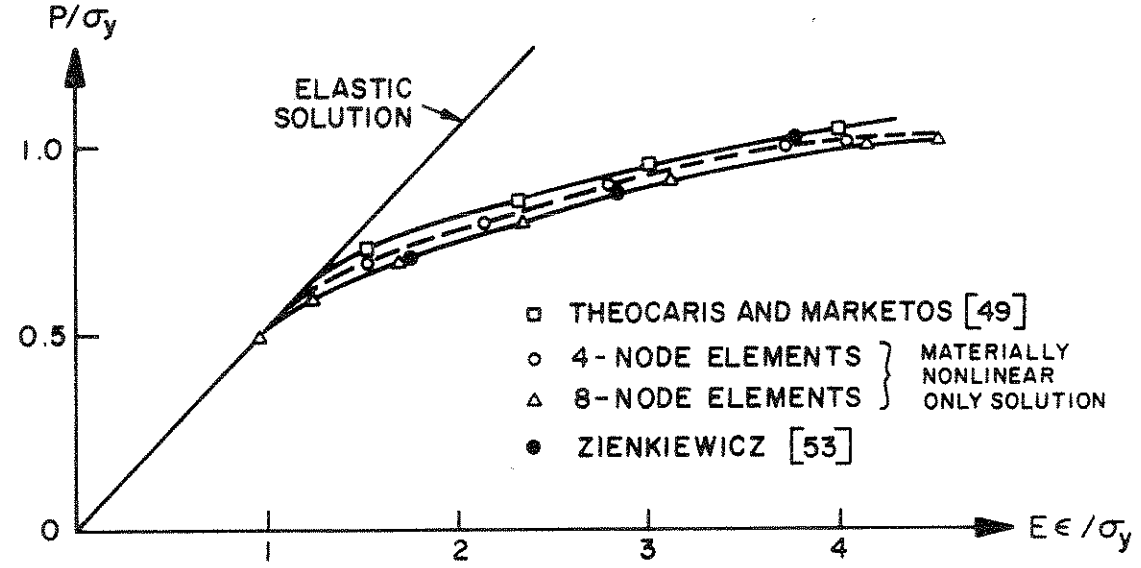

MAXIMUM STRAIN AT POINT OF FIRST YIELD
(POINT A IN [49] AND POINT C IN FIG. 6.25)

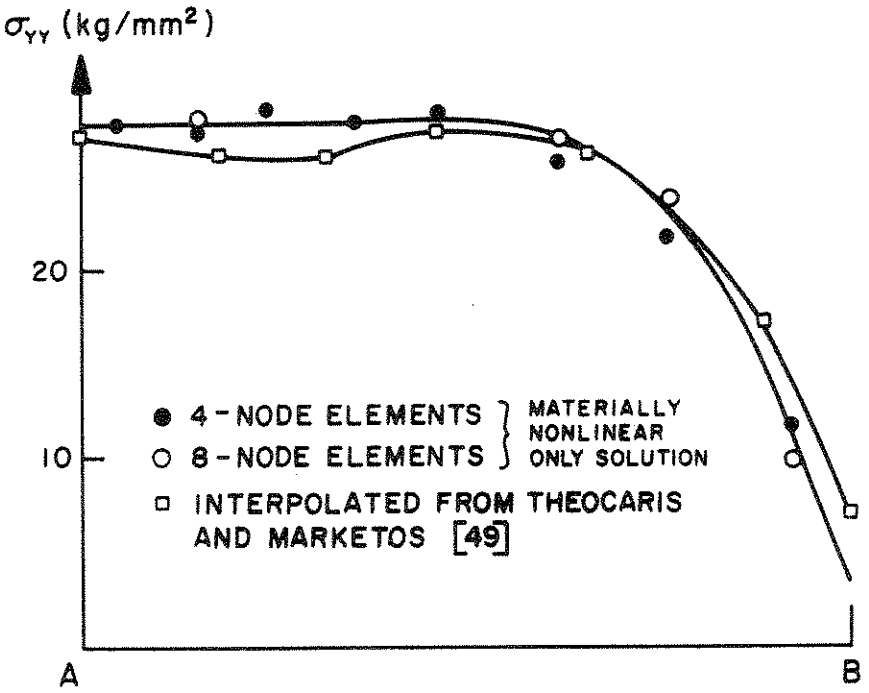

STRESS DISTRIBUTION ALONG SECTION A-B IN
FIG. 6.25 AT $P/\sigma_y = 1.0$

FIGURE 6.26 ELASTIC-PLASTIC DISPLACEMENT AND STRESS RESPONSE OF PERFORATED TENSION STRIP

6.12 Elastic-Plastic Small Displacement Dynamic Analysis of Simply-Supported Beam

The beam shown in Fig.6.27 was analyzed for the step loading indicated. The material of the beam was assumed to be elastic perfectly plastic using the von Mises yield condition. In the analysis small displacements were assumed, i.e. materially nonlinear only solutions were calculated. The purpose of the analysis was to compare the solutions predicted by NONSAP with results reported by Baron et al. [3] and Nagarajan and Popov [36].

Figures 6.28 and 6.29 show the response calculated using NONSAP with the Wilson θ and Newmark integration schemes. Using a time step $\Delta t = 0.5 \times 10^{-4}$ sec, which is approximately 1/100 th of the fundamental period, T_f, of the (linear elastic) beam, both integration schemes give almost identical results.

In Fig. 6.30 the response is shown normalized with respect to the static elastic deflection of the beam when subjected to p_0. The solutions obtained by Baron et al. [3] and Nagarajan and Popov [36], who used a rather large time step, are also shown. Nagarajan only presented the initial response solution and did not use equilibrium iteration. However, it should be realized that with too large a time step instabilities can develop at a later time. Indeed, using $\Delta t = 0.3 \times 10^{-3}$ seconds and the Newmark integration scheme, the solution obtained by Nagarajan was also predicted using NONSAP. However, at a later time the solution started to oscillate until, at the maximum times considered in Figs. 6.28 and 6.29, the solution was meaningless.

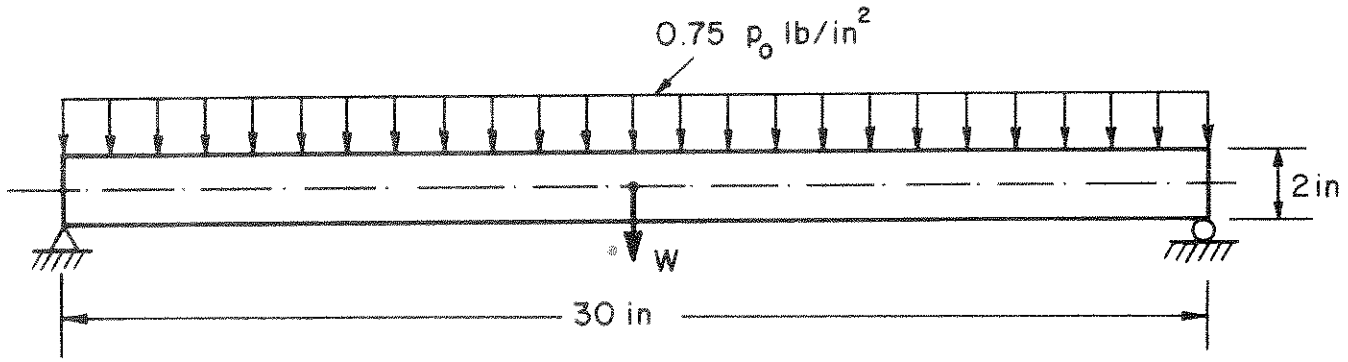

BEAM THICKNESS = 1 in

$E = 3 \times 10^4$ kip/in^2

$\nu = 0.3$

$\sigma_y = 50$ kip/in^2

$\rho = 0.733 \times 10^{-3}$ lb sec^2/in^4

p_o = STATIC COLLAPSE LOAD

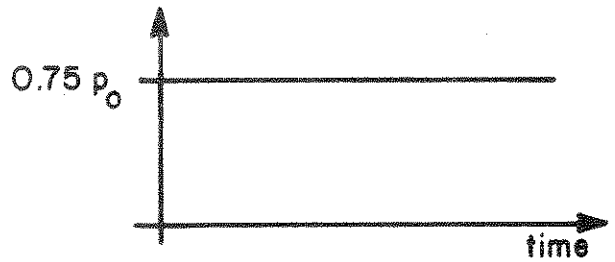

STEP PRESSURE

SIMPLY SUPPORTED BEAM AND APPLIED LOAD

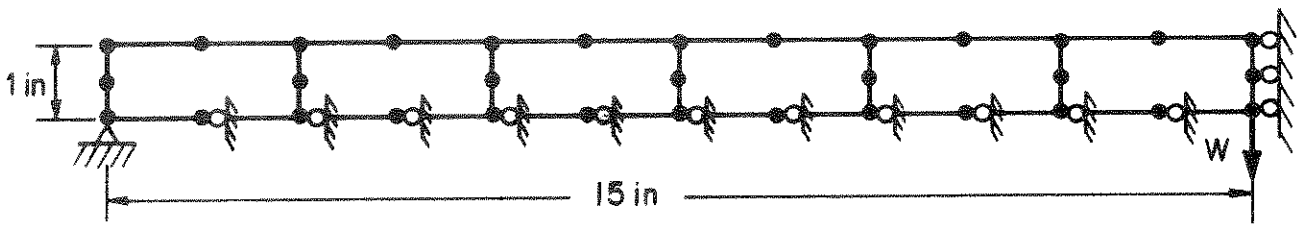

FINITE ELEMENT IDEALIZATION, SIX 8 NODE ELEMENTS

FIGURE 6.27 ELASTIC-PLASTIC DYNAMIC ANALYSIS OF SIMPLY-SUPPORTED BEAM

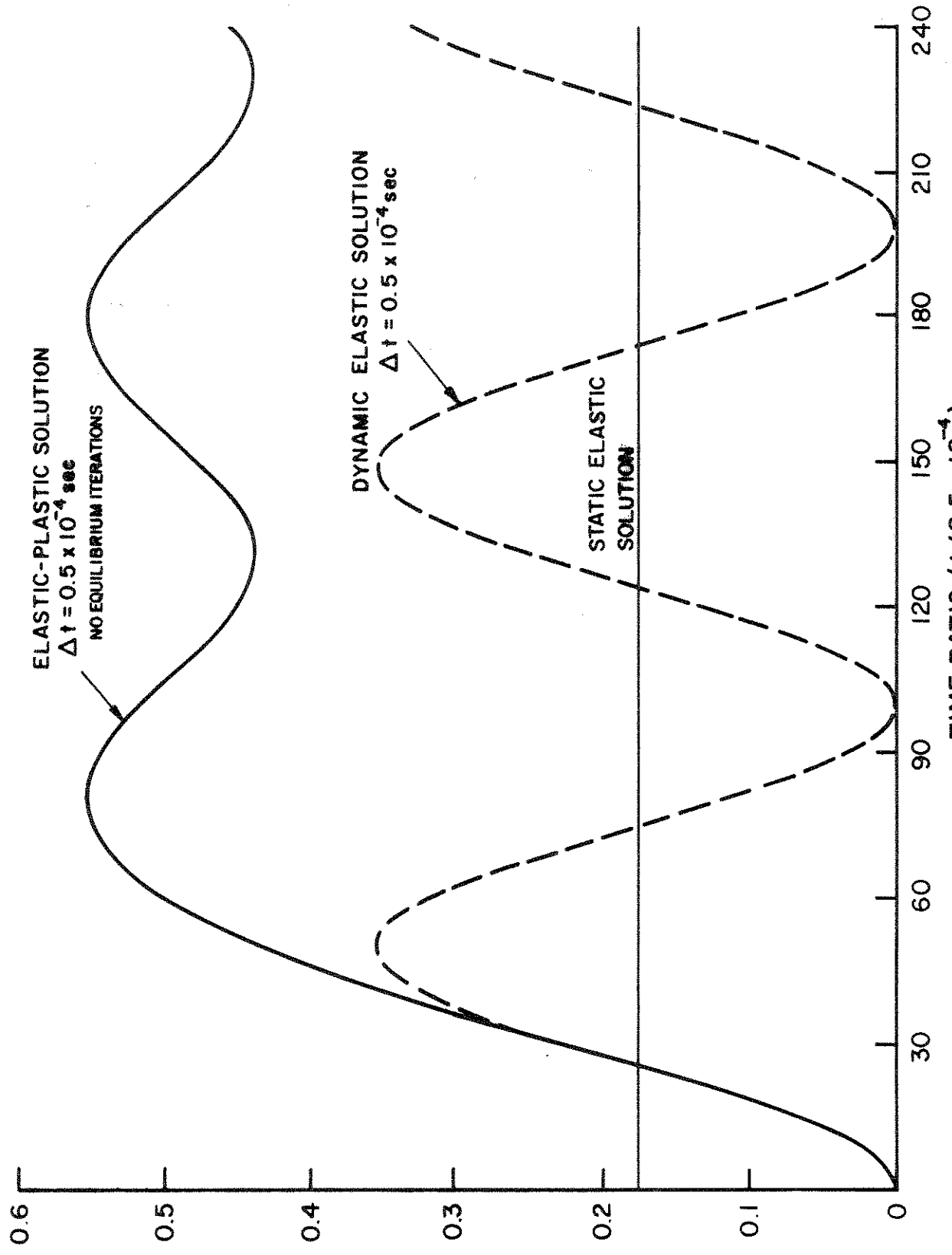

FIGURE 6.28 DYNAMIC SMALL DISPLACEMENT ELASTIC-PLASTIC RESPONSE OF SIMPLY SUPPORTED BEAM, WILSON θ-METHOD, $\theta = 1.4$

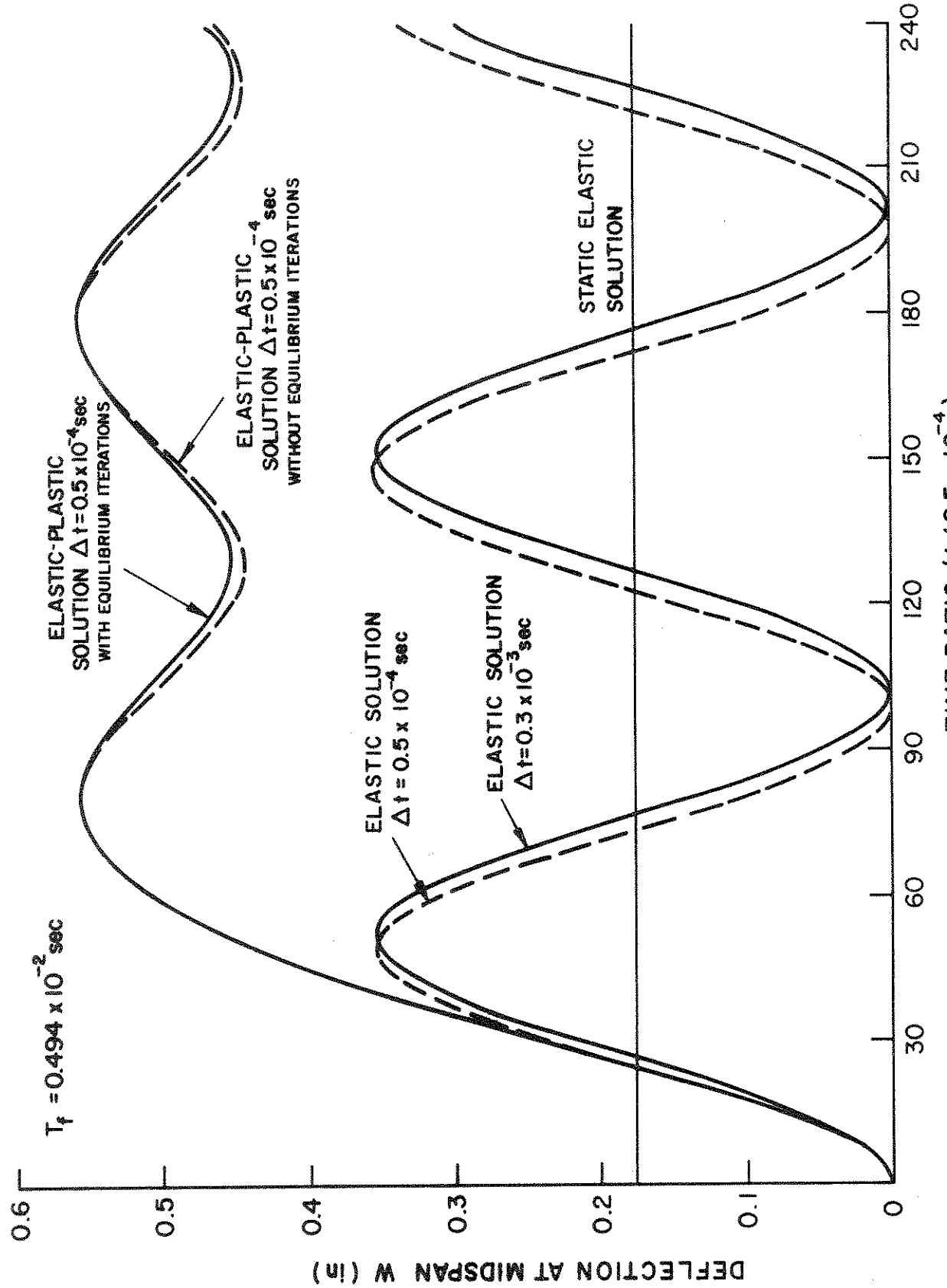

FIGURE 6.29 DYNAMIC SMALL DISPLACEMENT ELASTIC-PLASTIC RESPONSE OF SIMPLY SUPPORTED BEAM, NEWMARK METHOD, $\delta = 0.50$, $\alpha = 0.25$

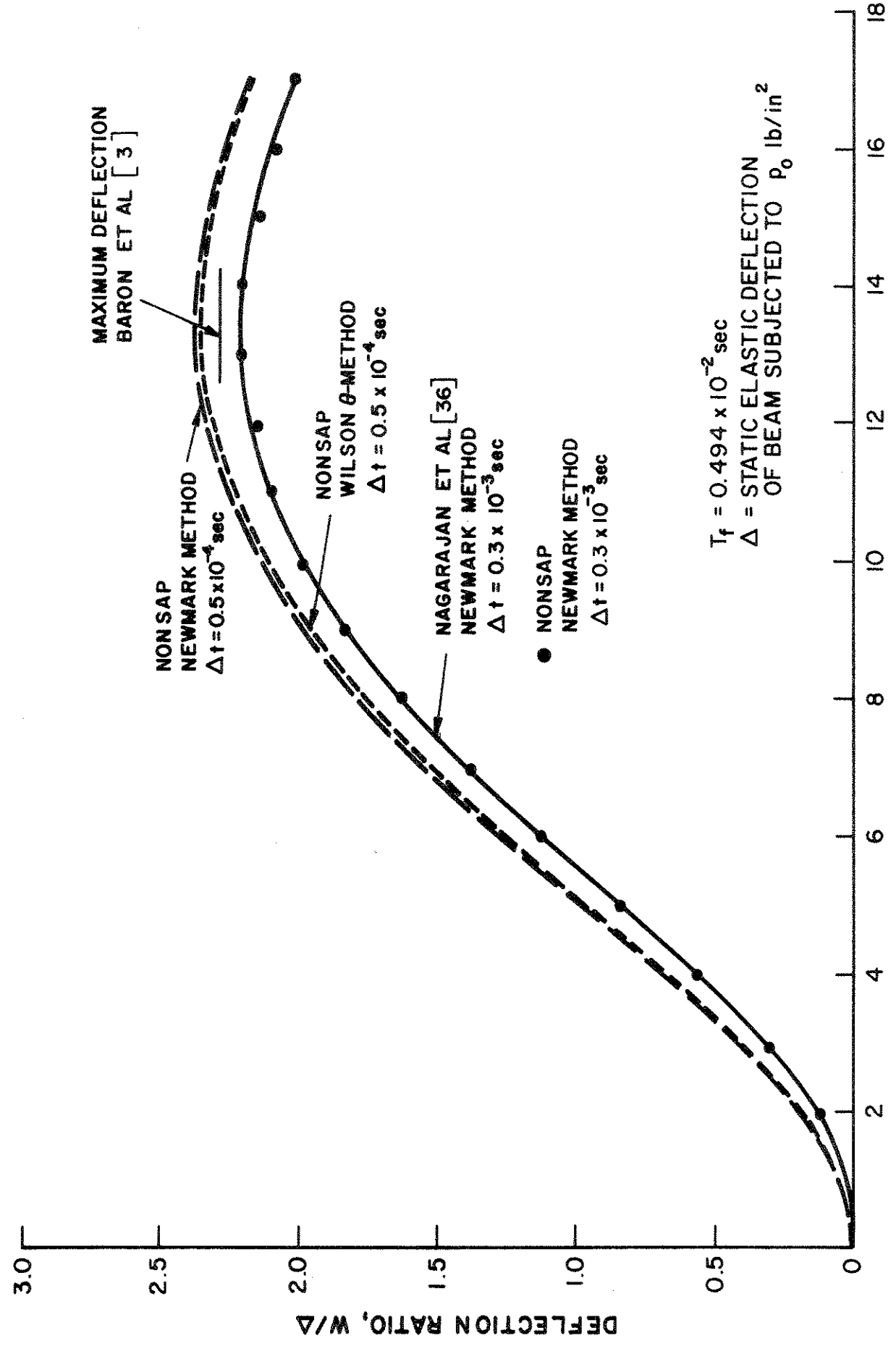

FIGURE 6.30 INITIAL ELASTIC-PLASTIC DISPLACEMENT RESPONSE OF SIMPLY SUPPORTED BEAM

The dynamic solution predicted by NONSAP shows the typical characteristics of elastic-plastic behavior; namely, since the system is softening due to plasticity, the effective period and amplitude of vibration of the system are larger than in linear elastic response. Also, the mean value of the beam mid-point deflection about which the beam is vibrating is much larger than predicted assuming elastic behavior.

6.13 Elastic-Plastic Large Displacement Dynamic Analysis of a Spherical Cap

The dynamic response of the spherical cap in Fig. 6.31 subjected to a distributed step pressure p = 600 lb/in^2 was calculated. The material was assumed to obey the von Mises yield condition with linear isotropic hardening. The purpose of this analysis was to compare the results obtained using the various nonlinear large displacement formulations available in NONSAP for elastic-plastic response calculations.

Figure 6.31 shows the dynamic response of the cap predicted using the Newmark time integration scheme in linear analysis, materially nonlinear only analysis, i.e. assuming small displacements and small strains, and combined geometrically and materially nonlinear analysis. In the fully nonlinear analysis the solutions using the T.L., U.L.(T) and U.L.(J) formulations have been obtained. It is observed that all three formulations predict essentially the same response. The reason for obtaining almost identical solutions lies partly in that the mathematical representation of the yield function is almost the same in the 2nd Piola - Kirchhoff stress space and the Cauchy stress space. Namely, in problems of small strains but large rotations, such as in the analysis of shells, the physical components of the Cauchy stress tensor in rotated (surface) coordinates are approximately equal to the Cartesian components of the 2nd Piola - Kirchhoff stress tensor.

The solutions in Figure 6.31 demonstrate the effect of including different degrees of nonlinearities. It is observed that the materially nonlinear only solution differs a great deal from the linear elastic response, and that the effect of large displacements is also significant.

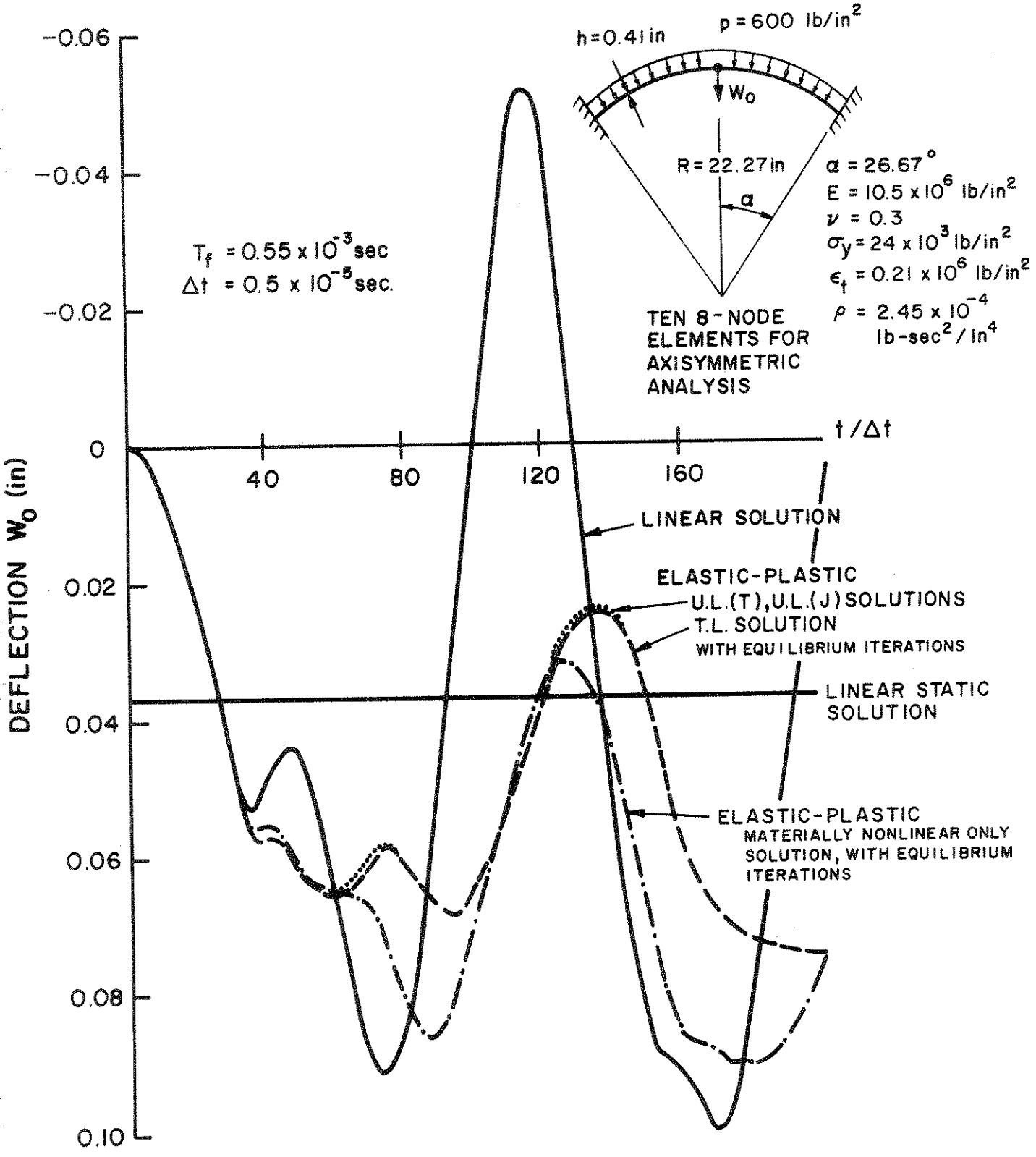

FIGURE 6.31 LARGE DISPLACEMENT DYNAMIC ELASTIC-PLASTIC ANALYSIS OF SPHERICAL CAP, NEWMARK METHOD, $\delta = 0.50$, $\alpha = 0.25$

The decrease in amplitude of vibration and increase in the mean deflection of the shell when nonlinearities are taken into account should be noted.

The response of the cap was also calculated using the Wilson θ-method and the results are given in Fig. 6.32. It should be noted that essentially the same response is predicted using the Newmark and the Wilson integration schemes.

A comparison of the results obtained using NONSAP with those calculated by Nagarajan [35] is given in Fig. 6.33. Nagarajan used degenerate isoparametric elements, in which it is assumed that the transverse normal stresses are negligibly small. This assumption affects the effective stress patterns which control plastic loading and contributes to the different response predicted using NONSAP.

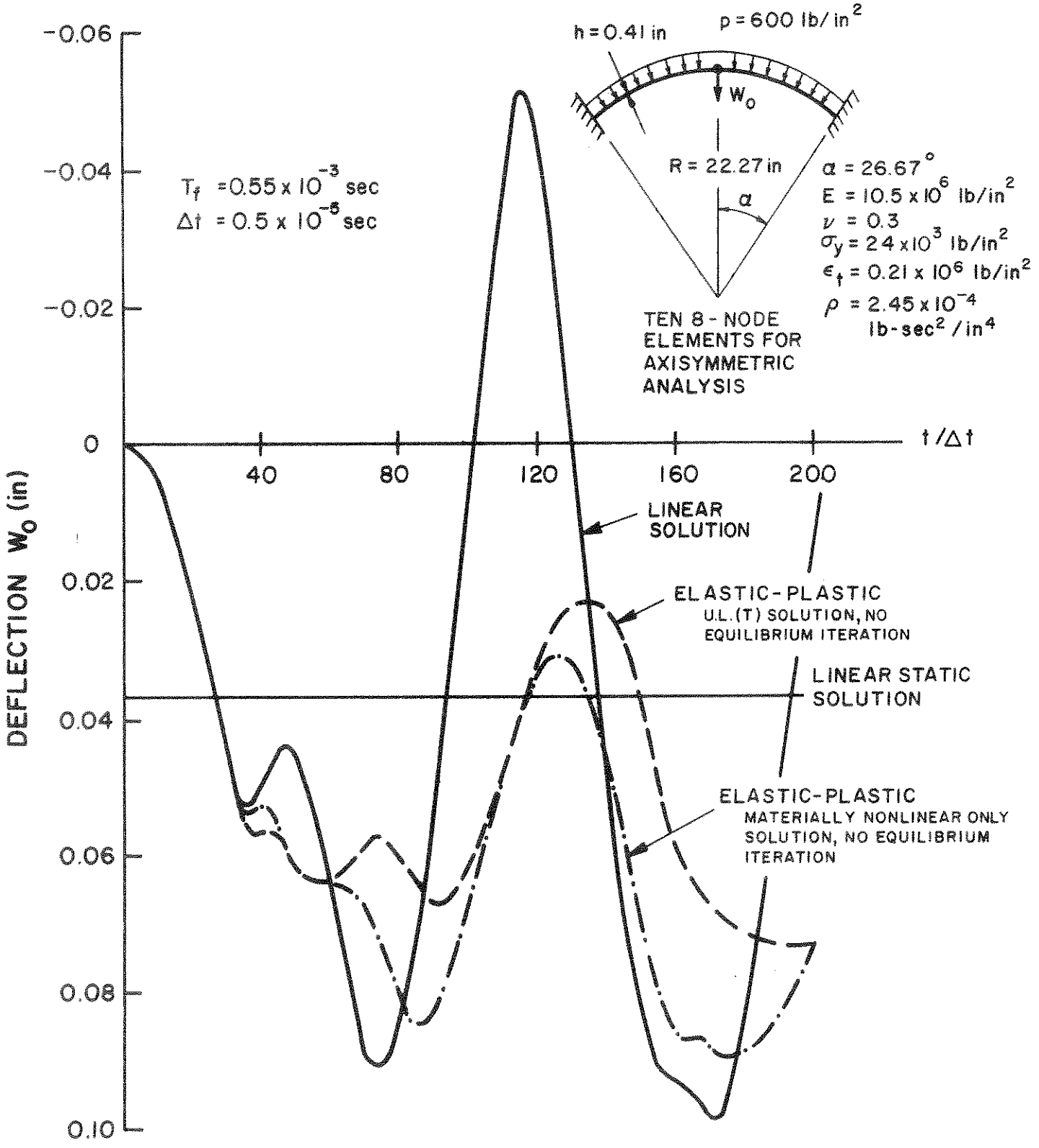

FIGURE 6.32 LARGE DISPLACEMENT DYNAMIC ELASTIC-PLASTIC ANALYSIS OF SPHERICAL CAP, WILSON θ-METHOD, θ=1.4

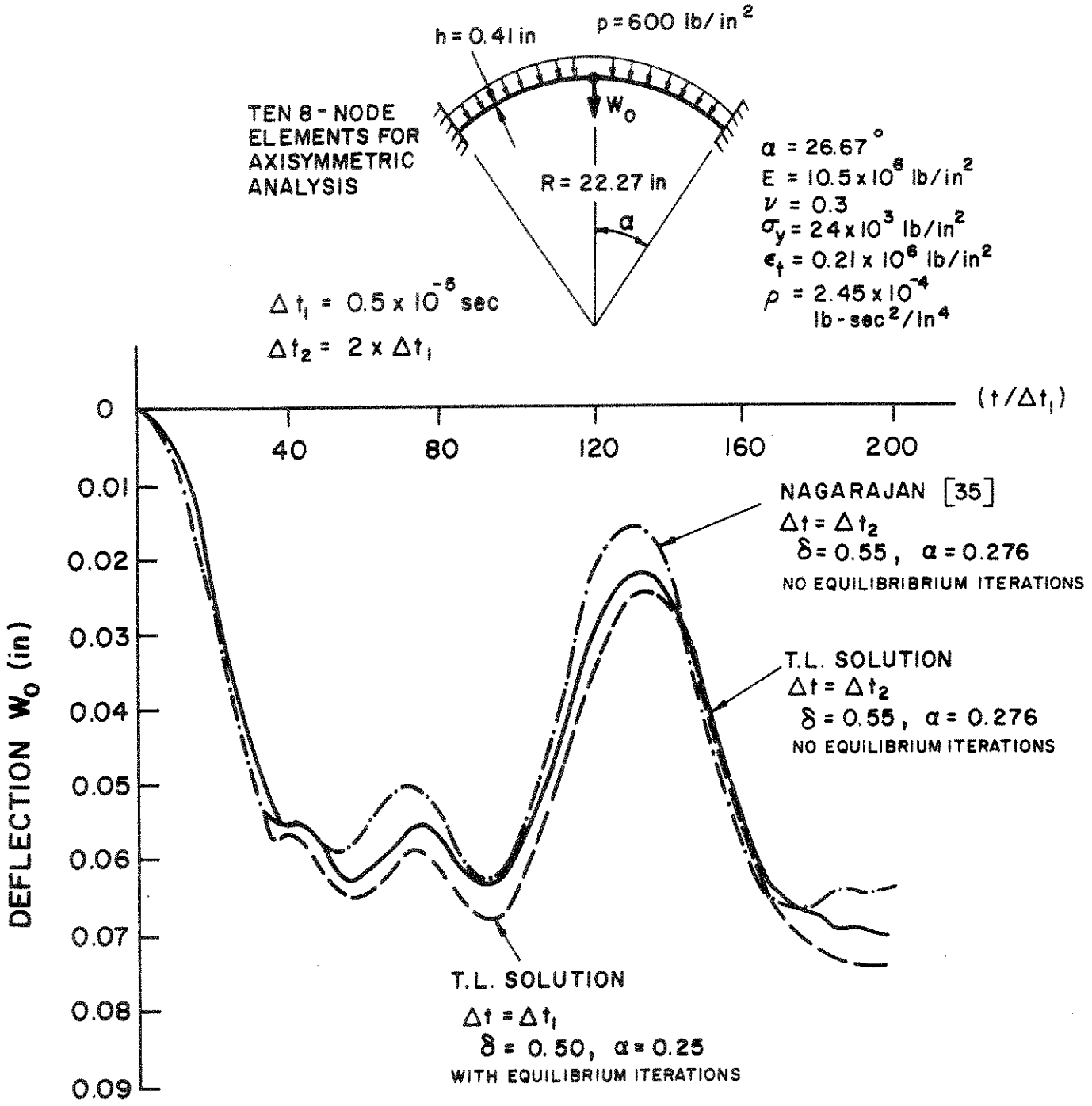

FIGURE 6.33 LARGE DISPLACEMENT DYNAMIC ELASTIC-PLASTIC ANALYSIS OF SPHERICAL CAP, NEWMARK METHOD

6.14 Static Analysis of Variable Tangent Moduli Model Test Specimen

A simple static analysis of a one element test specimen under cyclic loading was carried out. The material of the specimen was characterized using the variable tangent moduli model. Figure 6.34 shows the specimen with the static loading condition and the material parameters. Plane strain conditions are assumed.

The loading, unloading and reloading stress-strain response of the specimen as predicted using NONSAP is shown in Fig. 6.34, in which also results obtained by Nelson et al. [38] are given. Good correspondence is observed. It should be noted that the model does not predict a substantial hysteresis loop.

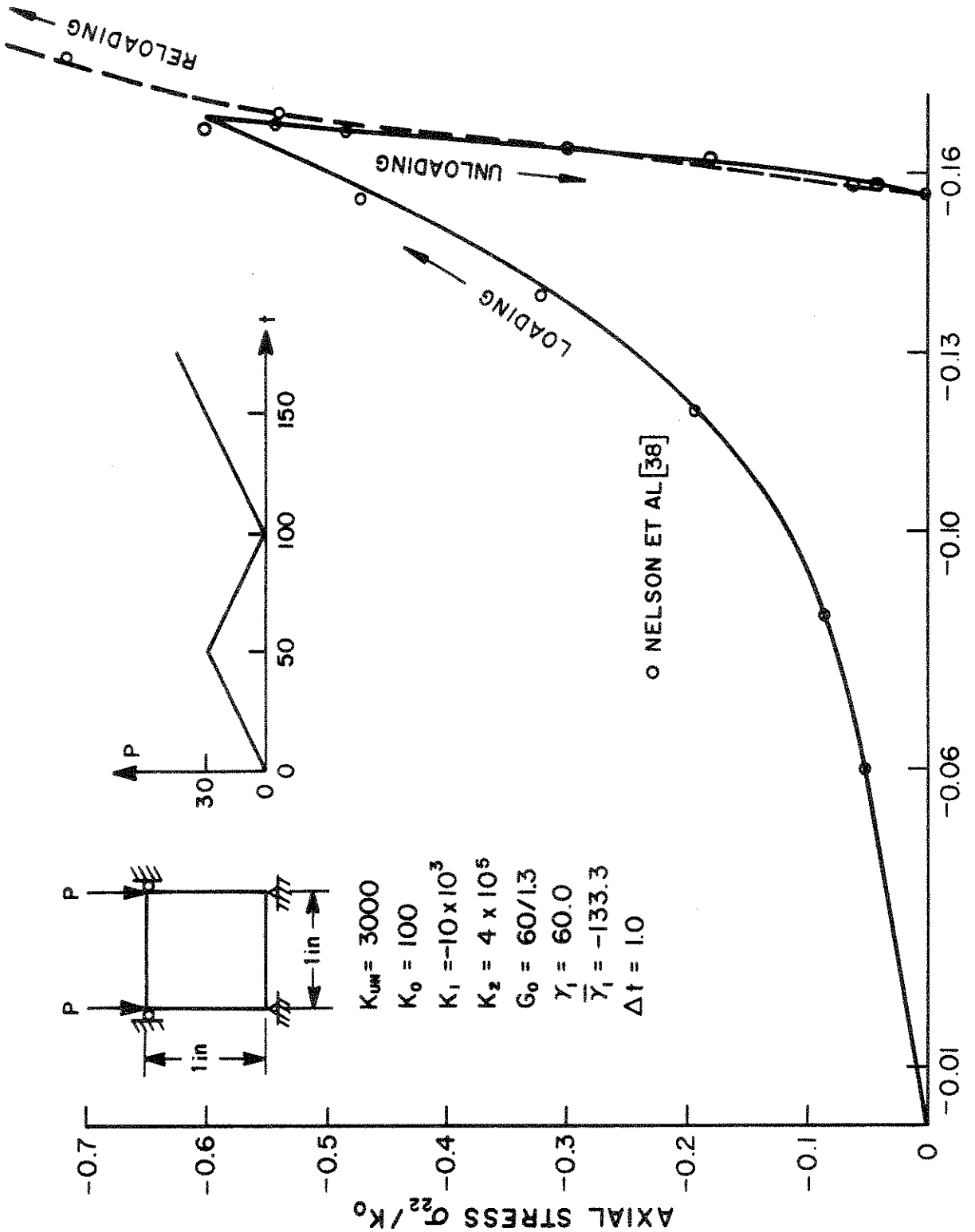

FIGURE 6.34 VARIABLE TANGENT MODULI MODEL STRESS-STRAIN RESPONSE OF TEST SPECIMEN

6.15 Static Analysis of an Underground Opening

To demonstrate the use of the curve description model with tension cut-off capability, a simplified analysis of an underground opening under static overburden pressure was carried out. Figure 6.35 shows the underground opening, the finite element mesh and the material data used. It should be noted that 4, 5 and 8 node elements have been employed and that γ was only used in the in-situ ground pressure calculations for the no-tension model (see Section 4.4.6), i.e. only surface loading P = 2000 lb/ft^2 per load step was applied.

The analysis was carried out using the materially nonlinear only formulation, i.e. large displacement effects were neglected. The rock material was assumed to be a no-tension material with constant Young's modulus and Poisson's ratio.

Figure 6.36 gives the load-deflection relations for two points of the opening. The influence of the no-tension material assumption on the displacements can be observed. Figure 6.37 shows the crack region around the opening at two load levels.

The purpose of this analysis was to give an application of the curve description model with tension cut-off and to show qualitatively what results can be expected. The material data, loading and the finite element mesh have been chosen for demonstration purposes only. It is apparent that the accuracy of the analysis can only be determined by comparison with actual experiments, from which also the different material properties need be determined.

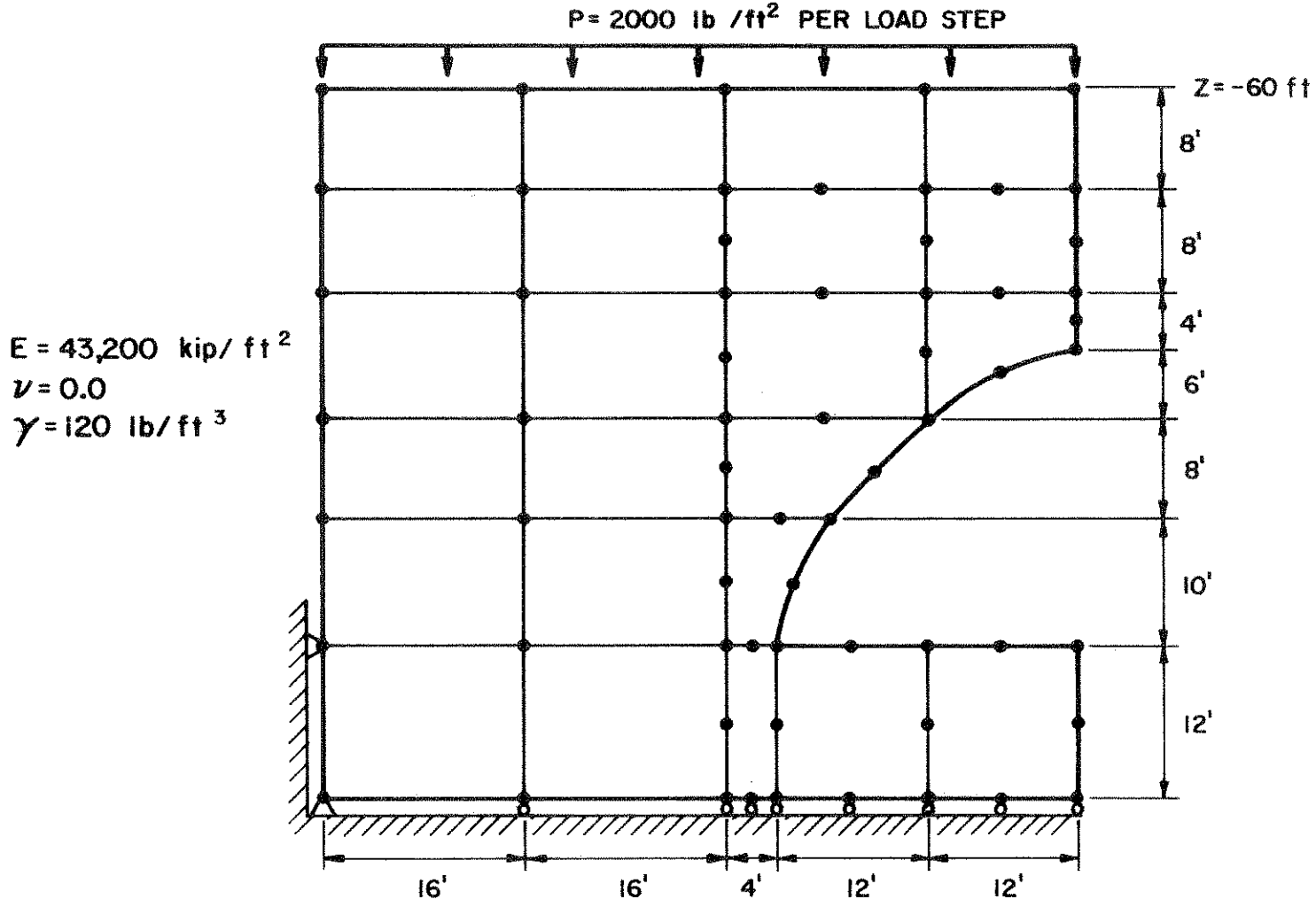

FIGURE 6.35 FINITE ELEMENT MESH FOR ANALYSIS OF UNDERGROUND OPENING

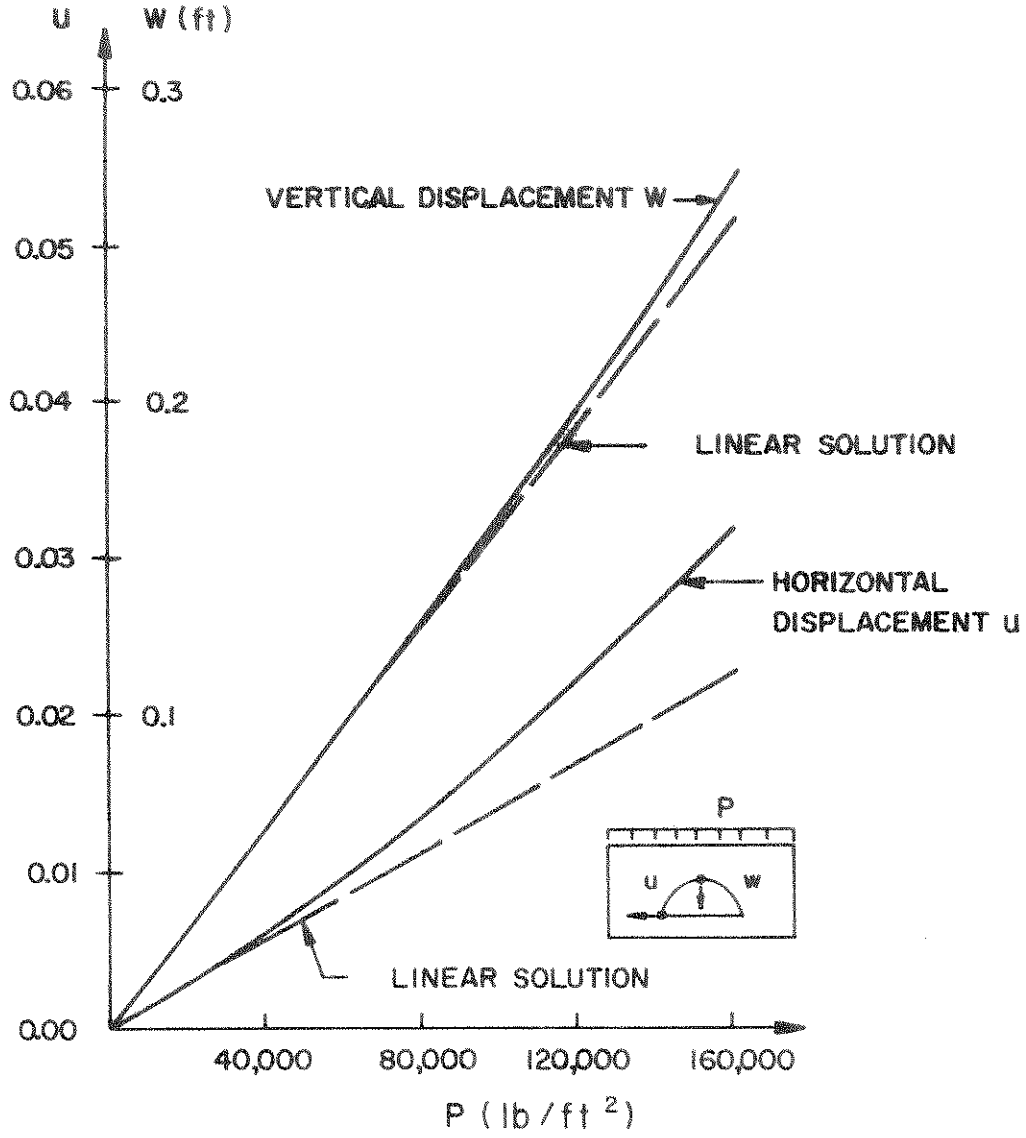

FIGURE 6.36 LOAD-DEFLECTION RESPONSE OF UNDERGROUND OPENING

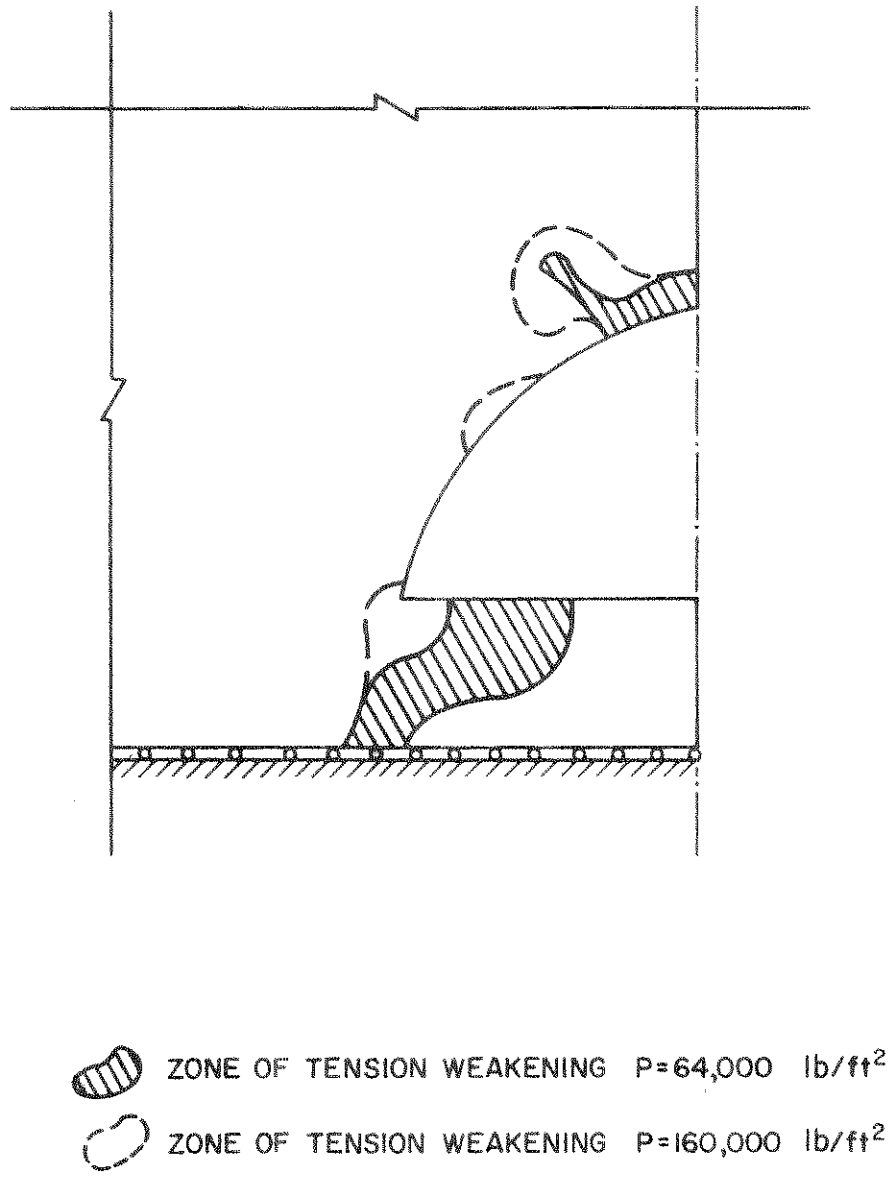

FIGURE 6.37 CRACKED REGIONS AROUND UNDERGROUND OPENING

6.16 Static and Dynamic Analysis of a Simply Supported Plate

A simply supported plate subjected to a concentrated mid-point load was analyzed for static and dynamic response. Figure 6.38 shows the finite element idealization used for one quarter of the plate. In the analysis, small displacements were assumed and the material was considered to be isotropic linear elastic (see Section 4.5.1). The Gauss integration order used in the derivation of element stiffness matrices was two in the r,s and t directions.

It should be noted that the finite element idealization of the plate is rather coarse and high accuracy in the analysis cannot be expected. Figure 6.39 shows the static and dynamic displacement response as predicted by NONSAP. The same element idealization was also used in an analysis with SAP IV [8]. Table 9 summarizes the frequency solution.

TABLE 9 VIBRATION PERIODS OF SIMPLY SUPPORTED PLATE

	PERIOD (SEC)		
MODE	Kirchhoff plate theory †	NONSAP consistent mass	NONSAP lumped mass
1	0.2366	0.2260	0.2264
2	0.0684	0.0609	0.0668
3	0.0362	0.0328	0.0359

† $T = 2\sqrt{\mu} \Big/ \left(\pi\sqrt{D}\left(\frac{n^2}{60^2} + \frac{m^2}{40^2}\right)\right)$; $D = \frac{Eh^3}{12(1-\nu^2)}$; $\mu = \frac{\rho}{h}$

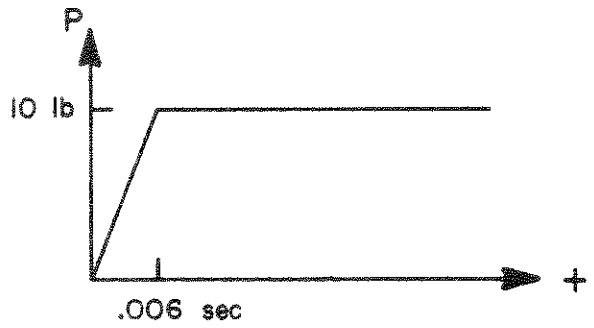

$\rho = 0.0003 \ \frac{\text{lb sec}^2}{\text{in}^4}$

$E = 3 \times 10^4 \ \text{lb/in}^2$

$\nu = 0.25$

STEP LOADING
(on one quarter plate)

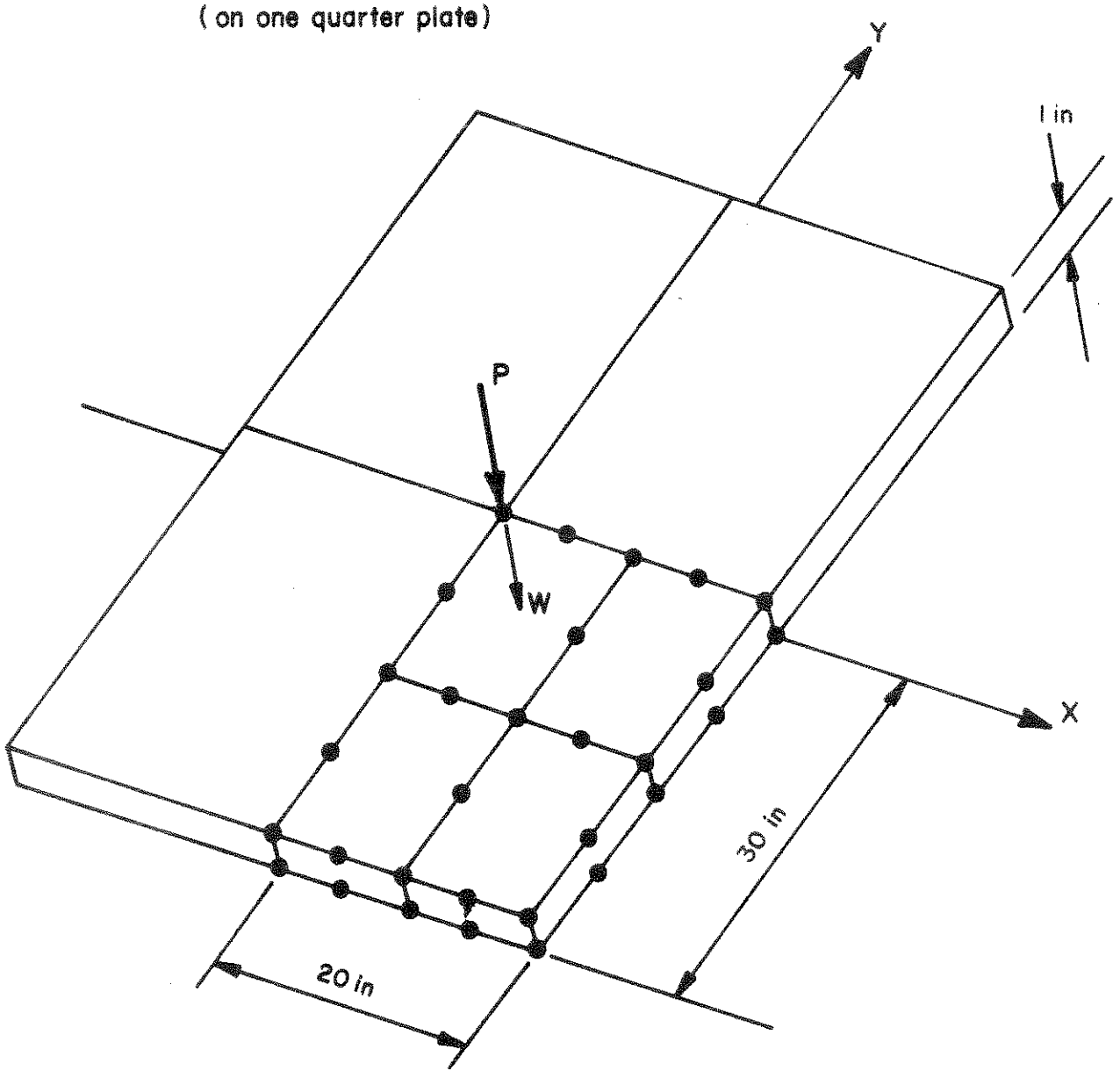

FIGURE 6.38 STATIC AND DYNAMIC ANALYSIS OF SIMPLY SUPPORTED PLATE

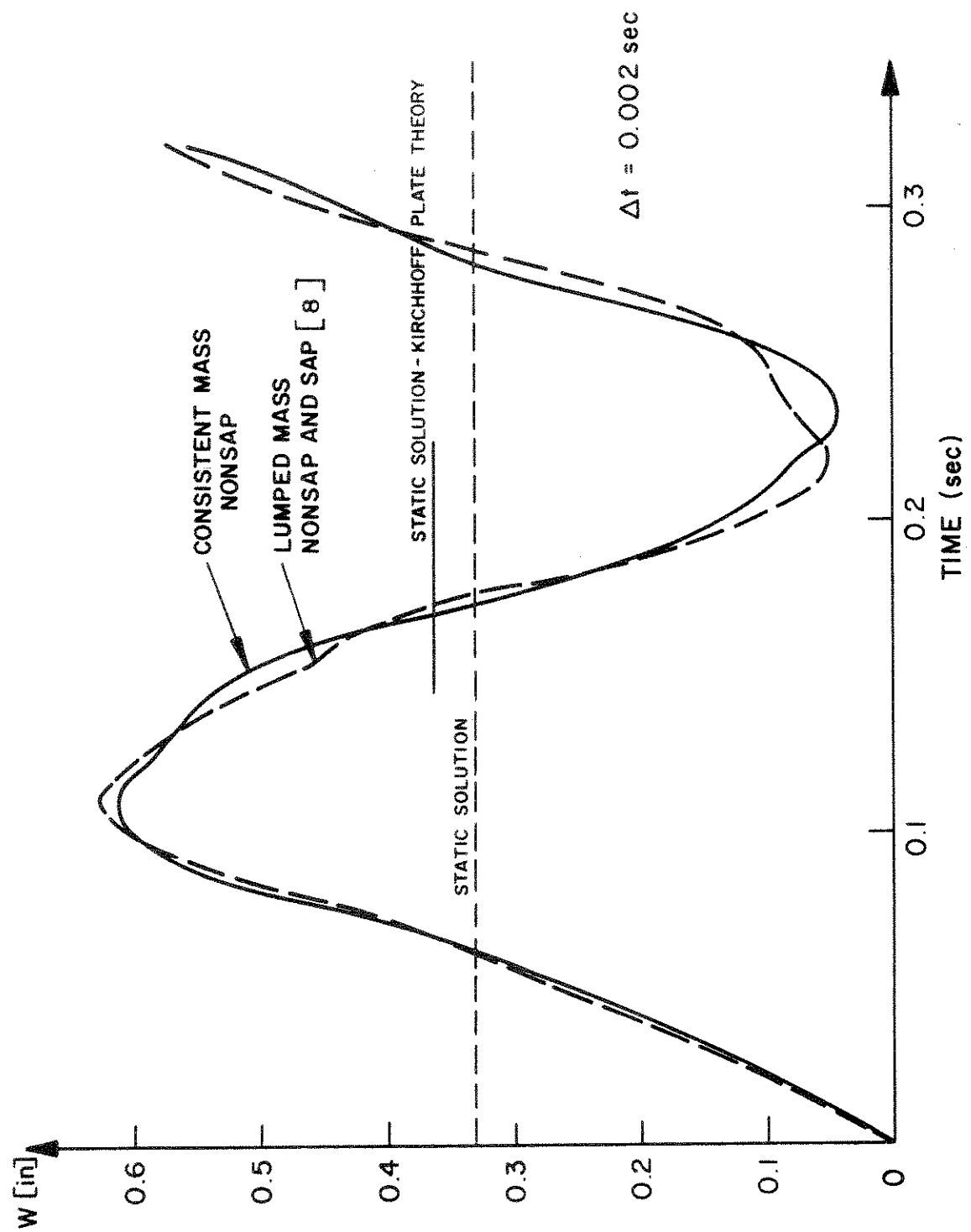

FIGURE 6.39 DISPLACEMENT RESPONSE OF SIMPLY SUPPORTED PLATE, WILSON θ-METHOD, $\theta = 1.4$

7. CONCLUDING REMARKS

The purpose of this report was to present the analysis techniques currently used in the nonlinear analysis program NONSAP. The finite element formulations, the actual finite elements implemented, the time integration schemes used and the nonlinear material models available in the program have been described. Sample analyses have been presented to demonstrate some of the current capabilities of the program. In the conclusions below, important observations made during the course of this work are summarized and the need for further research in various areas is pointed out.

The isoparametric finite element formulations implemented in this study have proven to be very effective. The T.L., U.L., U.L.(T) and U.L.(J) formulations are based on continuum mechanics principles and include all nonlinear effects due to large displacements, large strains and material nonlinearities. The analysis results obtained compare well with experiments and other existing analytical and numerical solutions.

A natural question is which one of the formulations should be adopted for a specific problem. As shown in this work, the choice between the different formulations is decided only by their relative numerical effectiveness, and largely depends on the material description employed, i.e. whether the constitutive law is given corresponding to the T.L. or the U.L. formulations. In the final current version of NONSAP, for elastic large deformation analysis, the U.L. formulation and the T.L. formulation are made available. However, for large displacement and large strain analysis including material nonlinearities, currently

only the T.L. formulation is made available, since nonlinear constitutive relations are relatively easy to implement in this formulation.

A number of material models have been programmed and tested. Using a specific nonlinear material description it is important to note the restrictions that are imposed on the use of the model. In particular, a material description may only be applicable to certain loading conditions or structural configurations. Since it is anticipated that additional nonlinear material models will be required for different analyses, NONSAP has been written to allow incorporating material subroutines without changes to the program.

For time integration in dynamic analysis, the Wilson θ and Newmark integration methods have been incorporated into NONSAP. Both schemes can be used with equilibrium iteration, in which case the solution corresponds to a modified Newton iteration within each time step. Without loss of solution accuracy, depending on the nonlinearities, the equilibrium iteration may allow to dispense with the calculation of a new effective stiffness matrix in each time step and in this way improve solution efficiency. Also, in some analyses, iterations were found to be necessary to obtain accuracy and possibly prevent solution instabilities. It should be noted that equilibrium iterations always improve the accuracy of analysis, and if convergence difficulties are encountered, the solution without iteration is likely to be inaccurate.

With regard to future research, important development is needed in practically all areas pertaining to nonlinear finite element analysis. The formulation of appropriate constitutive relations to be incorporated into the nonlinear equations of motion will still require a great deal more

attention for various classes of nonlinear materials. This phase of research need be based on experimental investigations. In addition, however, the formulations should be compatible with the computational techniques used in order not to cause numerical instabilities.

The stability, accuracy and cost of nonlinear analysis depends to a large degree on the numerical algorithms used and their effective computer implementation. Practical nonlinear analysis is only possible with the use of computers and the feasibility of an analysis depends to a large degree on efficient computer programming of the theoretical procedures.

A great deal more research is required for the design of reliable time integration operators, including algorithms for the automatic selection of variable time steps, and variable load steps in static analysis, in order to optimize the solution cost. However, in this context, it should be realized that effective time integration schemes must be based on consistent finite element formulations, in which stable constitutive relations are used, and on appropriate computer implementation. It is this interaction between the areas of numerical analysis, continuum mechanics, experimental investigation and computer implementation that makes the development of a general nonlinear analysis program a formidable and very rewarding challenge.

REFERENCES

1. Argyris, J.H., "Continua and Discontinua", Proceedings Conference on Matrix Methods in Structural Mechanics, Wright Patterson AFB, Ohio, 1965.

2. Argyris, J.H., Dunne, P.C., and Angelopoulos, T., "Nonlinear Oscillations Using the Finite Element Technique", Computer Methods in Applied Mechanics and Engineering, Vol. 2, pp. 203-250, 1973

3. Baron, M.L., Bleich, H.H., and Weidlinger, P., "Dynamic Elastic-Plastic Analysis of Structures", ASCE, J. Engng. Mech. Div., Vol. 87, pp. 23-42, 1961.

4. Bathe, K.J., Ramm, E., and Wilson, E.L., "Finite Element Formulations for Large Displacement and Large Strain Analysis", SESM Report No. 73-14, Department of Civil Engineering, University of California, Berkeley, September 1973.

5. Bathe, K.J., and Wilson, E.L., "NONSAP--A General Finite Element Program for Nonlinear Dynamic Analysis of Complex Structures", Paper M3/1, Proceedings 2nd Int. Conference on Structural Mechanics in Reactor Technology, Berlin, September, 1973.

6. Bathe, K.J., and Wilson, E.L., "Stability and Accuracy Analysis of Direct Integration Methods", International Journal of Earthquake Engineering and Structural Dynamics, Vol. 1, pp. 283-291, 1973.

7. Bathe, K.J., Wilson, E.L., and Iding, R., "NONSAP--A Structural Analysis Program for Static and Dynamic Response of Nonlinear Systems", SESM Report No. 74-3 , University of California, Berkeley, 1974.

8. Bathe, K.J., Wilson, E.L., and Peterson, F.E., "SAP IV--A Structural Analysis Program for Static and Dynamic Response of Linear Systems", EERC Report No. 73-11, University of California, Berkeley, 1973.

9. Belytschko, T., and Hsieh, B.J., "Nonlinear Transient Analysis of Shells and Solids of Revolution by Convected Elements", AIAA paper No. 73-359, AIAA/ASME/SAE 14th Structures, Structural Dynamics and Materials Conference, Williamsburg, Virginia, March, 1973.

10. Desai, S.C., and Abel, J.F., Introduction to the Finite Element Method, Van Nostrand Reinhold Company, New York, 1972.

11. Dupuis, G.A., Hibbitt, H.D., McNamara, S.F., and Marcal, P.V., "Nonlinear Material and Geometric Behavior of Shell Structures", Computers and Structures, Vol. 1, pp. 223-239, 1971.

12. Felippa, C.A., "Refined Finite Element Analysis of Linear and Nonlinear Two-Dimensional Structures", SESM Report No. 66-22, Department of Civil Engineering, University of California, Berkeley, 1966.

13. Felippa, C.A., and Sharifi, P., "Computer Implementation of Nonlinear Finite Element Analysis", Proceedings, Symposium ASME, Detroit, November, 1973.

14. Fung, Y.C., Foundations of Solid Mechanics, Prentice-Hall, Inc., Englewood Cliffs, New Jersey, 1965.

15. Gjelsvik, A., and Bodner, S.R., "The Energy Criterion and Snap Buckling of Arches", ASCE, J. Engng. Mech. Div., Vol. 88, pp. 87-134, 1962.

16. Haug, E., and Powell, G.H., "Finite Element Analysis of Nonlinear Membrane Structures", SESM Report No. 72-7, Department of Civil Engineering, University of California, Berkeley, 1972.

17. Heifitz, J.H., and Costantino, C.J., "Dynamic Response of Nonlinear Media at Large Strains", ASCE, J. Engng. Mech. Div., Vol. 98, pp. 1511-1527, 1972.

18. Hibbitt, H.D., Marcal, P.V., and Rice, J.R., "Finite Element Formulation for Problems of Large Strain and Large Displacements", Int. J. Solids Struct., Vol. 6, pp. 1069-1086, 1970.

19. Hodge, P.G., and White, G.H., "A Quantitative Comparison of Flow and Deformation Theories of Plasticity", J. Appl. Mech., Vol. 17, pp. 180-184, 1950.

20. Holden, J.T., "On the Finite Deflections of Thin Beams", Int. J. Solids Struct., Vol. 8, pp. 1051-1055, 1972.

21. Humphreys, J.S., "On Dynamic Snap Buckling of Shallow Arches", AIAA Journal, Vol. 4, pp. 878-886, 1966.

22. Iding, R.H., "Identification of Nonlinear Materials by Finite Element Methods", SESM Report No. 73-4, Department of Civil Engineering, University of California, Berkeley, 1973.

23. Iding et al., Private Communication, to be published.

24. Isenberg, J., "Analytical Modelling of Rock-Structure Interaction", Agbabian Associates, El Segundo, California, April, 1973.

25. Jensen, P.S., "Transient Analysis of Structures by Stiffly Stable Methods", Computers and Structures, to appear.

26. Kornishin, H.S., and Isanbaeva, F.S., "Flexible Plates and Panels", (in Russian), Nauka, Moscow, 1968.

27. Larsen, P.K., "Large Displacement Analysis of Shells of Revolution, Including Creep, Plasticity and Viscoelasticity", SESM Report No. 71-22, Department of Civil Engineering, University of California, Berkeley, 1971.

28. Lee, E.H., "Elastic-Plastic Deformation at Finite Strains", Transactions of the ASME, Journal of Applied Mechanics, March, 1968.

29. Mallet, R.H., and Berke, L., "Automated Method for the Large Deflection and Instability Analysis of 3-dimensional Truss and Frame Assemblies", AFFDL-TR-66-102, December, 1966.

30. Malvern, L.E., Introduction to the Mechanics of a Continuous Medium, Prentice-Hall, Inc., Englewood Cliffs, New Jersey, 1969.

31. Marcal, P.V., "The Effect of Initial Displacements on Problems of Large Deflection and Stability", Report of Brown University, Division of Engineering, 1967.

32. Martin, H.C., and Carey, G.F., Introduction to Finite Element Analysis, McGraw-Hill Book Co., New York, 1973.

33. McNamara, J.F., "Incremental Stiffness Method for Finite Element Analysis of the Nonlinear Dynamic Problem", Ph.D. thesis, Department of Civil Engineering, Brown University, 1972.

34. Mescall, J.F., "Large Deflections of Spherical Shells Under Concentrated Loads", J. Appl. Mech., Vol. 32, pp. 936-938, 1965.

35. Nagarajan, S., "Nonlinear Static and Dynamic Analysis of Shells of Revolution Under Axisymmetric Loading", SESM Report No. 73-11, Department of Civil Engineering, University of California, Berkeley, 1973.

36. Nagarajan, S., and Popov, E.P., "Elastic-Plastic Dynamic Analysis of Axisymmetric Solids", SESM Report No. 73-9, Department of Civil Engineering, University of California, Berkeley, 1973.

37. Nayak, G.C., and Zienkiewicz, O.C., "Elasto-Plastic Stress Analysis. A Generalization for Various Constitutive Relations Including Strain Softening", Int. J. Num. Meth. in Engng., Vol. 3, pp. 113-135, 1972.

38. Nelson, I., Baron, M.L., and Sandler, I., "Mathematical Models for Geological Materials for Wave Propagation Studies", Defense Nuclear Agency, Report No. 2672, Washington, D.C.

39. Nickell, R.E., "Direct Integration Methods in Structural Dynamics", ASCE, J. Engng. Mech. Div., Vol. 99, pp. 303-317, 1973.

40. Oden, J.T., Finite Elements of Nonlinear Continua, McGraw-Hill, 1972.

41. Peterson, F.E., and Bathe, K.J., "Nonlinear Dynamic Analysis of Reactor Core Components", Report S-104.3, Engineering Analysis Corporation, Berkeley, California, March, 1972.

42. Pugh, C.E., Corum, J.M., Liu, K.C., and Greenstreet, W.L., "Currently Recommended Constitutive Equations for Inelastic Design Analysis of FFTF Components", Report No. TM-3602, Oak Ridge National Laboratory, Oak Ridge, Tennessee, 1972.

43. Reyes, S.F., and Deere, D.U, "Elastic-Plastic Analysis of Underground Openings", Proceedings, First Congress, International Society of Rock Mechanics, Lisbon, 1966.

44. Schreyer, H., and Masur, E., "Buckling of Shallow Arches", ASCE, J. Engng. Mech. Div., Vol. 92, pp. 1-19, 1966.

45. Sharifi, P., and Popov, E.P., "Nonlinear Buckling Analysis of Sandwich Arches", ASCE, J. Engng. Mech. Div., pp. 1397-1412, 1970.

46. Sharifi, P., and Yates, D.N., "Nonlinear Thermo-Elastic-Plastic and Creep Analysis by the Finite Element Method", AIAA Paper No. 73-358, AIAA/ASME/SAE 14th Structures, Structural Dynamics and Materials Conference, Williamsburg, Virginia, March, 1973.

47. Stricklin, J.A., "Geometrically Nonlinear Static and Dynamic Analysis of Shells of Revolution", High Speed Computing of Elastic Structures, Proceedings of the Symposium of IUTAM, University of Liege, pp. 383-411, August 1970.

48. Stricklin, J.A., Von Riesemann, W.A., Tillerson, J.R., and Haisler, W.E., "Static Geometric and Material Nonlinear Analysis", Advances in Computational Methods in Structural Mechanics and Design, 2nd U.S.-Japan Seminar on Matrix Methods of Structural Analysis and Design, pp. 301-324, University of Alabama Press, 1972.

49. Theocaris, P.S., and Marketos, E., "Elastic-Plastic Analysis of Perforated Thin Strips of a Strain Hardening Material", J. Mech. Phys. Solids, Vol. 12, pp. 377-390, 1964.

50. Yaghmai, S., "Incremental Analysis of Large Deformations in Mechanics of Solids with Applications to Axisymmetric Shells of Revolution", SESM Report No. 69-17, Department of Civil Engineering, University of California, Berkeley, 1968.

51. Yaghmai, S., and Popov, E.P., "Incremental Analysis of Large Deflections of Shells of Revolution", Int. J. of Solids Struct., Vol. 7, pp. 1375-1393, 1971.

52. Yeh, C.H., "Large Deflection Dynamic Analysis of Thin Shells Using the Finite Element Method", SESM Report No. 70-18, Department of Civil Engineering, University of California, Berkeley, 1970.

53. Zienkiewicz, O.C., The Finite Element Method in Engineering Science, McGraw-Hill, London, 1971.